INVESTIGATION OF HULL-WATERJET INTERACTION EFFECTS

A THESIS PRESENTED IN FULFILMENT
OF THE REQUIREMENTS FOR
THE DEGREE OF
DOCTOR OF PHILOSOPHY
IN
MECHANICAL ENGINEERING
IN
THE UNIVERSITY OF CANTERBURY

BY
HAMISH GEORGE COOP, B.E.(HONS)

November, 1995

Department of Mechanical Engineering
University of Canterbury
Christchurch
New Zealand

TO MY FAMILY AND FRIENDS

Abstract

The project described in this thesis was undertaken in order to gain a better understanding of hull-waterjet interaction. The study has investigated interaction effects between a waterjet featuring a flush type intake and a planing hull, 7.4 metres in length.

Full and model scale resistance and propulsion tests have been conducted to accurately measure the thrust deduction fraction and interaction forces. Various techniques for measuring the waterjet thrust are discussed. Graphs of the thrust deduction fraction for a variety of towing positions are reported. Hull static pressure measurements are also reported.

A free body, vector approach was used to develop empirical, analytical models for both the towing and propulsion situations. Both models are based on the Savitsky planing performance equations. The propulsion model draws also on Hadler's work on propeller-hull interaction.

The analytical towing model was validated against full scale towing tests and small correction functions added. The adjusted model was found to compare favourably with model tests.

Using the correction factors developed for the towing model, an analytical propulsion model is constructed incorporating the waterjet momentum forces. A method is described whereby a vector, called the interaction vector, accounting for remaining interaction effects can be found. Two mechanisms are proposed which would account for the interaction vector.

By comparing the full scale propulsion tests with the propulsion model, the interaction vector is found. Its general magnitude and position are shown to be consistent with the combined proposed mechanisms.

Acknowledgments

I would like to offer my grateful appreciation to the following people and organisations:

To my supervisors, Dr A.J. Bowen of the University of Canterbury and Dr K.V. Alexander of C.W.F. Hamilton and Co. Ltd. who both supervised the project, providing guidance and much encouragement and support.

To the Tool Room Staff at C.W.F. Hamilton and Co. Ltd. for their interest, support and help in countless efforts of equipment construction and modification.

To the staff and technicians of the Department of Mechanical Engineering who have assisted in many different ways throughout the project.

To the Foundation of Research Science and Technology who have funded my salary for a period of four years.

And lastly to my friends and family, in particular Marjorie and David whose active interest, love and support has been essential to my perseverance with this project.

Table of Contents

page

1. Introduction 1

1.1 Project Objectives 1

1.2 Scope of the Project 2

1.2.1 Full Scale Tests 2

1.2.2 Model Tests 2

1.2.3 Computational Work 2

1.2.4 Wind Tunnel Work 2

1.2.5 Analysis 3

1.3 Introduction to Waterjet Propulsion 3

2. Aspects of Waterjet Propulsion 7

2.1 Introduction 7

2.2 Propulsion System - General Arrangement 7

2.2.1 Background to Existing Technology 7

2.2.2 Intake 8

2.2.3 Pump 9

2.2.4 Nozzle 10

2.2.5 Steering and Reversing Equipment 10

2.2.6 Other Designs 11

2.3 Waterjet Propulsion Theory 11

2.3.1 Introduction 11

2.3.2 System Definition 12

2.3.3 Definitions of Thrust 13

2.3.4 Wake Factor 15

2.3.5 Thrust Deduction Factor 18

2.3.6 Propulsive Efficiency 20

2.4 Conclusions 23

3. Aspects of Planing Hull Theory 25

3.1 Introduction 25

3.2 Types of Prediction Methods 25

3.2.1 Planing Hull Series 25

3.2.2 Regression and Empirical Methods 26

3.2.3 Prismatic Equations 26

3.3 Savitsky Method 28

3.3.1 Savitsky Long Form 28

3.3.2 Blount and Fox Modification Factor 34

3.3.3 Savitsky Short Form 35

3.4 Conclusions 36

4. Review Of Hull-Waterjet Interaction 37

4.1 Introduction 37

4.2 Early Work 38

4.2.1 Thrust deduction 38

4.2.2 Wake factor 39

4.3 Contemporary Knowledge and Experience 40

4.3.1 Analysis by Sub-system 40

4.3.2 Basic Descriptions 41

4.3.3 More Sophisticated Descriptions 46

4.3.4 Propeller Hull Interaction 58

4.4 Conclusions 60

5. Theoretical and Experimental Approach 61

5.1 Introduction 61

5.1.1 Vector approach 61

5.1.2 Hull as a free body 62

5.1.3 Likely Contributors to Hull-Waterjet Interaction 62

5.2 General Methodology 65

5.2.1 Stage 1 65

5.2.2 Stage 2 66

5.2.3 Stage 3 67
5.3 Appended Bare Hull Resistance: Computational Model 67
5.3.1 Savitsky Long Form 67
5.3.2 Aerodynamic lift and drag 70
5.3.3 Equations of Static Equilibrium 71
5.3.4 Blount and Fox Modification Factor 73
5.3.5 Correction Functions 73
5.3.6 Computational Procedure 74
5.4 Self Propelled Hull: Computational Model 75
5.4.1 Savitsky Long Form 75
5.4.2 Waterjet Forces 77
5.4.3 Interaction Vector 87
5.4.4 Equations of Static Equilibrium 87
5.4.5 Correction Functions 88
5.4.6 Computational Procedure 89
5.5 Finding Interaction Vector 90
5.6 Conclusions 91

6. Tow Testing 93

6.1 Introduction 93
6.2 Full Scale Tests 93
6.2.1 Introduction 93
6.2.2 Towing Site 93
6.2.3 Winch and chase boat 94
6.2.4 Hull geometry and loading condition 95
6.2.5 Instrumentation system 97
6.2.6 Measurements taken 99
6.2.7 Daily testing procedure 103
6.2.8 Results and data reduction 105
6.3 Model Tests 106
6.3.1 Introduction 106
6.3.2 Procedures 107

6.3.3 Results of model resistance tests 108
6.4 Discussion 108
6.4.1 Full scale tests compared to Savitsky 108
6.4.2 Model tests compared to Savitsky 111
6.5 Conclusions 113

7. Propulsion Testing 115

7.1 Introduction 115
7.2 Measuring Momentum Flux and Flow rate 115
7.2.1 Introduction 115
7.2.2 Outgoing Momentum: review of methods 116
7.2.3 Measurement of Thrust Using a Load Cell System 124
7.2.4 Measuring Momentum Fluxes: Chosen Method 128
7.2.5 Uncertainties 136
7.3 Full Scale Tests 139
7.3.1 Introduction 139
7.3.2 Site 139
7.3.3 Hull geometry and loading condition 139
7.3.4 Instrumentation 139
7.3.5 Measurements taken 140
7.3.6 Daily testing procedure 140
7.3.7 Results of full scale tests 141
7.3.8 Hull static pressure measurements 141
7.4 Model Tests 143
7.4.1 Model Test Procedures 143
7.4.2 Results of model propulsion tests 144
7.5 Discussion 145
7.6 Conclusions 147

8. Analysis of Results 149

8.1 Comparison of Bare Hull and Self Propulsion Tests 149
8.1.1 Comparison of Thrust Deduction Factor 149

8.1.2 Comparison of trim, wetted length and CG position 152
8.2 Interaction Vector 155
8.2.1 Review of approach 155
8.2.2 Presentation of results 155
8.2.3 Possible Contributing Factors to the Interaction Vector 157
8.3 Conclusions 158

9. Conclusions 159

9.1 Contribution to the Understanding of Hull-Waterjet Interaction 159
9.2 Summary of Conclusions 160
9.3 Recommendations for Further Work 162

References 165

Appendices

A-1 Results of Towing Tests 169
A-2 Results of Propulsion Tests 171
A-3 Manufacturing Drawing of Prandtl Rake 173
A-4 Hamilton Test Boat Specifications 174
A-5 Hamilton 273 Waterjet Specifications 174
A-6 Hamilton Test Boat Linesplan 175
A-7 Computer Program Listings 176
A-7.1 CALC_RESISTANCE() 176
A-7.2 SAV_CRL.C 179
A-7.3 SAV_CIR.C 182
A-7.4 FUEL.C 186
A-7.5 INTAKE.C 187

List of Figures

page

1.1 Hamilton 321 waterjet propulsion system (CWF Hamilton and Co. Ltd.) 3

1.2 Range of typical waterjet applications (CWF Hamilton and Co. Ltd.) 5

2.1 Sectioned view of Hamilton 212 waterjet 9

2.2 Waterjet system definition 12

2.3 Hull boundary layer 15

3.1 Free body diagram for Savitsky method 28

3.2 Savitsky long form compared to short form 35

4.1 Inlet and bottom plating lifting forces (Svensson) 43

4.2 Trim and net drag performance of a planing boat model (Ellis (1977)) 47

4.3 Model and test set-up (Burtness 1987) 48

4.4 Lift and drag coefficients for varying IVR 49

4.5 JIP thrust deduction fraction for varying intake throat geometry 54

4.6 Predicted and experimental results of self -propulsion tests (Hadler (1966)) 59

5.1 Dividing streamline and stream tube shapes (Griffith-Jones (1994)) 64

5.2 Schematic of investigation methodology 66

5.3 Model in wind tunnel test section (McLeod (1993)) 70

5.4 Aerodynamic coefficients for varying trim angles 71

5.5 Free body diagram (towing case) 72

5.6 Computational structure diagram (towing case) 74

5.7 Waterjet control volume 1 78

5.8 Hull/waterjet control volume 1 79

5.9 Hull/waterjet control volume 2 80

5.10 Crossection of stream tube at ramp tangency point 84

5.11 Streamlines on hull afterbody (MARIN (1991)) 85

5.12 Free Body Diagram (propulsion case) 87

5.13 Computational structure diagram (self propelled case) 89

5.14 Computational structure diagram used to find the interaction vector 90

6.1 Towing test site in Lyttelton harbour 94

6.2 Winch and test boat at test site 95

6.4 Data acquisition system 98
6.5 Trim meter 100
6.6 Hull markings 101
6.7 Immersion ruler 102
6.8. Typical immersion recording 102
6.9 Towing force transducer 103
6.10 Test boat under tow 104
6.11 Model test towing position 107
6.12 Graph showing predicted and full scale resistance 108
6.13 Graph showing predicted and full scale trims 110
6.14 Graph showing predicted and full scale wetted keel lengths 110
6.15 MARIN resistance 111
6.16 MARIN trims 112
6.17 MARIN wetted keel lengths 112
7.1 ASP tube and mounting plate 119
7.2 Cross-section of ASP tube 119
7.3 Rectangular notch weir 121
7.4 Weir test set up 122
7.5 Sectioned view of 273 waterjet with load cell and seal arrangement 124
7.6 Photograph showing waterjet and load cell installation 125
7.7 Prandtl rake 128
7.8 Nozzle extension complete with straightening vanes 130
7.9 Swirl probe 131
7.10 Swirl meter in use 131
7.11 Swirl data 132
7.12 Nozzle velocity profiles (2800 rpm) 133
7.13 Nozzle velocity profiles at 2300 rpm 134
7.14 Nozzle velocity profiles for a range of rpms 134
7.15 Tapping fittings and rotary valve 142
7.16 Results of pressure tapping measurements. (kPa) 142
7.17 Waterjet installation for model propulsion test 144
7.18 Graphs of full scale and model scale thrust 145

7.19 Graphs of full scale and model scale trim 146
7.20 Graphs of full scale and model wetted keel lengths 147
8.1 Graphs of thrust deduction fraction for varying towing position 150
8.2 Comparison of full scale and model thrust deduction factors 151
8.3 Difference between thrust and resistance 153
8.4 Difference between propelled and bare hull trim 153
8.5 Difference between propelled and bare hull wetted keel length..... 154
8.6 Difference between propelled and bare hull height of CG above free surface.. 154
8.7 Magnitude of ivector, IVR and ratio of ivector to intake momentum flux 156

List of Tables

page

2.1 Events pertinent to waterjet propulsion 7
2.2 Wake factor example 18
3.1 Summary of well known planing hull series 25
3.2 Summary of regression and empirical methods 26
3.3 Savitsky method input parameters 28
3.4 Savitsky calculation parameters 29
4.1 Some propulsive parameters (Bjarne(1990)) 41
4.2 Interaction effects caused by water jet on hull (Alexander et al(1994)) 55
4.3 Interaction effects caused by hull on waterjet (Alexander et al (1994)) 56
5.1 Possible interaction mechanisms 62
6.1 Sample loading calculation sheet 97
6.2 Recorded parameters 99
6.3 Full scale measurement uncertainties 106
6.4 Review of model resistance tests 106
6.5 MARIN resistance test results for test 50208 108
7.1 Input parameters for program INTAKE.C 136
7.2 Variables and uncertainties 137
7.3 Intake momentum calculation uncertainties 138
7.4 MARIN propulsion test results for test 50221 145
8.1 Interaction vector results 156

List of Symbols

description	*units*	*symbol*
frontal area	(m^2)	A_f
sectional area of intake duct at throat	(m^2)	A_{it}
sectional area of intake projected in bottom plane	(m^2)	A_{ip}
sectional area of nozzle	(m^2)	A_n
breadth of stream tube	(m)	b
beam	(m)	b or B
max. projected chine beam	(m)	B_{PX}
chord	(m)	c
boundary layer thickness coefficient	(-)	C_{bl}
drag coefficient	(-)	C_d
Schoenherr turbulent friction coefficient $0.242C_{f2}^{-\frac{1}{2}} = \log_{10}\mathrm{Re}.C_f$	(-)	C_f
centre of gravity	(-)	CG
a lift coefficient	(-)	C_L
lift coefficient, zero deadrise	(-)	C_{Lo}
lift coefficient for hull with deadrise b	(-)	$C_{L\beta}$
ratio of distance from transom to centre of pressure to the mean wetted length	(-)	C_p
velocity coefficient = $\frac{V_b}{(gb)^{1/2}}$	(-)	C_v

total drag force	(N)	D
appendage drag force	(N)	D_a
bracket drag force	(N)	D_b
viscous drag force	(N)	D_f
pitot static drag force	(N)	D_{ps}
rudder drag force	(N)	D_r
aerodynamic drag force	(N)	D_w
distance between N and CG measured normal to N	(m)	e
energy recovered by inlet	(Nm/s)	E_r
energy supplied to the pump	(Nm/s)	E"
distance between T and CG measured normal to T	(m)	f
distance between D_f and CG measured normal to D_f	(m)	f_f
between I and CG measured normal to force I	(m)	f_i
pressure force vector due to integrated pressure	(N)	**Fp**
pressure force acting on waterjet casing	(N)	$\mathbf{Fp_c}$
pressure force acting on hull	(N)	$\mathbf{Fp_h}$
pressure force acting on stream tube	(N)	$\mathbf{Fp_s}$
force vector due to weight of entrained water	(N)	**Fw**
length Froude number = $\frac{V_s}{\sqrt{g\, l_{wl}}}$	(-)	Fn_l (or Fn)
volume Froude number = $\frac{V_s}{\sqrt{g\, \nabla^{1/3}}}$	(-)	F_∇ (or Fv)

gravitational acceleration	(m/s^2)	g
height of jet centre line above free surface	(m)	h_j
submergence of inlet	(m)	h_I
interaction error	(-)	i_error
interaction vector	(N)	**I**
intake velocity ratio $= \frac{V_{it}}{V_s}$	(-)	IVR
duct loss coefficient	(-)	K_d
inlet loss coefficient	(-)	K_i
nozzle loss coefficient	(-)	K_n
dynamic wetted length	(m)	l
waterline length at $V_s=0$	(m)	l_{wl}
length in general	(m)	L
distance from centre of pressure to transom	(m)	L_{cp}
longitudinal distance from transom to CG	(m)	LCG
wetted keel length	(m)	L_K
mean wetted length measured from transom	(m)	L_m
Blount and Fox modification factor	(-)	M
mass flow rate	(kg/s)	$\dot{m}$
hull normal pressure force	(N)	N
boundary layer exponent	(-)	n

overall propulsive coefficient	$= \frac{R_T V_s}{P_B}$	(-)	OPC
static pressure at front face of protruding stream tube		(N/m^2)	p_{0A}
brake power developed by engine		(W)	P_B
effective power	$= R_{BH} V_s$	(W)	P_E
effective jet system power	$= Q H_0$	(-)	P_{EJS}
effective pump power	$= Q H_p$	(W)	P_{EP}
power absorbed by pump impeller	$= \frac{2\pi N}{60} Tq$	(W)	P_D
volumetric flow rate		(m^3/s)	Q
resistance increment fraction	$= \frac{\Delta R_{gf} + \Delta R_{lf}}{R_{BH}}$	(-)	r
Reynolds number		(-)	Re
bare hull resistance		(N)	R_{BH}
shaft power		(W)	shp
planform area of rudder		(m^2)	S_r
thrust deduction factor		(-)	(1-t)
thrust deduction fraction	$= \frac{T - R_{BH}}{T}$	(-)	t
a thickness		(m)	t
thrust		(N)	T
net thrust vector	$=-(\phi_{Mn}-\phi_{Mi})$	(N)	$\mathbf{T_N}$
jet unit input torque		(Nm)	Tq

local velocity	(m/s)	v
momentum intake velocity	(m/s)	V_i
jet velocity at vena contracta	(m/s)	V_j
nozzle velocity	(m/s)	V_n
mean bottom velocity	(m/s)	V_m
throat velocity	(m/s)	V_{it}
ship speed	(m/s)	V_s
wake factor $= \frac{V_s - V_i}{V_s}$	(-)	w
towing force	(N)	W
height of stream tube	(m)	y
elevation of CG above free surface	(m)	z
angle between D_w and horizontal	(deg)	α
hull deadrise angle	(deg)	β
boundary layer thickness	(m)	δ
hull dynamic displacement weight	(N)	Δ
hull static displacement weight	(N)	Δ_0
angle between net thrust vector and keel	(deg)	ε
angle between towing force and horizontal	(deg)	γ
overall propulsive efficiency $= \frac{P_E}{P_D}$	(-)	η_{DA}

intake duct efficiency		(-)	η_i
jet efficiency	$= \frac{TV_s}{E''}$	(-)	η_j
pump efficiency	$= \frac{E''}{shp}$	(-)	η_p
relative rotative efficiency		(-)	η_r
transmission efficiency		(-)	η_t
kinematic viscosity		(m^2/s^2)	ν
mean wetted length to beam ratio		(-)	λ
jet velocity ratio	$= \frac{V_s}{Vj}$	(-)	μ
density of working fluid		(kg/m^3)	ρ
momentum flux vector	$= \dot{m}\,\mathbf{V}$	(N)	ϕ_M
trim angle		(deg)	τ
displacement volume		(m^3)	∇
nozzle loss factor		(-)	ψ
a loss factor		(-)	ζ

SUBSCRIPTS:

i	intake
j	jet
M	momentum
n	nozzle
P	pump
s	ship
t	throat
0	free stream

1. Introduction

1.1 Project Objectives

The project was initiated by CWF Hamilton and Co. Ltd., a leading manufacturer and pioneer of waterjet propulsion systems. It was set up as a joint venture between the company and the Department of Mechanical Engineering in the University of Canterbury. The project began as a Masters however after 12 months it became apparent that the study was more suited to a doctoral level of investigation.

As waterjet applications increase in size, cost and complexity, the need for more precise thrust and resistance predictions arises. A problem exists for the naval architect and propulsion system supplier in knowing how a vessel will behave with the propulsion system fitted.

At the outset of the project the problem of hull-waterjet interaction had been topical in the industry for some time. There was also little understanding of the problem within the company and indeed generally there was almost no published work on the topic. Some competitors had been cloaking interaction with an air of mystery thus capitalising on the ignorance of the market. The company therefore identified the need for research to increase both its own understanding and that of the waterjet industry in general. Performance predictions must be accurate in such a competitive field. Knowledge of interactions and a reliable design process are necessary to achieve such accuracy. Therefore the prime objective of this work was to gain a better understanding of hull-waterjet interaction.

Hull-waterjet interaction occurs when operation of one system affects the performance of the other. In particular it was hoped that interaction effects could be split into various groupings each with a different mechanism. Also, it was anticipated that full scale resistance parameters would be measured.

Funding to support the author was sought from the Technology for Business Growth (TBG) program supported by the Foundation for Research, Science and Technology. The objective of the TBG program is to bring together research institutions and companies to provide mutual commercial and educational benefits. The company

supplied a vessel for the project while day to day labour and equipment costs were shared equally by the company and the university.

1.2 Scope of the Project

A variety of techniques were utilised in the investigation. The significant work which defines the scope of the project is outlined below.

1.2.1 Full Scale Tests

The project has relied heavily on full scale tests using the Hamilton 7 metre test boat. This craft was fully instrumented and then used to conduct series of towing tests to measure the resistance and later propulsion tests with the waterjet operational. The towing tests were used to, define the bare hull resistance at full scale and to help refine a computational towing model against which data from the propulsion tests were compared. In this manner the interaction effects were investigated. The full scale towing tests were also compared with model bare hull tank test results.

1.2.2 Model Tests

As the result of a commercial relationship between CWF Hamilton and Co. Ltd. and the Maritime Research Institute of the Netherlands (MARIN), an opportunity arose to conduct some model tests of the Hamilton test boat. Both resistance and propulsion tests were conducted and data used for useful comparisons to the full scale work. A "baby" waterjet was manufactured by CWF Hamilton and Co. Ltd. for use in the model propulsion tests.

1.2.3 Computational Work

Existing empirical and computational models were used to help form resistance prediction models for the test boat. Use was made of Hamilton's existing planing performance prediction software which was extensively modified to provide accurate computational models for both the towed and self propelled cases.

1.2.4 Wind Tunnel Work

Model tests were carried out in the Department of Mechanical Engineering closed circuit wind tunnel to determine aerodynamic characteristics of the test boat. Wind

tunnel data from a similar project in the department on waterjet intakes was also used.

1.2.5 Analysis

A physical model was developed of all forces acting on the hull with each parameter identified in order to define the experimental work and to assist in its interpretation.

1.3 Introduction to Waterjet Propulsion

Waterjet propulsion has enjoyed continuous development since it entered the marine industry as a serious propulsion alternative in the 1950s. Like propellers, thrust is achieved by accelerating water through the waterjet and so imparting a net force on the propulsion system.

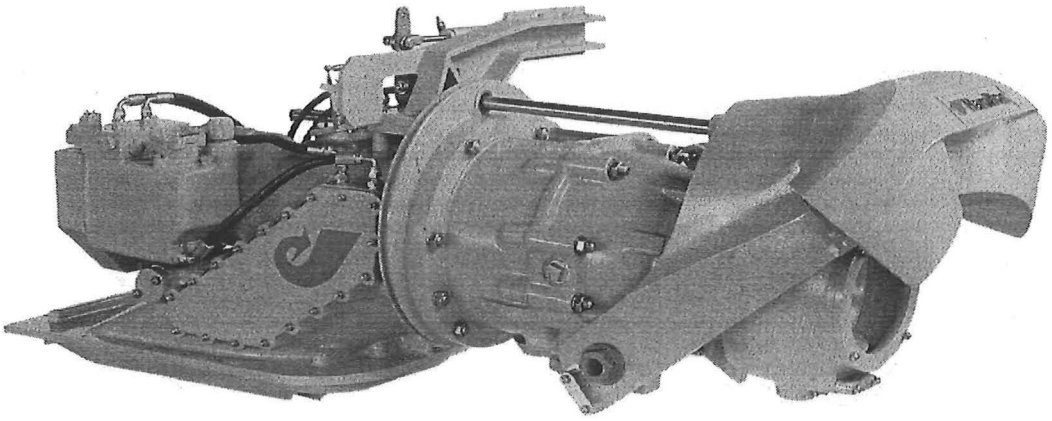

Figure 1.1 Hamilton 321 waterjet propulsion system (courtesy CWF Hamilton and Co. Ltd.)

Figure 1.1 shows mid-range waterjet propulsion system. The system is mounted predominantly within the hull. Water is drawn in through an intake duct and debris screen fitted flush to the bottom of the hull. The fluid passes through a pump before discharging via a nozzle projecting through a sealed transom opening.

Most medium to small waterjets can be direct coupled to the engine without the need for a gearbox. Units are often supplied as a complete package which includes steering and reversing systems.

Key features of waterjet propulsion systems are:

- Good manoeuvrability. The arrangement allows thrust to be applied in any direction. Steering thrust is available while stationary, allowing vessels to turn

in their own length. Reverse thrust can be applied at any speed for emergency braking.

- High Efficiency. Due to an efficient pump combining multi-bladed impellers and a stator set, and also to the lack of protruding appendages, efficiencies can match and even exceed those for propellers especially at medium to high planing speeds.
- Safety. Rotating parts are enclosed in the waterjet unit affording safety to people in the water and protection for machinery from debris.
- Shallow draft. Smooth hull bottom lines allows shallow water operation.
- Low noise and vibration. Waterjets are found to be relatively free from excessive noise and vibration and also exhibit a low underwater acoustic signature.

Waterjet propulsion systems are now available in many different sizes from a variety of manufacturers with power absorption ranging from 100 to 20 000 kW. Figure 1.2 is reproduced from the CWF Hamilton and Co. Ltd. application guide and shows a range of typical waterjet applications.

HamiltonJet

TYPICAL APPLICATIONS

With over 20,000 installations worldwide, HamiltonJet propulsion systems are well proven for providing efficiency, reliability and flexibility in a wide range of hull forms. With models available to suit power inputs ranging from 150kW to 3000kW, Hamilton waterjets can be used in single or multiple configurations in vessels up to typically 50 metres long.

FAST PASSENGER FERRIES

32 metre Catamaran Ferry—U.S.A.
Twin HM571 waterjets—25 knots

WORK BOATS

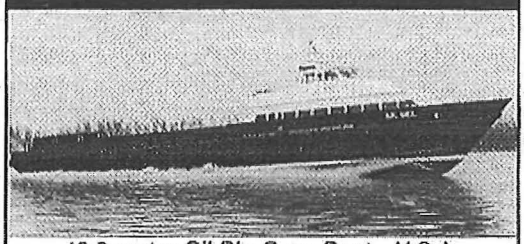

43.2 metre Oil Rig Crew Boat—U.S.A.
Quadruple HM571 waterjets—28 knots

PATROL CRAFT

21 metre Coast Guard Patrol Craft—India
Triple HM402 waterjets—40 knots

RESCUE CRAFT

14.4 metre R.I.B. Rescue Craft—Holland
Twin 362 waterjets—33 knots

ASSAULT CRAFT

10.6 metre Riverine Assault Craft—U.S.A.
Twin 271 waterjets—38 knots

PILOT BOATS

18.6 metre Pilot Boat—Holland
Twin HM571 waterjets—31 knots

PLEASURE CRUISERS

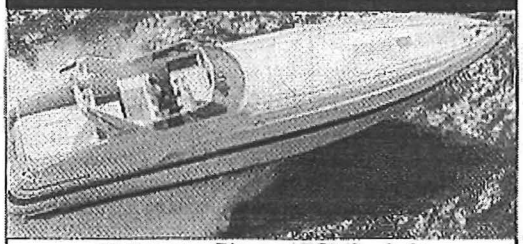

16.7 metre Pleasure Craft—Italy
Twin 362 waterjets—45 knots

FISHING BOATS

9.8 metre Salmon Fishing Boat—U.S.A.
Twin 321 waterjets—34 knots

Figure 1.2 Range of typical waterjet applications (Courtesy CWF Hamilton and Co. Ltd.)

2. Aspects of Waterjet Propulsion

2.1 Introduction

The purpose of this chapter is to give a general overview of waterjet propulsion technology and current theoretical understanding. Section 2.2 gives an overview of the principle of operation and describes the general equipment layout. Section 2.3 reviews general waterjet propulsion theory and also discusses definitions of thrust.

2.2 Propulsion System - General Arrangement

2.2.1 Background to Existing Technology

Waterjet propulsion works in a similar manner to conventional propeller (water screw) propulsion in that fluid is accelerated by the propulsor so as to provide a net thrust on the propulsor. The significant difference is that the propeller is replaced by a pump that is located within the vessel. Ducting leads water to and from the pump.

The concept of accelerating water to provide a forward thrust by using an internal pump is not new. The earliest serious and successful vessels using this concept were built for trials by the British Admiralty for comparisons with propeller driven craft. The waterjet driven craft did not perform well, probably due to the inferior pumps available at the time. Roy (1994) and Allison (1992) give excellent overviews of the development of waterjet propulsion. Table 2.1 is condensed from both papers and summarises some historical developments pertinent to waterjet propulsion.

A key step in the development of the waterjet was the move from using centrifugal to axial and mixed flow pumps. This allowed the development of a compact, robust and efficient package containing an intake duct, pump, nozzle, steering and reversing equipment.

Table 2.1 Events pertinent to waterjet propulsion

Year	*Person/Organisation*	*Achievement*
287-212 BC	Archimedes	Axial water pump
1452-1519	Leonardo Da Vinci	Axial water pump, Screw propulsion
1631	David Ramsey	Patented steam WJ ship propulsion
1661	Toogood and Hayes	Patent for waterjet propelled vessel
1775	Benjamin Franklin	Proposal for waterjet propelled boat
1782	James Rumsey	WJ propelled 80 ft ferry
1836-1845	Smith	Screw propellers
1840	Ericsson	Marine propellers, Sweden/USA

1853	Seydell	WJ Ship Albert
1863	British Admiralty	WJ Ship Nautilaus, 10 knots
1863	British Admiralty	WJ Ship Waterwitch v Viper
1870	Ramus, C.M.	Planing boat, rocket propulsion
1878	Swedish government	Comparative trials WJ v propeller
1883	Thorneycroft	Royal Navy WJ gunboat
1894	Royal National Lifeboat Inst.	WJ Lifeboat
1932	Riva Calzoni	First modern WJ
1950	W. Hamilton	First high speed WJ propulsion system
1968	Jacobson	Patent for personal watercraft
1968	KaMeWa	Mixed flow WJ pump
1968-1972	Tucumcari (PGH-2)	Boeing/Centrifugal pump
1971	Walker (RINA)	Claims WJ more efficient over 50 knots
1971-1980	SES 100	High speed inducer pump WJ
1973-1978	2K/3KSES	Most powerful WJ development
1974-	Boeing/Kawasaki	Jetfoil
1974-	Boeing/ALRC	Inducer/mixed flow
1989	Riva Calzoni	Atlantic Challenger WJ
1990	SES 200	WJ conversion
1991	KaMeWa 180 SII	Largest current WJ built
1992	SEC SES	Largest WJ ship
1992	Yamato	First Magneto-hydrodynamic WJ ship
1992	Destriero	Atlantic speed record 3 KaMeWa WJ
1992	OMC	High volume production WJ leisurecraft
1993	Aquastrada	1000 tonnes, 43 knots car and passenger ferry
1994	Jane's	Lists 88 models, 14 manufacturers, 8 countries

The 1994 edition of Jane's high speed craft has listed 88 different waterjet model from 14 manufacturers in 8 countries. A Hamilton 212 waterjet shown in Figure 2.1 is used to illustrate key features of a waterjet's construction. The 212 will absorb approximately 260 kW of power. Most components are cast in aluminium, using stainless steel, nylon and bronze for the more specialised items.

2.2.2 Intake

The intake casting performs several functions. Its main purpose is to deliver water from beneath the hull to the pump as efficiently as possible. In this case it also serves as the main structural element of the waterjet, providing a rigid mounting for the other housings and control equipment. The main shaft passes through the middle of the intake and out through the thrust bearing and main seal housing. This particular unit uses a ceramic mechanical seal. The intake is usually bolted to the hull, or in the case of larger installations welded in place.

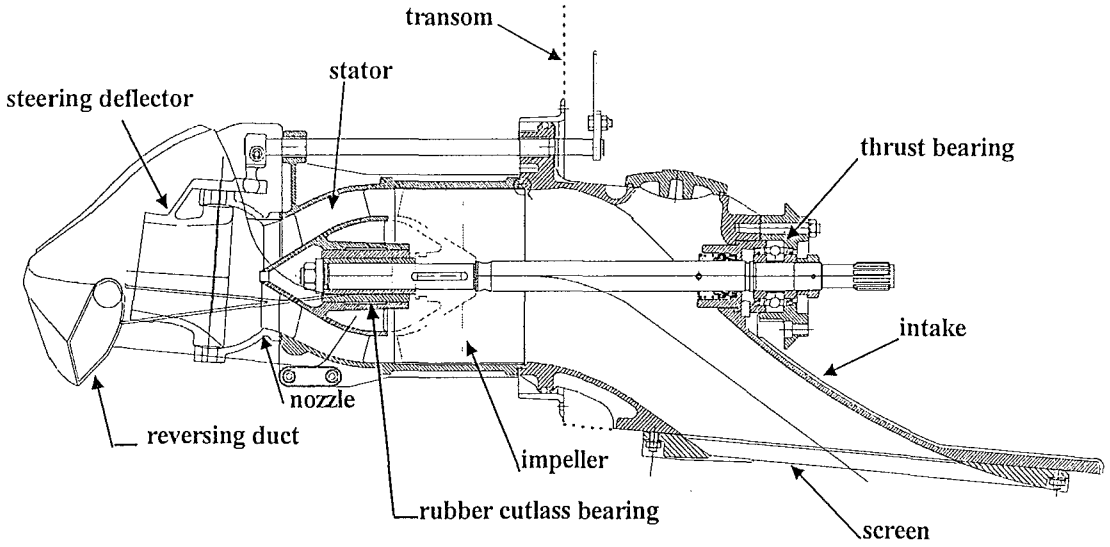

Figure 2.1 Sectioned view of Hamilton 212 waterjet

A screen is bolted to the bottom of the intake to prevent the ingress of debris and weed. In the unlikely event that a rope or some foreign object becomes wrapped around the shaft an inspection hatch on top of the intake allows access for disentanglement.

2.2.3 Pump

The pump is of semi-mixed flow type. Impellers of varying pitch are available to alter the power absorption of the pump for a given rpm. The impeller is a four, five or six bladed one piece stainless steel casting which has a flared hub to provide some mixed flow. It rotates within the impeller race which has an internal sleeve of stainless steel to provide wear resistance. It is of constant diameter for ease of manufacture.

Behind the impeller is fitted the tail pipe which has 8 integral stator blades. The stators are fitted to remove the rotation in the flow caused by the impeller. The stator blades converge to a central hub in which is pressed a water lubricated, rubber cutlass bearing that supports the aft end of the impeller shaft. The tail pipe is also fitted with a cooling water off-take. A small amount of water is drawn off from this high pressure region to cool the engine, usually via a heat exchanger such that the engine cooling circuit is isolated from whatever fluid the vessel is floating in.

A prime advantage of using a semi-mixed flow pump is that for many installations, direct coupling to the engine is possible. This means that heavy and expensive gearboxes can be omitted from the design.

2.2.4 Nozzle

After the stators the tail-pipe draws down in cross-section thereby accelerating the flow. The flow leaves the waterjet at the nozzle. Nozzle inserts of varying diameter are used to control the pump operating point and the jet velocity. At a given boat speed there is an optimum nozzle velocity which yields the greatest propulsive efficiency.

2.2.5 Steering and Reversing Equipment

The high speed jet stream has considerable momentum which may be used to produce substantial steering and reversing forces. A short pivoting tube is mounted at the nozzle to deflect the jet stream approximately 30 degrees to either side. This has the effect of creating a side load on the tube of up to 50% (sine30°) of the nozzle momentum flux while only reducing the available forward momentum flux by 13% (1-cosine30°). The tube is controlled by a rotating rod which runs back through the transom.

Reverse thrust is achieved by directing some or all of the jet stream back in a forward direction. This is accomplished by lowering a ducting arrangement consisting of two elbows. Analysis of the momentum equations shows that reverse thrust as much as 60% higher than forward thrust is possible. The raising and lowering of the reversing duct is again controlled by rotating a rod which runs back through the transom.

Zero net thrust can be achieved by a partial lowering of the duct which deflects only a portion of the jet stream. Equalising the forward and reverse momentum fluxes results in a zero net force on the boat. Steering forces are still available however enabling "zero speed" manoeuvrability such as turning the boat through 360° in its own length. The Hamilton system of having the reversing duct and steering nozzle independently mounted ensures that the steering sense is the same in both "forward" and "reverse".

2.2.6 Other Designs

There are many variations on the general theme described above. Different pump designs include fully mixed flow or purely axial flow. Cavitation resistance in high power applications is achieved by multi-staging of the pump configuration. Some manufacturers supply only the pump and control equipment, relying on the boat builder to supply the intake integral with the hull. Intake designs vary in length, width and cutwater design. Different steering and reversing configurations abound. A common variation is the mounting of the reversing equipment on the steering tube. Some manufactures use a duct or bucket while others rely on systems of gates and levers which can be more compact but often less effective.

The thrust bearing assembly can also be mounted in the stator hub. This has the advantage of removing axial loads in the shaft. It does however lead to complication in the hub with the need to feed lubrication oil inside stator blades and a more sophisticated and expensive bearing and seal arrangement.

2.3 Waterjet Propulsion Theory

2.3.1 Introduction

There are a large number of papers which give good summaries of general waterjet propulsion theory. Allison (1992)[1] gives an excellent review of existing literature presenting both a simplified analysis and a more sophisticated treatment which includes intake, pump and nozzle losses. The effect of elevation of the nozzle is also considered along with interaction effects including the wake factor and the thrust deduction factor.

This section begins with a description of the theoretical waterjet system and its boundaries. There follows some discussion of definitions of thrust and some basic theory is developed. The wake factor, and some thrust deduction theory is also introduced.

---

[1] pp 6-18 Note: Footnotes refer to page numbers in the referenced publication

2.3.2 System Definition

The following system definition is drawn from Allison (1992)[1] and van Terwisga (1993)[2] and is shown in Figure 2.2.

Starting at the upstream end, the waterjet system begins with the front face of the protruding stream tube, A'B. The stream tube is a tube of water, all of which will be drawn into the waterjet. Another boundary could be drawn across the horizontal intake plane, however the flow is hard to measure due to the screen and it is more convenient to extend the system out to plane A'B. The point A' is called the "ramp tangency point". It is the point where the curve of the intake roof or ramp meets the keel which is straight. The ramp should meet tangentially to provide minimal flow distortion. Van Terwisga (1993)[3] has made a case for extending the control volume forward 10% of the intake length to a'b as shown by the dotted line.

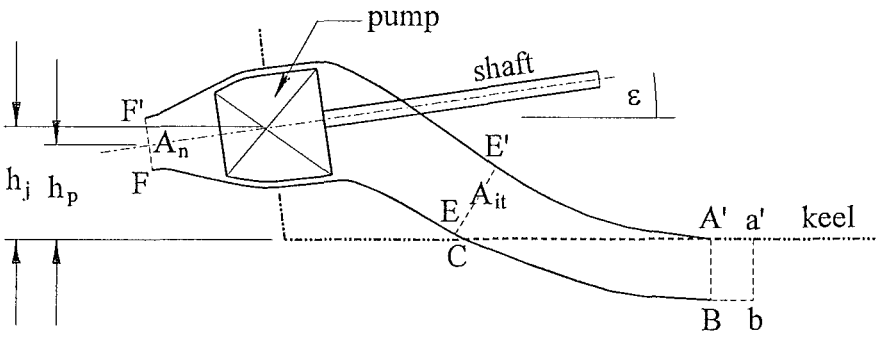

Figure 2.2 Waterjet system definition

The reason stated for this is *"avoid major flow distortions caused by the intake geometry"*. It is true that streamlines are not quite straight and parallel as shown by material presented in chapter 5 however it is unlikely that an increase of 10% would be sufficient in that case. Most previous studies (Etter (1980) and Wilson(1977)) use the ramp tangency point as does this study. In any case pressure variations between the tangency point and 10% ahead were found to be small (≈0-0.5 kPa).

The flow then enters the waterjet itself passing up the intake duct. The intake throat area, A_{it} is defined as being where the cross-sectional intake area is at a minimum. This area is used to define the important intake velocity ratio (IVR). The IVR is an

[1] p9
[2] p976
[3] p977

important dimensionless ratio that defines the flow conditions at the intake. It is defined as,

$$IVR = \frac{V_i}{V_s} \tag{2.1}$$

V_i is the average velocity and is found by dividing the flowrate through the waterjet by the intake throat cross-sectional area A_{it}. V_s is the ship speed through the water. It is also sometimes known as the free stream velocity. When comparing intakes it is important that kinematic similarity of flow is maintained. By making comparisons at the same IVR the general flow patterns in the region of the intake can be considered similar.

The flow then passes through the pump and on out to the nozzle. The nozzle area A_n is defined by the physical nozzle exit plane. In the case where a vena contracta is present, the area at the vena contracta is designated A_j.

2.3.3 Definitions of Thrust

While the concept of thrust would appear at first to be straightforward, closer analysis reveals a more complex situation. The International Towing Tank Conference (ITTC, 1987) has defined thrust as being the difference between the incoming and outgoing momentum fluxes passing through the waterjet system boundaries described in section 2.3.2 such that,

$$\mathbf{T_G} = \phi_{Mn} - \phi_{Mi} \tag{2.2}$$

where,

$\mathbf{T_G}$	=	gross thrust
ϕ_M	=	a momentum flux vector
n	=	subscript meaning at the nozzle
i	=	subscript meaning at the front face of the stream tube

Symbols shown in bold represent a vector whereas regular type represents a scalar quantity.

Allison (1992)[1] has moved away from calling the thrust defined in equation (2.2) "the gross thrust". Instead he has reserved this term for the nozzle momentum thrust, ϕ_{Mn} ($=\dot{m}V_n$). His justification for this in a private letter to the author is this:

"It is essential that the theoretical formulations, which may be mathematically correct, should not conceal important physical realities. In this case, the gross thrust is the force available for deflection for steering and for partial reversal for stopping and going astern."

Allison calls the thrust defined in equation (2.2) the net thrust, T_N. This definition will be used for the remainder of this work. Sometimes the subscript is dropped and the net thrust is symbolised by T. The thrust vector is sometimes decomposed into horizontal and vertical components

Other researchers have considered the concept of thrust. Bowen (1971) develops some control volume theory and rightly finds that the thrust force on the control volume should include the pressure across the intake plane. The British, Engineering Sciences Data Unit (1969) has prepared an information sheet which discusses various thrust definitions for jet aircraft. There are no less than five commonly accepted thrust definitions. Most definitions consider not only the momentum fluxes but also the pressures acting across the exit and entry planes. A more detailed analysis of the waterjet situation is conducted in chapter 5.

The ITTC also recommends Etter's 1980 definitions, however Etter defines the net thrust as:

$$T_{net} = T_{gross} - D_{inletsystem} = \dot{m}(V_n - V_m) - D_{inletsystem} \qquad (2.3)$$

The inlet system drag accounts for pressures acting on the protruding stream tube and losses due to the external lip at the cutwater. As Allison (1992)[2] points out, if the inlet is truly flush then the inlet drag tends to zero.

---

[1] p6
[2] p12

In the following analysis in chapter 5, pressures acting on the stream tube will be considered as a separate force component. For most flush waterjet installations there is little or no external lip.

To reiterate the thrust definition, the momentum flux leaving the nozzle and available for steering and reversing is known as the gross thrust. The difference between the outgoing and incoming momentum flux is known as the net thrust. Both these forces may be decomposed into horizontal and vertical components.

2.3.4 Wake Factor

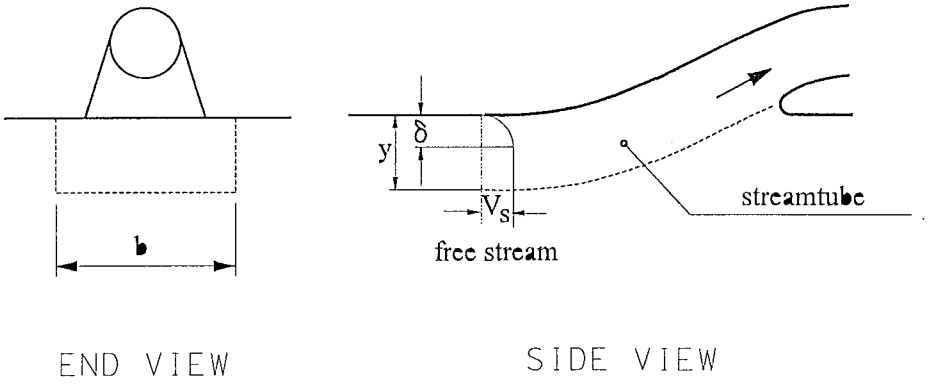

Figure 2.3 Hull boundary layer

The water entering the inlet beneath the boat is in reality travelling slower than V_s, due mainly to the boundary layer under the hull as shown in Figure 2.3. This has the effect of improving the performance slightly, as less power is required to accelerate the water to get the same momentum change and hence thrust.

To achieve this modification in the theory, a new inlet velocity, V_i is defined as the momentum average velocity of water entering the intake to provide the same overall momentum as the flow with its boundary layer in the real case such that,

$$V_i = V_s(1-w) \tag{2.4}$$

where w is defined as the wake factor. Useful approximations for this velocity can be found from standard boundary-layer theory, even though this does not account for such effects as the longitudinal pressure gradient and its effect on boundary layer growth beneath the hull. Basic theory assumes that the stream tube is rectangular in

cross-section with a height y and width b. In practice the stream tube is likely to be elliptical. Calculations based on cruise conditions for the Hamilton test boat and using equations (2.15) and (2.25) show that for an elliptical stream tube 50% wider than the intake the wake factor w is 0.069. If the simple rectangular stream tube the same width as the intake is used then w is equal to 0.051. The jet efficiency is 0.6% higher for the wider, elliptical stream tube. For most purposes then the simple rectangular inlet assumption is adequate if conservative. The theory is developed further below for the rectangular stream tube.

Assuming a power-law velocity profile with local velocity V within the turbulent boundary layer:

$$\text{Boundary layer depth, } \delta = \frac{0.37l}{(\mathrm{Re})^{0.2}} \tag{2.5}$$

$$\text{Velocity profile, } \frac{V}{V_s} = \left(\frac{y}{\delta}\right)^{\frac{1}{n}} \tag{2.6}$$

Using equation (2.6) the flowrate is equal to,

$$\begin{aligned} Q &= b\int_0^{\delta} V dy + (y-\delta)bV_s \\ &= bV_s\int_0^{\delta}\left(\frac{y}{\delta}\right)^{\frac{1}{n}} dy + (y-\delta)bV_s \\ &= \frac{bV_s}{\left[n+1/n\right]}\delta + (y-\delta)bV_s \\ &= bV_s\left(y - \frac{\delta}{n+1}\right) \end{aligned} \tag{2.7}$$

Equation (2.1) can be rearranged to give the depth of ingested flow in terms of the flow rate:

$$y = \frac{Q}{bV_s} + \frac{\delta}{n+1} \tag{2.8}$$

$$\text{Then } \frac{V_i}{V_s} = \frac{\frac{n}{n+2} + \frac{y}{\delta} - 1}{\frac{n}{n+1} + \frac{y}{\delta} - 1} \quad \text{for } \frac{y}{\delta} \geq 1 \tag{2.9}$$

$$\frac{V_i}{V_s} = \frac{n+1}{n+2}\left(\frac{y}{\delta}\right)^{\frac{1}{n}} \quad \text{for } \frac{y}{\delta} < 1 \tag{2.10}$$

n is the power law index, usually between 7 and 9, used in the assumed fluid velocity profile. For derivation of the above, see the ALRC (1981)[1] report. The wake factor, w, is related to V_s and V_j,

$$w = \frac{V_s - V_i}{V_s} \tag{2.11}$$

and would typically be about 0.03 - 0.08. In the usual case, the depth of ingested flow is greater than the boundary layer depth (i.e. $\frac{y}{\delta} > 1$). Assuming this, equations can be derived to give w in terms of μ, the jet velocity ratio where $\mu = V_s/V_j$ (assuming $V_j = V_n$, i.e. vena contractor appears at the nozzle exit plane):

$$\frac{V_i}{V_s} = \frac{\frac{n}{n+2} + \frac{y}{\delta} - 1}{\frac{n}{n+1} + \frac{y}{\delta} - 1} \tag{2.12}$$

$$\text{Now, } y = \frac{Q}{bV_s} + \frac{\delta}{n+1} \quad \text{and } Q = A_n V_n$$

$$\text{so } y = \frac{A_n}{b\mu} + \frac{\delta}{n+1} \tag{2.13}$$

[1] p3

$$\text{and by substitution:} \quad \frac{V_i}{V_s} = \frac{\frac{n}{n+2} + \frac{A_n}{b\delta\mu} - \frac{n}{n+1}}{\frac{n}{n+1} + \frac{A_n}{b\delta\mu} - \frac{n}{n+1}} \tag{2.14}$$

For example, assuming inlet stream width is equal to b and n = 7,

$$\text{wake factor, } w = 1 - \frac{V_i}{V_n} = \frac{7}{72}\frac{b\delta\mu}{A_n} \tag{2.15}$$

Using equation (2.5), w can be found easily for a known intake and jet unit geometry. The net effect of the wake factor is to increase the thrust from that predicted from simple theory with no wake factor, or conversely, to increase the expected unit efficiency for a given thrust.

An example of the effect of the wake factor follows:

To develop 10 kN of thrust at a boat speed of 10 m/s at w=0 and w=0.05 (assume fresh water, density = ρ = 1000 kgm^{-3}, and nozzle area $A_n = 0.05\ m^2$).

Table 2.2 Wake factor example

Parameter	*w=0*	*w=0.05*
V_s	10 m/s	10 m/s
V_i	10 m/s	9.5 m/s
V_n	20 m/s	19.67 m/s
$\dot{m}$	1000 kg/s	983 kg/s
T	10 kN	10 kN
jet power	150 kW	145.7 kW
η_j	66.7%	68.63%

As can be seen in Table 2.2, the wake factor gives a distinct improvement in the jet efficiency (which is defined later, equation (2.25)).

2.3.5 Thrust Deduction Factor

A vessels hull resistance can be calculated or measured by testing a model or towing a full scale bare hull. Appendage, wave and aerodynamic resistances can be calculated and added to the bare hull resistance. This then is the vessels total resistance.

However it has been found that when the vessel is self propelled the total resistance changes. The hull's propulsor influences the flow under the hull and so causes a change in the total resistance. Also, the propulsor may impart thrust forces in a direction different from that assumed during the towing test. Both these factors may cause the hull to move to a new equilibrium planing position. The new planing condition will inevitably have a new total resistance.

A thrust deduction factor (1-t) is now introduced to allow for this and any other changes in total resistance:

$$(1-t) = \frac{R_T}{T} \qquad (2.16)$$

Barnaby (1969)[7] outlines a basis for finding the thrust deduction factor for a propeller driven craft as follows:

"R_T is the resistance when the vessel is towed at speed V_s with propeller removed. Therefore R_T takes into account all appendage (shafting and rudders etc), air and wave resistance. T is the thrust when self propelled. However the two forces are not equal and T-R_T represents the additional resistance caused by the action of the propulsion system. The term (1-t) is known as the thrust deduction factor while t is the thrust deduction fraction. The fraction can be positive or negative.

In the case of testing a jet propelled boat the propeller should be replaced with the whole jet unit. R_T will be measured with the intake blocked off as for the bare hull case but should include any other appendages and the effects of self-weight of the jet unit and entrained water. The thrust deduction factor will then include any reduction in resistance due to the reduced wetted area. T will be the thrust transmitted from the jet unit to the hull in the direction of V_s."

Waterjet propelled craft are unusual in that t can be negative which causes the factor to be greater than one. This means that at the given boat velocity a jet propelled vessel will require less thrust than many other propulsion systems where thrust deduction factors are less than one. Waterjet thrust deduction factors as high as 1.07 have been reported (Bjarne(1990)), resulting in a 7% decrease in required thrust at the given speed.

2.3.6 Propulsive Efficiency

The overall propulsive efficiency of the propulsion system is of prime importance as it is a measure of the power supplied to the propulsor compared to the delivered power. It is of course finally the delivered power which the waterjet operator must pay for by way of fuel costs. A common definition of efficiency is called the overall propulsive coefficient, OPC, which is defined as effective power divided by the engine power,

$$OPC = \frac{R_T V_s}{P_B} \tag{2.17}$$

where,

R_T = towed resistance
V_s = ship speed
P_B = brake power developed by engine

The advantage of using the OPC is that it can be used to compare engine power from a variety of propulsion installations against a constant baseline, the effective towed power. It therefore includes interaction effects.

The analysis conducted by Allison(1992)[1] is repeated here in abbreviated form. The simplifying assumptions made initially are:

- The vena contracta occurs at the nozzle exit plane ($V_j = V_n$)
- The velocity of the approaching fluid across inlet plane A'-B is $V_i = (1-w)V_s$ where w is the wake factor
- Pump losses include stator losses
- The jet exits horizontally
- There is no external inlet drag
- The static pressure at the inlet is equal to the submergence of the intake
- Pressure changes on the hull due to the presence of the inlet are assumed to be included in the thrust deduction factor t

The inlet losses can be expressed as a fraction of the available inlet energy so that the energy recovered is given by:

$$E_r = (1-\zeta)\frac{1}{2}\dot{m}V_i^2 \tag{2.18}$$

[1] p9

where ζ is a loss factor, V_i is the momentum average inlet velocity and $\dot{m}$ is the mass flow rate. The inlet efficiency may be defined as:

$$\eta_i = (1-\zeta) \tag{2.19}$$

The energy lost by the nozzle while converting the available energy to useful axial velocity can also be expressed as a fraction of that supplied to the nozzle. Energy supplied to the nozzle is given by:

$$E_n = (1+\psi)\frac{1}{2}\dot{m}V_n^2 \tag{2.20}$$

where ψ is a loss factor, and V_n in the velocity at the nozzle exit plane. In addition to the above losses, the pump must raise the water to the height of the jet centreline above the free surface, h_j. The additional work is given by:

$$W_e = \dot{m}gh_j \tag{2.21}$$

Combining equations (2.18), (2.20) and (2.21), and substituting V_i for V_s by using the wake factor the useful energy supplied by the pump is then:

$$E'' = \frac{\dot{m}}{2}\left[V_n^2(1+\psi) - \eta_i(1-w)^2V_s^2 + 2gh_j\right] \tag{2.22}$$

The jet efficiency is defined as the work done on the ship over the power supplied by the pump:

$$\eta_j = \frac{TV_s}{E''} \tag{2.23}$$

$$= \frac{\dot{m}(V_n - (1-w)V_s)V_s}{\frac{\dot{m}}{2}\left[V_n^2(1+\psi) - \eta_i(1-w)^2V_s^2 + 2gh_j\right]} \tag{2.24}$$

Dividing top and bottom by V_n^2 and $\frac{\dot{m}}{2}$, and letting the jet velocity ratio, $\mu = \frac{V_s}{V_n}$:

$$\eta_j = \frac{2\mu(1-(1-w)\mu)}{1+\psi-\eta_i(1-w)^2\mu^2+\frac{2gh_j}{V_n^2}} \tag{2.25}$$

The energy supplied to the pump will be greater than that supplied by the pump due to losses in the pump. The pump efficiency, η_p is often known from a uniform flow performance test such that the shaft power, shp = E"/η_p. A further efficiency is used to account for losses due to the non-uniformity of the flow reaching the pump in the real case. This is called the relative rotative efficiency, η_r and is drawn from propeller theory. The transmission efficiency, η_t, accounts for mechanical losses between the pump input shaft and the engine such that, $\eta_t = P_D/P_B$ where P_D is the power delivered to the pump input shaft. Then,

$$E'' = \eta_p\eta_r\eta_t P_B \tag{2.26}$$

The actual thrust required will differ from the total towed resistance due to interaction effects between the hull and the propulsor. This is accounted for by the thrust deduction factor, (1-t) such that,

$$T = \frac{R_T}{(1-t)} \tag{2.27}$$

Using equation (2.23), (2.26) and (2.27),

$$R_T = \frac{(1-t)\eta_j\eta_p\eta_r\eta_t P_B}{V_s} \tag{2.28}$$

From equation (2.17) and using equation (2.28),

$$OPC = (1-t)\eta_j\eta_p\eta_r\eta_t \tag{2.29}$$

2.4 Conclusions

This chapter has considered various aspects of waterjet propulsion. The various points covered are summarised below.

- A large number of companies worldwide manufacture and market waterjet propulsion systems for installation high performance vessels.
- There is a reasonable understanding of waterjet propulsion. Existing theory handles basic questions of waterjet system efficiency and performance satisfactorily. Most theory breaks the machine down into discrete parts and attaches an efficiency to each part.
- Thrust definitions have been set down and common agreement exists.
- Some aspects of the incoming flow field can be predicted by the theory. The effect of the hull's boundary layer on the waterjet is well understood. Pressure effects at the intake are not generally included.
- Interaction between the waterjet and the hull is known to occur however is accounted for with an empirical factor.

3. Aspects of Planing Hull Theory

3.1 Introduction

This chapter briefly reviews the various planing hull performance prediction methods available. Special attention is paid to the Savitsky method which forms the basis for the computational model developed later in this work. The Savitsky method is widely used in industry generally but is also the method of choice at CWF Hamilton and Co. Ltd.

3.2 Types of Prediction Methods

Almeter (1991) presents an excellent review of resistance prediction methods. Much of the material in this section is drawn from Almeter's paper. The following three sections briefly mention the types of prediction method available. The final section covering prismatic type prediction methods examines the varying techniques of this type in a little more detail.

3.2.1 Planing Hull Series

Resistance can be predicted by using data gathered from a series of model tests. A nominally representative initial geometry (the parent) and loading condition is chosen and tested. Models of similar geometry are then tested, extending the database both in terms of geometry and loading condition. Series data give good results if the hull in question is of similar geometry and within the loading range of the original data. Table 3.1 summarises the well known hull series.

Table 3.1 Summary of well known planing hull series

Series	*Features*
Series 50	Semi-planing, dated, does not reflect modern planing hull designs
Series 62	Pure-planing, low constant deadrise, tapered transom
Series 65A and B	Larger pre-planing, deep vee, 65A very high beam taper and not normally used
Naval Academy Series	Pre-planing, round bilge and hard chine, small data set
Dutch Series 62	Pre and semi-planing, high deadrise
BK Series	Semi-planing, very large
MBK Series	Semi-planing smaller hulls
Norwegian Series	Semi and pure planing post hump speed range

3.2.2 Regression and Empirical Methods

Using multilinear regression techniques, equations can be developed to interpolate between data from a discrete number of model tests. There is great potential for misuse and designers must be careful not to use input data which goes beyond the range of applicability of the regression model being used. Some of the currently used methods are summarised in Table 3.2.

Table 3.2 Summary of regression and empirical methods

Method	*Features*
US Naval Academy Series Regression	Uses hard chine data, applicability very limited
Series 62/65 Regression (Hubble)	Covers wide speed range, used for rough approximation
Series 62/65 Regression (Radojvic)	Variable accuracy
Japanese Regression	Large database, semi-planing, difficult to use
Empirical "rule of thumb" Methods	Can be good but best for rough approximation

3.2.3 Prismatic Equations

There are several techniques which assume a prismatic hull shape and use a variety of equations to determine the planing characteristics. The prismatic assumption is quite appropriate for many modern hulls which have constant deadrise and straight buttock lines. Once up to planing speeds the curved bow sections are not in contact with the water. These methods are really a conglomeration of empirical regression equations and classical fluid dynamic theory bought together into one technique. Almeter (1991)[1] has the following to say about prismatic methods:

"One of the advantages of using prismatic shapes is that drag is simply considered to be the product of the tangent of the trim angle and the craft's weight plus frictional drag. Prismatic models have been tested in a variety of ways for lift and torque or longitudinal moment. From these tests researchers have developed equations that relate the lift and longitudinal moment to wetted planing shape, trim and speed. The equations are often based on a flat plate whose planing characteristics have been modified in various ways to account for deadrise."

Three commonly used prismatic prediction methods are summarised below.

[1] p11

3.2.3.1 Savitsky Method

The Savitsky method is probably the most commonly used (Almeter (1990)[1]) method for the prediction of resistance of planing hulls. Blount and Fox (1976)[2] also refer to it as *"the predominant prediction method used within the small-craft technical community"*. The first and still generally referred to presentation of the method can be found in Savitsky (1964). The core equations in this work relate trim, lift and centre of pressure to the mean wetted length to beam ratio. By a process of iteration the trim is adjusted until a free body in which all hull forces are applied is bought to a condition of static equilibrium. The Savitsky method and versions of it are covered in greater detail in section 3.3.

3.2.3.2 Shuford Method

The Shuford method is better suited to the pure planing regime where buoyancy forces are negligible. It predicts well for deep vee hulls travelling at very high speeds. Clement (1959) modified the method to include spray drag. Brown (1980) also made some modifications which extended the method for use at lower speeds.

3.2.3.3 Lyubomirov Method

The Lyubomirov method is similar to the Savitsky method but has however several key differences. The wetted surface, lift and trim are calculated as if a flat plate were used. The trim and wetted surface are then corrected to allow for deadrise. The Lyubomirov method also has wetted surface increasing with deadrise.

3.2.3.4 Comparison of Methods

Almeter (1990) compared all three methods to the same sets of test data. Using data taken from a test of a 20° deadrise hull, the non-dimensional wetted length, λ, was compared. All three methods were in close agreement with the test data.

Comparisons of trim results however were found to vary with different sets of data. Almeter (1990)[3] states, *"The Savitsky method will tend to give the highest prediction because of its higher running trim..."* Analysis of the graphs shown in Almeter's

---

[1] p12
[2] p14
[3] p16

figure 16 reveal trim predictions by Savitsky that are between 0.8 and 1.2 degrees higher than the model test data. In this project small experimentally determined correction factors are used to correct the Savitsky prediction.

3.3 Savitsky Method

Savitsky's 1964 paper brought together a variety of previous studies and data into one method that could be applied to a large range of prismatic planing hull configurations. The method requires a relatively small amount of input data due to the assumption that the hull geometry is prismatic. Only the hull beam, deadrise, static displacement, position of the shaft centreline and position of the centre of gravity are required. These are summarised in Table 3.3. Savitsky presents two methods, the long form and the short form.

Table 3.3 Savitsky method input parameters

Symbol	Parameter
b	chine beam (m)
β	hull deadrise (deg)
Δ_0	vessel's static displacement (kg)
ε	angle between the propeller shaft and the keel (deg)
f	distance between the centre of gravity (GC) and the shaft line (m)
LCG	distance (parallel to the keel) from the CG to the intersection of the transom and the keel (m)

3.3.1 Savitsky Long Form

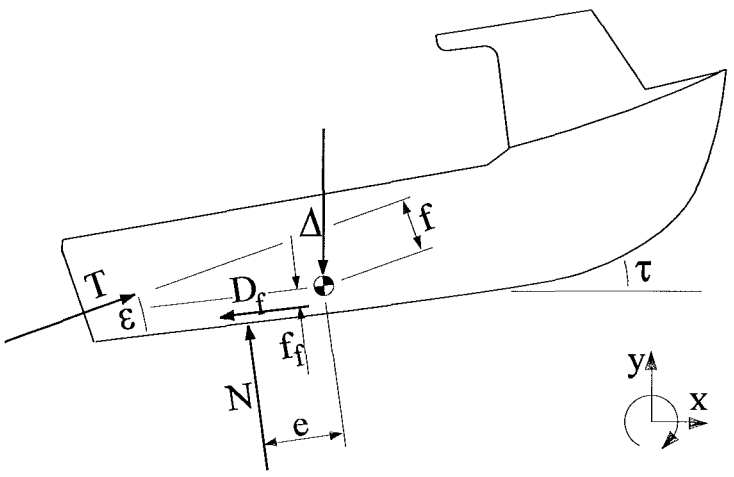

Figure 3.1 Free body diagram for Savitsky method

In this section, the key physical factors contributing to the planing performance analysis are reviewed. This section is essentially a condensed review of Savitsky's 1964 paper. Figure 3.1 shows the free body diagram used by Savitsky. The nomenclature is however a little different in places. Hadler's (1966) nomenclature has been adopted in some cases.

The Savitsky method involves conducting a computational iteration until all forces in the free body diagram are balanced. This is achieved at a given speed by assuming a trim angle and then calculating the parameters shown in Table 3.4.

Table 3.4 Savitsky calculation parameters

Key Parameters		***Subsidiary Parameters***	
mean wetted length to beam ratio	λ	flat plate lift coefficient	C_{L0}
deadrise surface lift coefficient	$C_{L\beta}$	Reynolds number	Re
mean bottom velocity	V_m	Schoenherr friction coefficient	C_f
total drag force	D		
viscous drag force	D_f		
position of centre of pressure	e		

Equations of static equilibrium are then solved simultaneously to find the thrust or resistance and the net moment on the hull in terms of these parameters. The trim is then varied and the parameters recalculated until the net moment on the hull is zero and the hull can then be considered to be in static equilibrium.

3.3.1.1 Normal hull pressure force

The normal hull pressure force N, is the resultant of integrating all dynamic and buoyancy forces acting on the hull. The sum of vertical components of all forces acting on the hull must balance the weight of the vessel (assuming that it is not accelerating vertically). The normal hull pressure force N will provide most of the lift however other forces may provide some lift, (i.e. aerodynamic loads, forces from appendages) but also some added displacement (downwards component of viscous drag force). The longitudinal position of N in relation to the centre of gravity, e, is found using Savitsky's empirical equation for the position of the centre of pressure,

$$e = LCG - \frac{L_{cp}}{L_m}\lambda b \qquad (3.1)$$

where LCG is the position of the longitudinal centre of gravity measured from the intersection of the transom and the hull bottom. The mean wetted length to beam ratio λ, is defined as L_m/b where b is the beam and is found iteratively from Savitsky's empirical equation for the flat plate lift coefficient, equation (3.3) and L_m is the mean wetted length measured from the transom.

The ratio $\frac{L_{cp}}{L_m}$ is found using equation (3.2):

$$\frac{L_{cp}}{L_m} = 0.75 - \frac{1}{\frac{5.21C_v^2}{\lambda^2} + 2.39} \qquad (3.2)$$

where C_v is a Froude number speed coefficient based on the beam and τ in the angle of trim of the hull measured between the keel and the horizontal. L_{cp} is the distance from the centre of pressure to the transom.

The hydrodynamic lift can be attributed to two separate effects.

- dynamic reaction of the fluid against the moving surface
- buoyancy contribution

At very low velocity coefficients, the buoyancy contribution predominates while at high speeds the dynamic contribution to lift is high and the static pressure effects are small. Over the speed range normally considered however, both components must be considered.

The formulation of an empirical lift equation for a zero deadrise angle was based on classical aerodynamic theory and involved the combination of the static and dynamic components. Sottorf's (1932) analysis of high speed planing, where the hydrostatic term is negligible, along with empirical evaluation of a large collection of data resulted in enabled the formulation of an expression for the lift coefficient for a planing surface with zero deadrise, C_{L0}:

$$C_{L0} = \tau^{1.1}(0.0120\lambda^{1/2} + \frac{0.0055\lambda^{5/2}}{C_v^{\,2}}) \qquad (3.3)$$

where λ = mean wetted length to beam ratio

C_v = a Froude number coefficient of velocity = $\frac{V_b}{\sqrt{g\,b}}$

(3.4)

Expression (3.3) above is applicable for

$$0.60 < C_v < 13.00$$
$$2^o < \tau < 15^o$$
$$\lambda < 4$$

Increasing the deadrise of a surface decreases the planing lift. An empirical expression was formulated by Savitsky for $C_{L\beta}$, the lift coefficient for a planing surface with deadrise angle β, by mapping experimental values to those already derived for a surface with zero deadrise and having the same dimensions such that,

$$C_{L\beta} = C_{L0} - 0.0065\beta C_{L0}{}^{0.60}$$

(3.5)

where $C_{L\beta}$ is the deadrise lift coefficient and β is the deadrise angle. The deadrise surface lift coefficient is calculated in the same manner as classical aerodynamic coefficients, i.e. based on a planform area (usually the beam squared), the fluid density, the free stream velocity squared and the static displacement weight:

$$C_{L\beta} = \frac{\Delta_0}{\frac{1}{2}\rho V_s^2 b^2}$$

(3.6)

It should be noted that the displacement weight used in the calculation of the deadrise coefficient remains constant. In fact the weight supported by the fluid forces will change as other forces such as aerodynamic lift and forces from the propulsion system act to change the dynamic displacement. Due to the extra computational complication and the lack of computing power in the 1960s it can be assumed that Savitsky had good reason to consider these changes to be of negligible significance.

3.3.1.2 Hydrodynamic Drag

The hydrodynamic drag on the hull can be divided into two categories, pressure drag and viscous drag. Pressure drag is the horizontal component of the normal hull pressure force which acts in the rearward direction. The total hydrodynamic drag is then given by equation (3.7).

$$D = \Delta \tan\tau + \frac{D_f}{\cos\tau} \tag{3.7}$$

The viscous drag force, D_f, is found using Savitsky's empirical equation based on classical drag theory. It is assumed that there is no side wetting. Hadler (1966) uses a small addition in the friction area wetted length to beam ratio to account for the spray drag. However Savitsky justified dropping this for trim angles at and below 4 degrees as he and Ross (1952) found it to be negligible. The addition is included here however for completeness. The viscous drag force, D_f is described as,

$$D_f = \frac{\rho}{2}\frac{b^2 V_s^{\,2}}{\cos\beta}(C_f + \Delta C_f)\left[\left(\frac{V_m}{V_s}\right)^2 \lambda + \Delta\lambda\right] \tag{3.8}$$

where,

V_m = the average velocity near the hull surface,
C_f = Schoenherr friction drag coefficient
ΔC_f = friction coefficient allowance for surface roughness
$\Delta\lambda$ = effective increase in friction area length-beam ratio due to spray contribution to drag
other parameters as before

A relationship for the average bottom velocity, equation (3.9), has been developed by Savitsky and Ross in terms of trim, wetted length and deadrise.

$$\frac{V_m}{V_s} = \left[1 - \frac{0.012^{1/2}\tau^{1.1} - 0.0065\,\beta\,(0.012\,\lambda^{1/2}\tau^{1.1})^{0.60}}{\lambda\cos\tau}\right]^{1/2} \tag{3.9}$$

The Schoenherr friction coefficient, C_f, is determined iteratively such that equation (3.10) is satisfied.

$$\frac{0.242}{C_f^{1/2}} = \log_{10} \mathrm{Re}\, C_f \qquad (3.10)$$

The Reynolds number Re is defined by equation (3.11), where υ is the kinematic viscosity.

$$\mathrm{Re} = \frac{b\lambda V_m}{\upsilon} \qquad (3.11)$$

The viscous drag force is assumed to act at a point midway between the keel and the chine.

3.3.1.3 Equations of static equilibrium

The remaining variables are then found in terms of those already calculated by simultaneously solving equations of static equilibrium. A moment equation can then be written in terms of the known variables. The development of the equations concerned follows.

Consider the hull free body diagram shown in Figure 3.1.

For vertical equilibrium of forces (sign convention: positive up):

$$0 = N\cos\tau + T\sin(\tau + \varepsilon) - D_f \sin\tau - \Delta_0 \qquad (3.12)$$

For horizontal equilibrium of forces (sign convention: positive forward):

$$0 = T\cos(\tau + \varepsilon) - D_f \cos\tau - N\sin\tau \qquad (3.13)$$

For equilibrium of pitching moments (sign convention: positive bow down):

$$0 = Ne + D_f f_f - Tf \qquad (3.14)$$

By a process of substitution and assuming that the cosine of ε is approximately equal to 1, T and N can be expressed in terms of the known variables as follows.

$$T = D_f + \Delta_0 \sin\tau \qquad (3.15)$$

$$N = \frac{\Delta_0(1-\sin(\tau+\varepsilon)\sin\tau) + D_f(\sin\tau - \sin(\tau+\varepsilon))}{\cos\tau} \tag{3.16}$$

Equations (3.16) and (3.15) can now be substituted into equation (3.14) to produce the moment equation:

$$0 = \left[\frac{1-\sin(\tau+\varepsilon)\sin\tau}{\cos\tau}e - f\sin\tau\right]\Delta + (f_f - f - e\sin\varepsilon)D_f \tag{3.17}$$

Equation (3.17) differs from Savitsky's equation 35 due to an error which crept into the analysis in his equation 33. The term esinε is omitted from the final bracket. However using typical values for the Hamilton test boat, the term appears to make no noticeable difference to the output. Hadler (1966)[1] also reports this omission. It may have been left out deliberately by Savitsky.

Once the process of iterating trim to satisfy equation (3.17) is complete, the horizontal resistance or thrust may be calculated using equation (3.15).

3.3.2 Blount and Fox Modification Factor

It was found that in reality true prismatic hull forms were scarce, and that most hulls had curved bow sections in contact with the water and reducing beam towards the stern. As a result the Savitsky method was found to be under-predicting resistance especially in the hump region. Consequently Blount and Fox (1976) made an effort to improve the Savitsky prediction method by developing a multiplying factor that could be applied to the resistance. This factor, know as the Blount and Fox modification factor M, was found by analysing predictions and existing model test data for sensitivity to hull form and loading parameters. The resulting expression[2] was:

$$M = 0.98 + 2\left(\frac{LCG}{B_{PX}}\right)^{1.45} e^{-2(F_\nabla - 0.85)} - 3\left(\frac{LCG}{B_{PX}}\right) e^{-(3F_\nabla - 0.85)} \tag{3.18}$$

where F_∇ is the volumetric Froude number,

[1] p582
[2] p16

$$F_{\nabla} = \frac{V_s}{\sqrt{g\nabla^{\frac{1}{3}}}} \qquad (3.19)$$

B_{PX} is the maximum projected chine beam and ∇ is the displaced volume found by dividing the displacement by the fluid density. Equation (3.18) is valid for,

$$F_{\nabla} \geq 1.0$$

$$\text{and } \frac{LCG}{L_{cp}} \leq 0.46$$

3.3.3 Savitsky Short Form

Savitsky mentions various assumptions which can be used to simplify the analysis. The simplest approach is to assume that all forces pass through the centre of gravity. It is then simply a question of finding the trim which will provide the correct lift to support the hull. This method requires much less computing power as the results can be calculated directly without the need to perform substantial iteration. The short form method is known to give reasonable results as on many hulls, forces are applied close to the centre of gravity.

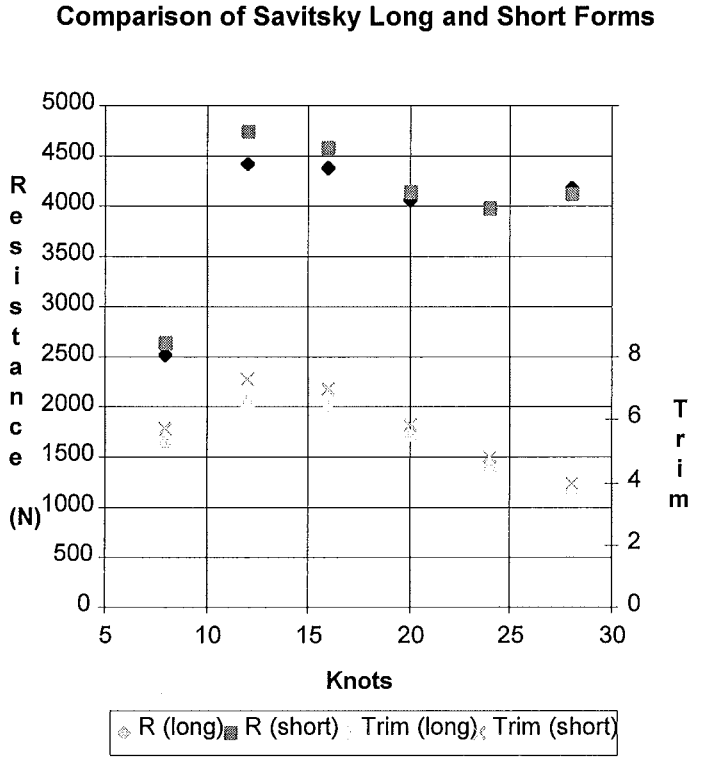

Figure 3.2 Savitsky long form compared to short form

Figure 3.2 shows a graph comparing the long form method to the short form method. The data has been calculated neglecting air, wave and appendage drag. It can be seen from the graph that the methods are reasonably close especially at higher speeds when the hull is stiffer longitudinally and less susceptible to pitching moments. However around the hump the short form has over-predicted the resistance by 7%.

3.4 Conclusions

- Various types of planing hull performance prediction methods are available: planing hull series, regression and empirical methods and prismatic equation methods.
- Computational methods based on a prismatic hull geometry give the greatest flexibility and have been found to be reliable.
- The Savitsky long form method has been chosen as a key tool for this project due to its wide acceptance, reliability and ease of use. The key equations and assumptions used in method have been outlined.

4. Review Of Hull-Waterjet Interaction

4.1 Introduction

The study of hull-propulsor interaction has its beginnings with the advent of the screw propeller. Hull-waterjet interaction has borrowed much of the general concepts and terminology, in particular the thrust deduction and wake factors. The thrust deduction factor is an empirically based coefficient that is used to correct the thrust for interaction effects that may occur between the hull and waterjet propulsion system. The wake factor allows for the decrease in ingested momentum due to the hulls boundary layer.

Very little work on hull-waterjet interaction has been published in the public domain. This is so because much of the research has been carried out by manufacturers who are keen to hold commercially sensitive knowledge.

Knowledge of the hull-waterjet interaction falls into several categories. The most common treatment is a passing mention of thrust deduction in papers devoted to matters of waterjet propulsion. Occasionally some estimates of its magnitude can be found but these are rare and tend to be constant in nature rather than a statement of a trend or characteristic. Typical papers of this nature are Allison (1992), Stricker et al (1993), Bjarne (1990).

Mr T. van Terwisga of the Marine Research Institute of the Netherlands appears to be the most prolific researcher to date. He has published several papers (1991, 1993) and made a contribution to the 20th ITTC Workshop on Waterjets.

This author has contributed several conference papers (Coop et al (1992) and Coop and Bowen (1993)) outlining the proposed experimental approach and reporting some early findings of this project.

To the knowledge of the author, two manufacturers have also contributed work. Svensson (1991) for the Swedish company KaMeWa and Keith Alexander (1994) for CWF Hamilton and Co. Ltd. have both discussed interaction in general terms.

Estimates of interaction effects vary considerably from application to application as hull shape and loading and waterjet geometry are all significant factors.

Consequently it has been difficult to form any general theory. In some cases interaction is said to lead to a reduction in hull resistance, in others an increase. Recent propulsion testing by van Terwisga of MARIN (1991) in The Netherlands has indicated thrust changes due to interaction ranging from 20% to -6% for a particular vessel. Bjarne, (1990), has also published tabulated data of thrust deductions for a variety of propulsion systems. The flush inlet waterjet was the only system which exhibited a negative thrust deduction factor. Bjarne quotes thrust deduction fractions from -7% to +8% (t = -0.07 to 0.08) for waterjets. A significant negative thrust deduction is of great interest to waterjet manufacturers keen to emphasise such benefits and attribute them to the use of their product.

4.2 Early Work

Early work on hull-propulsor interaction is restricted to propeller propelled vessels. It is only in recent decades that waterjet propulsion has gained sufficiently wide use to warrant the growth of general understanding.

4.2.1 Thrust deduction

The earliest known work on hull-propulsor interaction is that conducted by R.E. Froude in England in the later part of the nineteenth century. Mr Froude published two papers, one in 1883 and then in 1886, (Froude 1886) which first considered the problem of interaction between the propulsor and the hull.

Froude initiated the terminology used when describing the difference between the resistance of a hull without a propulsor and the thrust required to propel the same hull when the propulsor is fitted. He called this difference *thrust deduction.* The terminology has remained to this day. Robb (1952) discusses the definition in his book on naval architecture:

Froude adopted this description rather, than augment of resistance, because the extent of the difference is dependent on the amount of thrust; the quantity indicates the amount by which the thrust is "discounted" in order that the remainder shall exactly balance the net resistance.

The difference between bare-hull resistance and self-propelled thrust is currently accounted for by a factor known as the *thrust deduction fraction*, t. This is defined in equation (4.1) where T is the net thrust[1] applied by the propulsor to the hull and R_{BH} is the bare-hull resistance when towed in a defined manner

$$t = \frac{T - R_{BH}}{T} \tag{4.1}$$

Alternatively this may be written as:

$$\frac{R}{T} = (1 - t) \tag{4.2}$$

where the bracketed term is known as the *thrust deduction factor.*

Froude considered that the extra thrust was required because of pressure effects caused by the propeller on the hull. This mechanism is described by Luke (1910) in what Robb describes as the "*first extensive series of systematic experiments on propulsion.*" Mr Luke writes:

"It must be remembered that the influence of the screw pervades a column of water of substantial dimensions in the fore-and-aft directions, and this influence extends far enough forward to cause a marked diminution of pressure on the after part of the ship, thereby causing a virtual increase in resistance. The thrust exerted by the screw when propelling the ship is therefore greater than the tow-rope resistance at that speed by an amount sufficient to balance this diminution of pressure."

4.2.2 Wake factor

Froude also considered interaction effects impinging on the propulsor as caused by the hull. Friction between the hull and the water causes energy to be transferred into the water from the hull. If one considers the propulsor to be stationary and the surrounding fluid to be moving, then a layer of water near the hull surface is slowed by friction on the hull. If the propulsor is acting in this region of slowed fluid then

[1] defined in section 2.3.3

the momentum change and therefore thrust produced will increase. The wake factor has been covered in greater detail in section 2.3.4.

4.3 Contemporary Knowledge and Experience

4.3.1 Analysis by Sub-system

As with many scientific investigations, particularly in the physical sciences, many attempts at solving the problem of interaction begin by breaking the problem into smaller parts. The hull and waterjet system are separated and attention focused on each system in turn. This approach is excellent for a careful analysis of the system in question especially in free stream conditions, that is, unaffected by other systems. For example the standard approach for predicting powering requirements of planing hulls has been as follows:

1. Find the bare hull resistance of the hull system without the waterjet system over a range of speeds.
2. Calculate the thrust that could be developed from the waterjet system given a constant level of input power, for a range of speeds. The wake factor is usually included here.
3. Choose a thrust deduction factor and apply it to the thrust characteristic calculated in 2 above.
4. Find the predicted speed, thrust and required power at that speed from the intersection of the resistance characteristic and the speed characteristic.

The difficulty with this approach is that it relies on accurate knowledge of the thrust deduction factor over all possible hull and waterjet configurations. This knowledge does not exist.

4.3.1.1 Waterjet system

Bowen (1971) uses a control volume to help analyse the waterjet system. Control volumes are also used by Etter(1980), Allison(1992) and Van Terwisga (1993). Bowen's control volume extends right to the front of the vessel and into the

undisturbed flow ahead. The other authors use a control volume similar to that shown here. Further discussion can be found in section 2.3.2.

4.3.1.2 Hull system

The hull system is, by definition the rest of the hardware exposed to fluid that is not included in the waterjet system. It includes all the hull surfaces in contact with the water and air. The hull system boundary meets the waterjet system boundary at the upper edges of the protruding stream tube.

4.3.2 Basic Descriptions

Bjarne (1990)[1] makes only a passing reference to propeller-hull interaction but is however one of the few authors to include some estimates of t. Some of the data is reproduced here in Table 4.1.

Table 4.1 Some propulsive parameters (Bjarne(1990))

Propulsion concept	***Speed Range***					
	Displacement		Semi-planing		Planing	
	w	t	w	t	w	t
Propeller on inclined shaft at 6 deg.	0.01 to -0.02	0.01	0 to 0.04	0.01 to 0.02	0 to -0.10	0.03
Propeller on inclined shaft at 12 deg.	0.02 to -0.02	0.05	0.04 to -0.05	0.05 to 0.07	0.03 to -0.05	0.07 to 0.11
Flush inlet waterjet	0 to 0.02	0.05 to 0.08	0.02 to 0.04	0.05	0.05	-0.02 to -0.07

A notable point in this set of data is the *negative* thrust deduction fraction which is reported to range from -0.02 to -0.07. Several manufacturers have taken advantage of reports of negative thrust deduction and used this fact as a marketing tool. In such a case it is possible to say *"...that by fitting our waterjet you will require less thrust than that required by your resistance predictions"*. Clearly this is a very powerful marketing point.

Haglund et al (1982) considers the overall propulsive performance in a manner analogous to propeller theory such that the hull efficiency, η_h appears in the expression for the overall propulsive efficiency. This comes about by removing the

[1] Table 1, p13

wake factor term from the jet efficiency such that the jet efficiency is then based on free stream conditions. The hull efficiency is defined as:

$$\eta_h = \frac{1-t}{1-w} \tag{4.3}$$

The propulsive efficiency is then:

$$\eta_D = \frac{P_E}{P_D} = \eta_H \eta_{jet} \eta_{pump} \eta_r \tag{4.4}$$

Equation (4.4) is the same as equation (2.29) with the exception of the transmission efficiency.

Haglund reports that the *"...measure of the effectiveness of the interaction between the propulsor and the ship's hull depends primarily upon the location and shape of the inlet and outlet openings. A low thrust deduction and a high inlet wake factor are beneficial for the hull efficiency...in the top speed range t was close to zero but at reduced power, values around 0.06 were found".*

Svensson (1989)[1] from KaMeWa introduces the thrust deduction fraction in the same way also quoting equation (4.1). He quotes a number of sources for this interaction:

- *The thrust combined with the natural dynamic trim creates an additional aft trim increasing the hull resistance , especially at low speed.*
- *The pressure distribution on the bottom plating of the vessel is strongly influenced by the action of the inlets. The resulting force on the surrounding bottom plating and on the inlet channel itself is shown in* Figure 4.1[2]. *When the water flow through the inlet is large in relation to the ship speed there is a downward force from the inlet. However, this force is more than balanced by a lifting force on the surrounding bottom plating. When the flow rate is low compared to the vessel speed the inlet creates a substantial lifting force. In this*

[1] p22
[2] p28

condition the bottom plating contributes less to the lifting force. Thus, the design of the inlet is extremely important to get an optimum performance. The total lifting force generated by the inlets can be in excess of 5% of the displacement for a high speed craft. The lifting force can thus exceed the weight of the units. This will be recognised as a negative thrust deduction reducing vessel resistance.

- *The altered pressure distribution on the aft hull and possibly the jet, might change the wave resistance.*

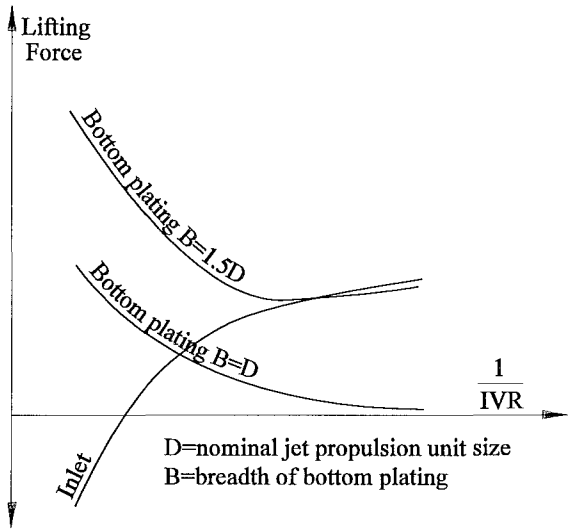

Figure 4.1 Inlet and bottom plating lifting forces (Svensson)

Svensson has correctly noted the effect of the thrust line on trim and therefore the hull resistance. However it is not possible to say whether the new thrust line will increase or decrease resistance as this depends on the hull loading and the bare hull towing position all of which may vary from case to case.

Interesting comments are made regarding integrated intake and bottom plating pressures. It is assumed that the intake pressure is recorded along the roof of the intake. The intake lift forces are low at lower ship speed but increase as would be expected for higher ship speeds and the increased ram effect on pressure. Lift on the plating surrounding the intake can be seen to decrease with speed. The inference that by combining the integrated lift forces a substantial net lift can be measured is

not supported with data. It is not clear if the lift force acting on the bottom plating is occurring in excess of that found with the intake blocked off or if it is the total force which may be little different from the bare hull situation.

The final point that the pressure field set up by the intake may change the wave making resistance is quite correct.

As is commonly found with papers emerging from the technical departments of manufacturers, hard data is frequently omitted. In this case the axes are left unscaled. A control volume analysis is conducted in section 5.4.2.1 which shows that for an intake located in the centre of a large plate, the net lift effects on the system would be zero.

Svennson's final comments in this section are worthy of repetition here:

"A propeller on a displacement hull normally reduces the pressure on the stern of the hull resulting in an increased resistance and a positive thrust deduction. As indicated above, the thrust deduction with waterjet propulsion is of quite a different nature and positive as well as negative values t-values are possible."

"The t-factor should be as low as possible. For most vessels the lift generated by the jet units tends to reduce t. It is important to have areas aft of the inlet to take advantage of the high pressure zones.."

The mention of high pressure zones aft of the intake is significant. This fact is considered to be a strong player in hull-waterjet interaction and is studied in greater depth in chapters 5 and 8.

Svensson introduces[1] a coefficient similar to the familiar wake factor to account for what he calls a *"potential wake field"*. He defines a pressure coefficient C_p for the portion of the hull where the inlet is located. There is already an elevation term in the jet efficiency definition however the pressure coefficient is added to account for deviations in the static pressure at the inlet from the corresponding submergence pressure. The coefficient is defined as:

[1] p22

$$C_p = \frac{p_{0A} - pgh_I}{\frac{1}{2}\rho V_s^2} \qquad (4.5)$$

where,

p_{0A} = static pressure at the front face of the protruding stream tube
h_I = submergence of the inlet

Svensson provides the following example. For an assumed C_p of 0.1 the power requirement for a 175 tonne catamaran is reduced by 4% at 33 knots. No data other than the assumed value of C_p is given. Svensson recommends the measurement of C_p during hull resistance tests.

In the case of large installations where a change in efficiency of only several percent is important economically Svenssons recommendation should be followed. Measurements presented in chapter 7 reveal that C_p may indeed be of the order of 0.0 - 0.1.

Allison (1992)[1] covers the material presented by Svensson but also adds some interesting points:

"When a vessel starts to move forward under the influence of its propulsor, there is an increase of draft at the stern due to the reduction of static pressure caused by the acceleration of the boundary layer. This is very noticeable in the case of planing or semi-planing hulls."

Allison also reaches the following conclusion from Svensson's Figure 4.1 work:

"At usual speeds the pressure around a waterjet is found to increase relative to the value it would have been if there were no waterjet inlet."

He goes on to discuss other possible interaction effects in general terms. Changes to the wave making resistance caused by a change to flow patterns around the hull are mentioned as are interaction effects due to a change in the frictional resistance. Forces and moments due to the momentum flux through the jet are also mentioned.

[1] p14

He finishes with a comment that a wider intake will increase the wake factor as recommended by Purnell.

4.3.3 More Sophisticated Descriptions

Wilson (1977) conducted a survey of propulsor-vehicle interactions. The paper presents some interesting pressure distribution data taken from measurements of static pressures around a flush intake on a surface effect ship operating at various intake velocity ratios. He comments[1] that "*One can easily imagine net interaction forces arising from the external pressure integration.*"

Wilson[2] also presents data from some towing basin experiments reported by Ellis et al (1977). Two graphs from this report are reproduced in Figure 4.2. Wilson comments: "*It is seen that the trim is always greater for the waterjet installed cases. The model evidently experienced a positive added drag at low speeds, and a negative added drag at speeds above 12 knots. Just how all the interaction effects fit together to give this result is not clear. Added on-board weight (not included in the static trim) acted to increase the trim over the bare hull values. It was anticipated that the expected suction pressures on the ramp roof at higher IVRs (lower forward speed) would have acted to provide a negative added drag in the low speed range.*"

Several points can be made concerning the above statement. The model has definitely experienced a trimming down by the stern however there is mention of a change in loading conditions due to some added on-board weight. This would render any comparison unclear. The data is plotted against knots rather than a Froude number so comparisons of the data with other workers results can not be conducted without knowledge of the hull geometry. It is correct to say that a forward component of the low ramp pressures would act to reduce the drag however a reduction in lift caused by the intake would serve to produce an increase in drag or resistance. Wilson is certainly correct in stating that the interaction issues are unclear.

Finally, in the section entitled Comments and Recommendations he states:

---

[1] p230
[2] p234

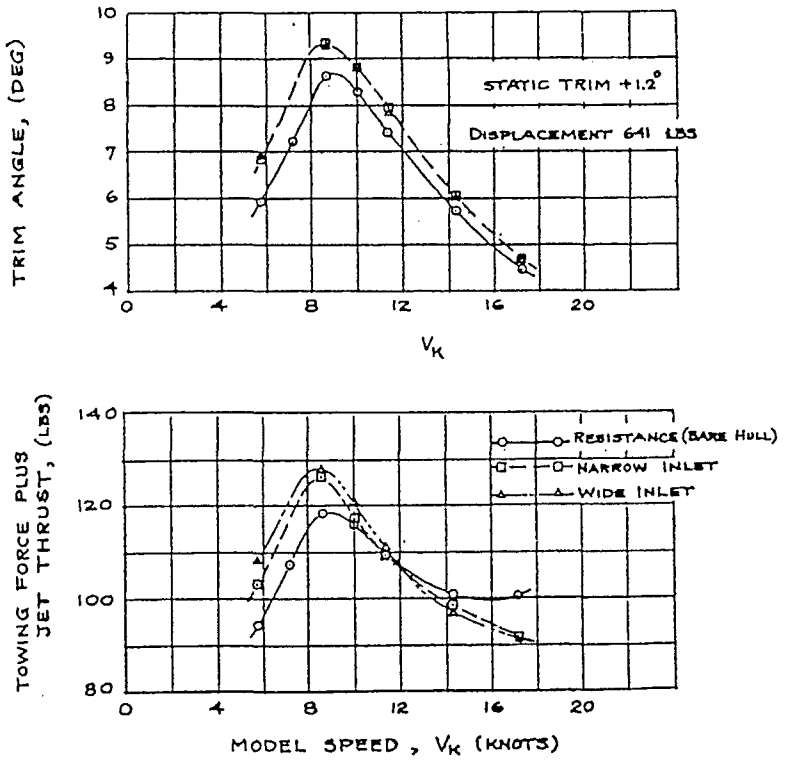

Figure 4.2 Trim and net drag performance of a planing boat model versus speed (from Ellis (1977))

"Further towing basin experiments should be conducted on the details of propulsive performance of flush inlets mounted in planing hulls. Important problems to be considered include the effects of angle of attack (trim), ingestion of air bubbles, and the complex interactions caused by the IVR-dependent pressure distributions acting near the operating inlet."

Similar work was conducted by Burtness (1987) at the Stevens Institute of Technology to evaluate the performance of several waterjet configurations suitable for installation on a high water speed amphibian landing craft. The objective was to investigate alternative combinations of inlet length and transition length and to use these data to design an optimum waterjet system with minimum losses.

Figure 4.3 is reproduced from Burtness's report and shows the model and test set-up. A scale model of the landing craft's hull was fitted to a moving carriage at an optimum trim setting which was determined by bare hull tests. The hull set-up includes a hinge point just ahead of the intake which allowed wedges to be inserted thus enabling the rear section of the hull to be inclined at a greater angle. The intake

under test was fitted to the centre of the hull and connected to a pump and duct system. Water leaving the intake was ducted through the pump and then expelled horizontally in a direction perpendicular to the direction of travel so as to not impart any thrust on the model.

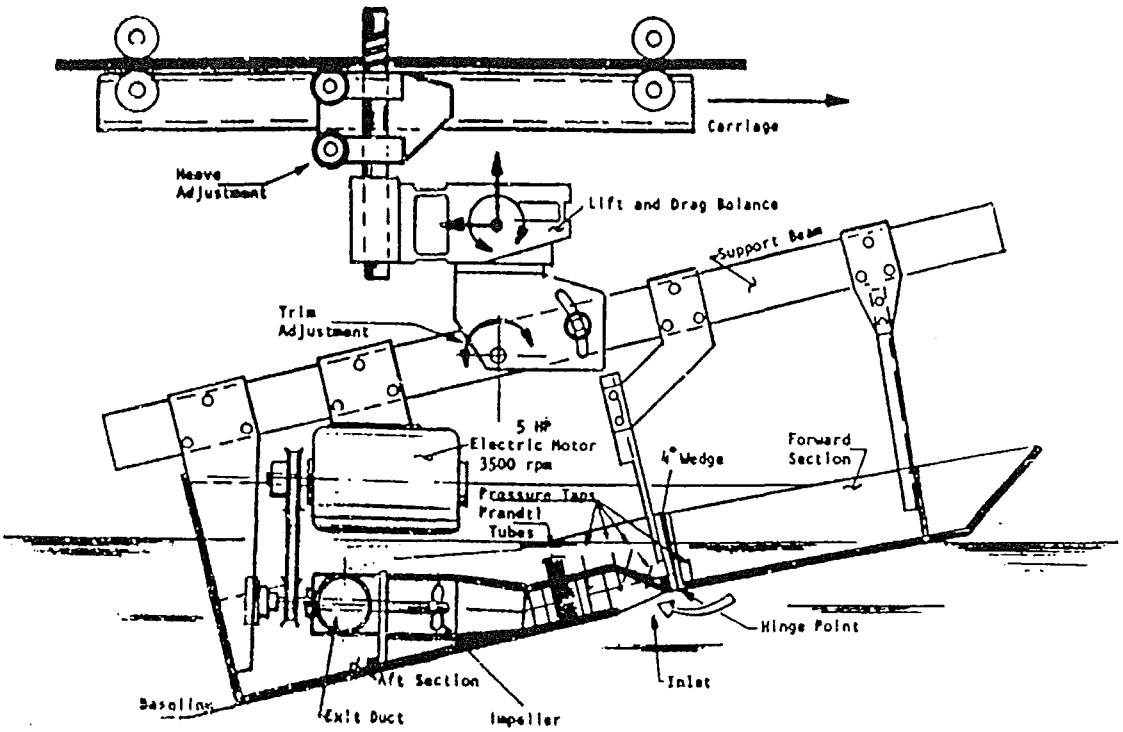

Figure 4.3 Model and test set-up (Burtness 1987)

Differences in lift and drag between the bare hull tests and tests conducted with the intake operating were measured and recorded. The forces were then expressed as lift and drag coefficients based on the inlet length and width and the free stream velocity. The lift force for example is expressed as:

$$F_L = C_L \frac{1}{2} \rho A V_s^2 \qquad (4.6)$$

The model inlet drag coefficient for all the inlets varied from -0.006 to 0.002 over the IVR range of 0.9 to 1.2. The lift coefficients for both inlets were similar varying from -0.016 at an IVR of 0.95 to -0.025 at an IVR of 1.2.

Graphs of the lift and drag coefficients, converted for use with SI units, are shown in Figure 4.4.

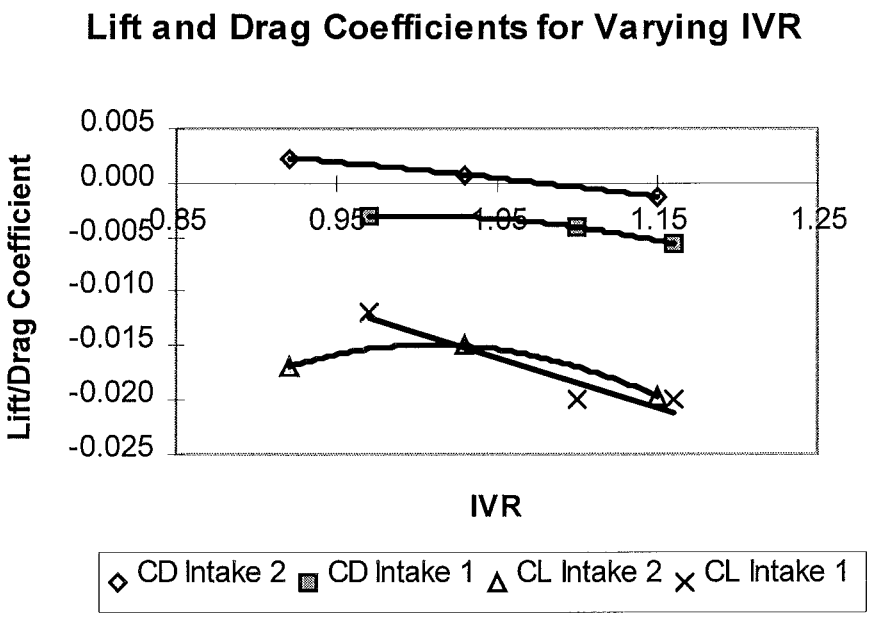

Figure 4.4 Lift and drag coefficients for varying IVR

The drag coefficient can be seen to be negligible however the lift coefficients are of greater significance. The lift acts in the negative or downwards direction, ie. if the hull were free to heave it would trim lower by the stern.

Care should be exercised in interpreting the results. It is not true to say that the physical arrangement of the exit ducting will not impart thrust on the model. If the usual $\dot{m}\Delta\mathbf{v}$ definition for thrust is used then a thrust force will result if the outgoing and incoming velocity vectors are different in magnitude or direction, assuming the mass flow to be constant. Considering velocity components relative to the model and in a direction lying in a vertical plane parallel to the direction of travel, the incoming velocity vector will be parallel to the keel and approximately equal to the forward speed. The outgoing velocity vector is perpendicular to the direction of travel and therefore does not contain any momentum flux in the directions under consideration. The force acting on the model therefore will be equal to $\dot{m}\mathbf{v}$ where $\dot{m}$ is the mass flow and $\mathbf{v}$ is the incoming velocity vector. This analysis assumes that pressure changes across the intake are negligible, further discussion of this topic can be found in section 5.4.2.1. It is not clear whether this thrust force has been allowed for in the calculation of the various lift and drag coefficients.

Using the lift coefficient and data for the intermediate IVR and assuming a jet velocity ratio of 0.66, the lift force and thrust can be calculated where,

IVR	= 1.03
Q	= 0.045 m^3/s
Inlet area, A	= 0.01 m^2
ρ	= 1000 kg/m^3
V_s	= 8.01 m/s

The lift force then from equation (4.6):

$$F_L = 0.015 \times 0.5 \times 1000\ kg/m^3 \times 0.010\ m^2 \times 8.01^2\ m/s = 4.8\ N$$

Assuming a jet velocity ratio, μ = 0.66 the thrust can be calculated using equation (2.2) as approximately,

$$T = 1000\ kg/m^3 \times 0.045\ m^3/s \times (12\ m/s - 8\ m/s) = 180\ N$$

It can be seen that the lift force is small compared to the thrust. Assuming a hull lift to drag ratio of 7, the lift force, which is downwards would be less than 0.5% of the hulls displacement and so practically negligible.

Dyne and Lindell (1994) have presented a way of avoiding the thrust deduction factor by calculating what they call the actual net thrust directly. This is achieved by including the stream tube pressure in the thrust equation as part of the wake factor as follows:

$$T_N = \rho Q_j (V_j - V_s(1 - w_{fm})) \tag{4.7}$$

The frictional wake is related to the local velocity, u and the static pressure coefficient C_p as follows:

$$1 - w_{fm} = \sqrt{\left(\frac{u}{V}\right)^2 + C_p} \tag{4.8}$$

The difficulty with this approach is that it requires measurement of the pressure coefficient and the friction wake for the self propelled case. It also only considers forces in the axial direction and does not allow for trim and draft changes that might be caused by the action of the waterjet at the speed under consideration.

Mr T. van Terwisga of MARIN has produced by far the greatest body of work on hull-waterjet interaction to date. His 1993 paper is effectively continuation of the work which was presented in the 1991 paper. He has also co-authored a paper with K.V. Alexander and this author which presents some of the ideas and approaches to the problem outlined in this work.

A significant contribution to the topic was also made by the Joint Industry Project (JIP) on Waterjet Application which was written by Van Terwisga but published by the ship research department of MARIN (1991). This project was supported by ten, mainly Dutch companies. A key focus was interaction effects. Much of Van Terwisga's work has flowed from the work initially carried out on this project.

The 1993 paper essentially develops a framework for describing the influence of interaction effects on the powering characteristics. Van Terwisga also introduces a new definition for the thrust deduction factor. The paper begins by describing the waterjet control volume. This is the same as the commonly used waterjet control volume shown in Figure 2.2 with the exception that the front face of the protruding stream tube has been moved forward a distance equal to 10% of the intake length. Van Terwisga states that *this position is selected to avoid major flow distortions by the intake geometry.* [1]

The traditional thrust deduction factor t, is renamed the total thrust deduction factor t_t where,

$$1 - t_t = \frac{1 - t_j}{1 + r} \tag{4.9}$$

t_t still accounts for the difference between the thrust (as calculated by a change to the momentum flux through the control volume) and the bare hull resistance. The thrust deduction factor t_j accounts for the fact that the protruding stream tube is prone to a pressure field that is subject to distortion by the hull and free surface effects.

$$1 - t_j = \frac{T_{net}}{T_g} \tag{4.10}$$

[1] p977

where in this case T_{net} is calculated from equation (4.7) and T_g from equation (2.2).

The hull resistance increment factor 1+r is used to account for changes in the hull resistance caused by a change to its planing condition from the bare hull case. The resistance increment factor is defined as:

$$1 + r = \frac{T_{net}}{R_{BH}} \tag{4.11}$$

An overall efficiency, η_{OA}, is derived from a number of component system efficiencies such that:

$$\eta_{OA} = \eta_I \eta_{duct} \eta_P \frac{\eta_{eI}}{(1+r)\eta_{mI}} \tag{4.12}$$

η_I is the ideal jet efficiency in free stream conditions:

$$\eta_I = \frac{P_{TE0}}{P_{JSE0}} \tag{4.13}$$

where P_{TE0} is the free stream effective thrust power and P_{JSE0} is the hydraulic jet system power. Energy losses occurring in the ducting and nozzle are accounted for by using a ducting efficiency η_{duct} such that,

$$\eta_{duct} = \frac{P_{JSE}}{P_{PE}} \tag{4.14}$$

where P_{PE} is the effective pump power. In a similar fashion, a pump efficiency is defined to account for losses within the pump:

$$\eta_P = \frac{P_{PE}}{P_D} \tag{4.15}$$

where P_D is the power delivered to the pump.

Interaction effects on the momentum fluxes are accounted for by a momentum interaction efficiency η_{mI} such that:

$$\eta_{mI} = \frac{T_{net0}}{T_{net}} \tag{4.16}$$

The momentum interaction efficiency accounts for the ingested boundary layer.

Van Terwisga has also introduced an energy interaction efficiency to allow for changes in jet system energy that may be required if the nozzle is submerged or the nozzle height changed. So:

$$\eta_{eI} = \frac{P_{JSE0}}{P_{JSE}} \tag{4.17}$$

The overall efficiency is subsequently broken down into the product of a free stream efficiency η_0, and an interaction efficiency η_{INT}, where

$$\eta_0 = \eta_I \eta_{duct} \eta_P \tag{4.18}$$

and

$$\eta_{INT} = \frac{\eta_{eI}}{(1+r)\eta_{mI}} \tag{4.19}$$

Now,

$$\eta_{OA} = \eta_0 \eta_{INT} \tag{4.20}$$

Subsequent analysis which will not be repeated here, decomposes the interaction efficiency further leaving a number of velocity parameters which must be determined by propulsion tests. The explanation of the various interaction efficiencies is useful however the analysis requires the measurement of various parameters. What is really required is a means to predict interaction.

The joint industry project (JIP) on waterjet application was essentially experimental in nature. A model representing a large (full scale length = 33 m) twin waterjet propelled hull was tested in both the bare hull condition and waterjet propelled. Tests were conducted for two different configurations of intake. The height to width ratio of the intake throat was varied plus and minus 30% around the value of 1. Paint smear tests were also conducted to find streamlines at the hull surface.

Of primary interest are the graphs of thrust deduction which was measured over the speed range. Figure 4.5 displays thrust deduction fraction for intakes of varying throat, height to width ratio. It can be seen that there is little change in thrust deduction factor with throat geometry.

The general trend is for a substantial increase in required thrust in the lower speed range. The thrust deduction fraction reaches nearly 0.25 at low volumetric Froude number. This means that considerably more (25%) thrust is required to propel the vessel at this speed with a waterjet fitted than is required to tow the bare hull.

Paint smear tests confirmed that the ingested stream tube is at least 30% wider than the intake width over the range of speeds tested.

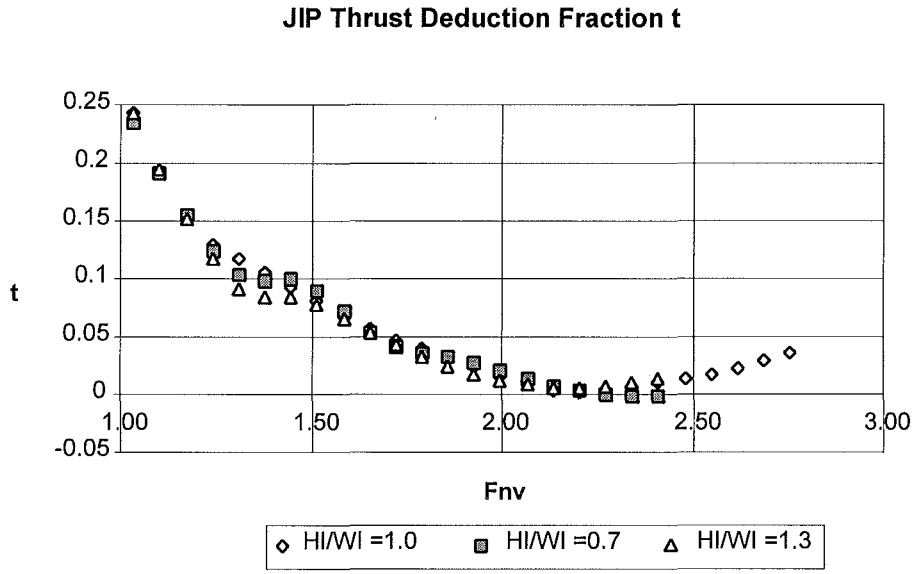

Figure 4.5 JIP thrust deduction fraction for varying intake throat geometry

The author has been involved with several papers on the subject of hull waterjet interaction. Coop et al (1992) and Coop and Bowen (1993) both present early material from this project. Alexander and van Terwisga (1992) canvas various

issues and also report some early findings of this project however Alexander's 1994 paper includes this material and more. Alexander et al (1994) is the last paper to report early findings and thinking from this work. The key points are summarised here.

Table 4.2 Interaction effects caused by water jet on hull (Alexander et al(1994))[1]

Intake Opening Hole (lost planing surface)	A CHANGES	Potential Flow	CHANGES	[Trim / Rise of C of G]	CHANGES	Wetted Length Wave Drag	CHANGES	Frictional Resistance
	B CHANGES	Wetted Length	CHANGES	Boundary Layer Aft of the Opening (lost)	CHANGES	Skin Friction		
Intake Flow (potential sink)	A CHANGES	Potential Flow	CHANGES	[Trim / Rise of C of G]	CHANGES	Wetted Length	CHANGES	Frictional Resistance
						Wave Drag		
	C CHANGES	Boundary Layer Around Opening	CHANGES	Frictional Resistance				
Water in the Jet (lost buoyancy or entrained water)	No change because this is taken into account with the addition of ballast during tests							
Thrustline Height	No change if the model is assumed to be waterjet propelled at the time of testing because the model towing force should be at the jet nozzle (Reference 1).							
Compared to model tests for a Propeller driven hull	D CHANGES	Moment on hull	CHANGES	Trim	CHANGES	Wetted Length Wave Drag	CHANGES	Frictional Resistance
Thrustline Angle	No change because the model towing force should be in line with the 'jet thrust' (Reference 1)							
If model towing tests towing force is not in the direction of jet thrust (assumed in Reference 2)	E CHANGES	[Trim / Rise of C of G]	CHANGES	Wetted Length Wave Drag (Potential Flow)	CHANGES	Frictional Resistance		
Trim of the Boat	I CHANGES	Vertical Component of Incoming Momentum to Jet	CHANGES	Rise of C of G of hull	CHANGES	Wetted Length	CHANGES	Frictional Resistance
		Vertical Component of Outgoing Momentum to Jet	CHANGES	Rise of C of G of hull	CHANGES	Wave Drag		

[1] p14

Table 4.3 Interaction effects caused by hull on waterjet (Alexander et al (1994))

Hull Ahead of Jet	Normally taken into account by waterjet designer											
	F **CHANGES**	Velocity Profile at Intake	**CHANGES**	Incoming Momentum	**CHANGES**	Thrust						
			CHANGES	Flow Through Jet	**CHANGES**	Outgoing Momentum	**CHANGES**	Thrust				
	G **CHANGES**	Potential Flow Field at Jet Intake eg. Transverse Flows and Static Pressures	**CHANGES**	Height of Streamtube	**CHANGES**	Incoming Momentum	**CHANGES**	Thrust				
					CHANGES	Flow Through Jet	**CHANGES**	Outgoing momentum	**CHANGES**	Thrust		
Trim of the Boat	H **CHANGES**	Wetted Length	**CHANGES**	Velocity Profile at Intake	**CHANGES**	Incoming Momentum	**CHANGES**	Thrust				
						Flow Through Jet	**CHANGES**	Outgoing Momentum	**CHANGES**	Thrust		
	G **CHANGES**	Potential Flow Field at Jet Intake eg. Transverse Flows and Static Pressures	**CHANGES**	Height of Streamtube	**CHANGES**	Incoming Momentum	**CHANGES**	Thrust				
						Flow Through Jet	**CHANGES**	Outgoing Momentum	**CHANGES**	Thrust		
	H **CHANGES**	Horizontal Component of Incoming Momentum	**CHANGES**	Thrust (Horizontal)								
		Horizontal Component of Outgoing Momentum	**CHANGES**	Thrust (Horizontal)								

Two tables are presented showing possible contributions to interaction. These are reproduced here in Table 4.2 and Table 4.3. The most significant interaction contributors were identified as,

1. the waterjet momentum forces causing lift and a moment
2. stream tube forces which are incompletely reacted on the hull
3. loss of planing surface at the intake
4. consequences of boundary layer changes
5. minor influences due to flow field changes

Item 2 deserves special mention as the importance of this mechanism will be expanded on in chapter 5. The paper states *"...not all of the stream tube force will be reacted on the hull bottom, and some of it will appear as momentum in the wake."*

Free body diagrams of the towed and self propelled hull are presented. A concept known as the *interaction vector* is presented. It is intended that this vector may be added to a free body diagram of the self propelled hull and that it will account for all the unknown interaction forces not present in the existing theory. A method is proposed whereby the magnitude and position of the interaction vector may be calculated from comparative experimental tests. This is achieved by comparing towing and self propulsion tests of the hull at the *same trim and draft*, measuring and calculating all of the known forces in each case and then comparing forces to find the interaction vector.

For practical reasons described in chapter 5, a variation of this technique was finally adopted for use in this thesis. However the basic philosophy has remained the same.

Supporting computational and experimental work is presented. Wind tunnel tests confirming the size and shape of the protruding stream tube are noted. This work is referred to in section 5.4.2.2. There is also mention of previous propulsion testing undertaken by this author where the waterjet was supported by a system of load cells between the waterjet and the hull. This work is reviewed in section 7.2.3. Early findings of and some analysis of the tests conducted at MARIN for this project are presented. However this material is examined in chapters 7 and 8 so is omitted here.

4.3.4 Propeller Hull Interaction

It is worthwhile to consider techniques that have been developed for the analysis of propeller-hull interaction. Hadler (1966) has developed a computational method for predicting the powering requirements of propeller driven craft. A key feature of this method compared to the Savitsky method is that it includes interaction effects between the propeller and the hull. In particular the effect of the induced velocities outside the propeller slipstream on the hull are considered.

The planing hull characteristics are calculated using the Savitsky equations outlined in the previous chapter. Appendage lift and drag are also added to the model using generally accepted formulas and assumptions.

Forces arising from the propeller are attributed to two separate effects: forces that are transmitted to the hull through the shafting and struts and pressure forces induced on the planning surface and appendages due to the action of the propeller beneath the hull. Hadler uses existing knowledge of the velocity field around the propeller to calculate the pressure force acting on the hull. Given that the velocity is known at any given radius from the propeller and at any distance fore and aft of the propeller plane, the Bernoulli equation is used to calculate the pressure on the hull surface which is assumed to be a flat plate. Hadler presents charts of contours of integrated pressure coefficients and centroids so that the magnitude and position of the induced pressure force on the hull may be calculated. A method for calculating the additional forces on the rudder caused by the propeller slipstream is also presented.

Now sufficient forces acting on the hull and propulsion system are known to solve the problem. In a similar manner to the Savitsky method, the hull is treated as a free body and equations of static equilibrium written to eliminate unknowns. Calculations are conducted at varying hull trim angles until the free body system is found to be in static equilibrium.

A key assumption in Hadler's approach to the problem is that it is possible to superimpose all forces acting on the hull and appendages and that they do not interact with one another. This is of course a necessary assumption to make if any progress is to made with the problem, and one which is made later in this thesis.

Hadler commented that this assumption should be examined further, however experimental results showed reasonable correlation with the theory which suggest that the assumption is not unreasonable. MARIN use the methods proposed by Hadler.

Graphs of thrust, trim, RPM and shaft power are shown below Figure 4.6. Trim predictions at and below the hump vary by approximately half a degree, however there is good agreement above the hump speed. The predicted value of thrust is low through the hump range however it is generally accepted that in this part of the speed range the Savitsky equations tend to under-predict resistance. This is due to the bow sections of the hull being in contact with the water and the Savitsky assumption of prismatic geometry falling down. The Blount and Fox modification factor was introduced to account for this effect. This factor is discussed further in section 3.3.2. Thrust is predicted well through the intermediate speed range.

Thrust deduction fractions for propellers tabulated by Bjarne earlier in the chapter are normally in the range 0-0.1.

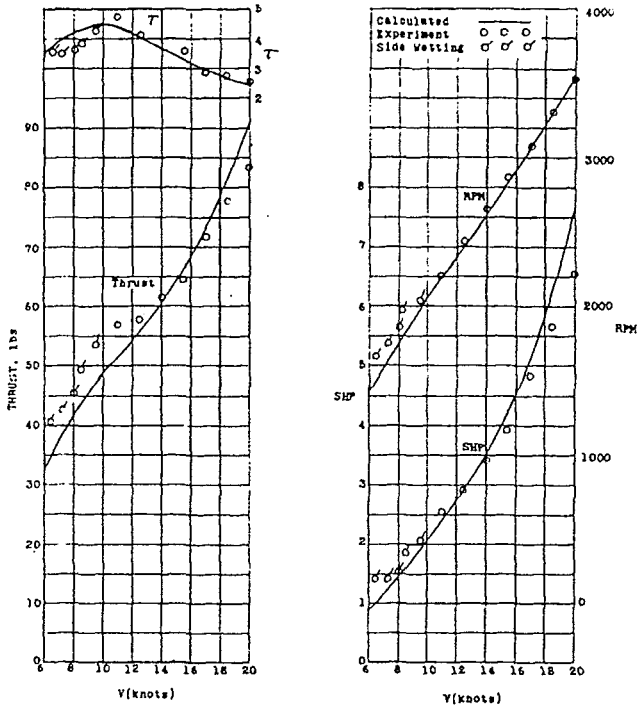

Figure 4.6 Predicted and experimental results of self-propulsion tests (Hadler (1966))

4.4 Conclusions

With respect to the review of existing literature above, but excepting those papers which have emerged as a product of this work, the following summary of points reflect the state of understanding of hull-waterjet interaction at the outset of this project.

- The thrust deduction and hull wake factors are well established in the existing theory. The wake factor is well understood however the thrust deduction factor is an experimental correction factor which as yet can only be found experimentally.
- Some existing theory includes a pressure coefficient as an extension to the wake factor, however supporting data is lacking.
- A number of contributing factors to hull waterjet interaction have been suggested. The most likely causes are seen as being the lift and moment forces due to the momentum increase through the waterjet and a changed hull pressure force at the stern due to the action of the intake.
- Several workers have presented integrated pressure distributions around the intake however hard data supporting the results is not supplied. Contrary opinions exist as to whether the intake supplies a net lift or net load.
- There is some general agreement on shape of the thrust deduction characteristic. It appears to be high, of the order of 20 to 30% at low Froude numbers, $F_\nabla \cong 1$ reducing to near zero at planing speeds, $F_\nabla \cong 3$.
- There is no detailed data or theoretical understanding of the contributors to the thrust deduction factor.
- There is no unified method for the calculation of planing performance which includes hull-waterjet interaction.
- Hadler's (1966) work on hull-propeller interaction may provide a useful framework for a similar method which accounts for hull-waterjet interaction.

5. Theoretical and Experimental Approach

5.1 Introduction

The conclusions drawn from the previous chapter state that there is little theoretical understanding of interaction effects and no unified method for the calculation of performance of the combined hull-waterjet system. This work is intended to go some way toward meeting both these needs. The theoretical and experimental approach outlined in this chapter is geared toward finding a vector, to be termed the *interaction vector,* which can be added to Savitsky type performance prediction theory. In doing so it is hoped that the understanding of the causes of interaction will be improved. The chapter presents three distinct stages to the approach. Computational models and experimental requirements are described.

As the project was initiated by a waterjet manufacturer, the problem has understandably been tackled from a practical, industry view-point. It was important that the approach used to solve the problem made the best use of the resources available. There were limited resources for extensive computational fluid dynamic (CFD) or test tank work. The 7m Hamilton test boat was available however so a full-scale experimental approach was adopted. During the project a relationship was formed with Mr T. van Terwisga of MARIN. As a result of this relationship some tank testing at competitive rates was possible. It became clear at an early stage that the Savitsky method for predicting planing hull performance, already in everyday use at CWF Hamilton and Co. Ltd. would also become an essential tool.

5.1.1 Vector approach

A key factor in maintaining a straightforward way of understanding the problem was to use vectors to represent all forces acting on the hull. This had the advantage of assisting in the visualisation of what was going on and enabled equations of static equilibrium to be written easily.

A fundamental assumption when working with vectors is that the principle of superposition applies. This is not necessarily the case when considering pressures. For example, a manifold coupled to a number of different pressure sources may not

experience a pressure equal to the sum of the sources. There will be flows from high to low pressure areas and associated energy losses in the system. Soon the analysis of the simple averaging manifold becomes complex. Care therefore, must be exercised when adding pressure fields. The principle of superposition can only be assumed to hold if the pressure distribution is constant across the region.

5.1.2 Hull as a free body

The hull is in contact with two fluids, seawater and air. All forces felt by the hull are either pressure forces which act perpendicular to surfaces or viscous drag forces which act parallel to surfaces. All forces can be thought of as vectors acting on a free body. The problem is then reduced to one of calculating or measuring each force in turn. This process forms the basis for the computational models which have been constructed in this chapter to better understand the problem of hull-waterjet interaction.

Table 5.1 Possible interaction mechanisms

Interaction Mechanism	*Significance*
Effects due to momentum change through waterjet system	
• pitching moment	moderate
• lift	moderate
Effects of lost momentum in wake	
• pitching moment	high
• loss of lift	moderate
Loss of planing surface at intake	
• pitching moment	high
• loss of lift	moderate
• new pressure distribution on the rest of the hull	low
• lower skin friction	low
Miscellaneous effects	
• boundary layer changes	low
• transverse flows	low

5.1.3 Likely Contributors to Hull-Waterjet Interaction

There are a number of possible mechanisms contributing to the overall interaction effect. Using existing theory covered in chapters 2 and 3 and a combination of wind tunnel work, computational fluid dynamics studies and experience gained at CWF Hamilton and Co. Ltd., estimates have been made of the relative significance of these possible interaction effects on the Hamilton test boat. These are tabulated in Table 5.1, the most significant being, waterjet momentum forces causing lift and a

moment about the centre of gravity, momentum losses in the wake and the loss of planing surface at the intake. Effects due to boundary layer changes and flow field changes were estimated to be small.

Some approximate calculations in the following sections indicate the likely relative magnitude of the various effects tabulated in Table 5.1.

5.1.3.1 Momentum change through waterjet system

It can be seen that the most significant effects are expected to be due to the momentum change through the waterjet system which produces lift and moment effects on the hull. Using the Hamilton 7m Test Boat (henceforth referred to as "the test boat") planing at 24 knots (F_∇ = 3.34) as an example the net thrust vector produced by the waterjet system is 4474 N acting at an angle of 12° to horizontal. The vertical or lift component of this vector is 925 N upwards which is equivalent to 3.4% of the hulls static displacement. The bow down moment about the CG caused by the thrust vector is 940 Nm which is equivalent to a person moving 1.3 m forward from the CG.

5.1.3.2 Momentum loss in wake

It is also possible that the presence of the protruding stream tube under the hull causes an extra down-load. This would not be the case if the intake were located in the middle of a large flat plate. It is not however, the cutwater being only 205 mm or approximately a third of the intake length from the transom. Analysis in section 5.4.2 predicts that there will be a loss of lift. The following calculations can be made to estimate what magnitude of loss may exist.

Consider the drawings of dividing streamlines measured by Griffith-Jones (1994)[1] for varying IVR settings in Figure 5.1. A typical IVR for the test boat is 0.55. Assume that for an average case a similar mass flow as that entering the intake is flowing past the transom at an angle of 10° to the keel. The component of momentum perpendicular to the keel is given by sine10°$\rho Q V_s$ which is calculated as

[1] p45

$0.17 \times 1026\ kg/m^3 \times 0.328\ m/s \times 12.3\ m/s = 704\ N$. This creates a force down at the transom and a bow-up moment of 1760 Nm about the CG.

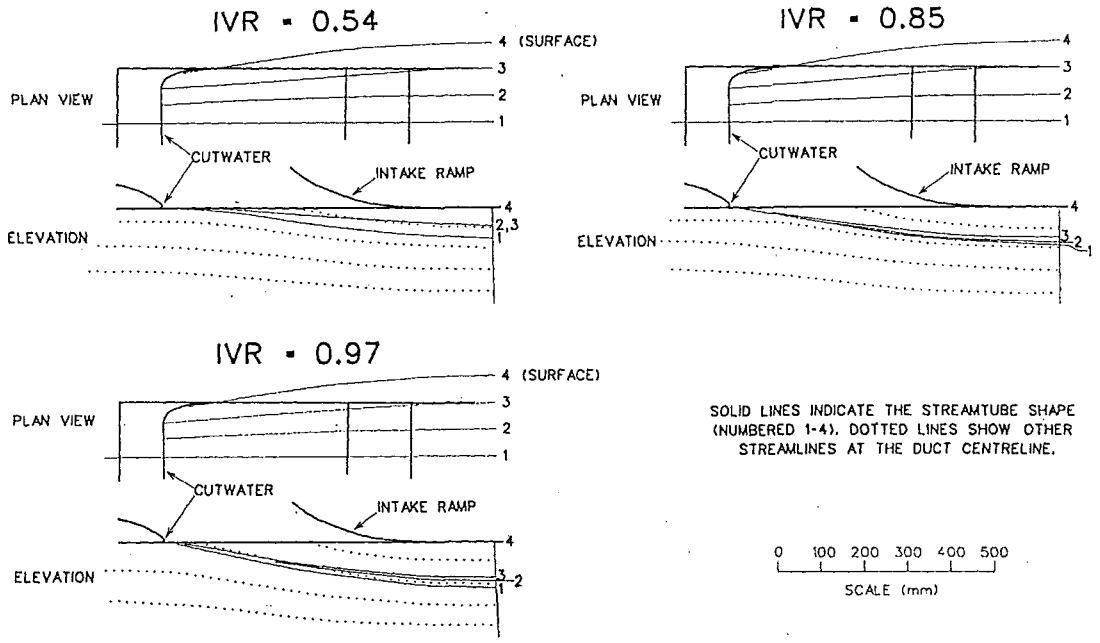

Figure 5.1 Dividing streamline and stream tube shapes (Griffith-Jones (1994))

5.1.3.3 Loss of planing area

The removal of the intake area also reduces the hull's planing area and the wetted surface friction area. The removal is not logically an interaction effect, but the bare hull against which the propelled hull is compared must have a cover over the intake so the cover's removal will be considered under the umbrella of interaction. The area where the cover plate was, is now occupied by waterjet intake. Pressure forces that were acting on the intake cover plate are now acting on the waterjet system and are taken into account when the waterjet forces are added to the theoretical model. However the calculations of hull pressure force must be adjusted to account for loss of lift on the hull otherwise the pressures in this area will be considered twice.

For the calculation of the reduction in drag force due to viscous friction it is assumed that a fresh turbulent boundary layer is grown from the cutwater. The boundary layer theory discussed in sections 2.3.4 and 3.3.1 is used in the calculations. At planing speeds the drag reduction was found to be 20 N which results in an 11 Nm

reduction in bow down moment due. As a comparison the total frictional drag force was 1786 N so the reduction is certainly small, a little over 0.5%.

The removal of dynamic planing pressure area however may have a more significant effect. The intake region which in this case is less than a quarter of one beam width from the transom is in a region of low dynamic pressure as discussed by Pierson and Leshnover (1950)[1]. There is not sufficient data or theory to exactly predict the pressure in the region of the intake for the test boat bare hull condition. However it is assumed that the pressure in this region is equal to the average pressure calculated by dividing the hull displacement by a typical wetted surface area. A typical wetted area from Savitsky calculations is 8 m^2. Given the test boat nominal displacement of 2800 kg, calculation yields an average pressure of 3.4 kPa. If this is multiplied by the intake area the lost lift would be approximately 800 N causing a bow up moment of 1600 Nm.

It should be remembered that the above calculations consider each effect acting in isolation and assumes no interaction between effects.

5.2 General Methodology

The following three sections present the method used to find the size of the interaction vector which would need to be added to the existing theoretical model to correct it for interaction.

5.2.1 Stage 1

Figure 5.2 shows a schematic of the process which was used to find the likely interaction forces. The first stage involved constructing an accurate Savitsky long form type computational model of the towing case and checking this against full scale data. At a *given ship speed*, three key performance characteristics were identified, the resistance R, wetted keel length L_k, and the keel trim, τ. These were compared with the same characteristics measured at full scale in order that the accuracy of the computational model could be checked. Non-dimensional correction functions were developed to make small adjustments to the computational model to

[1] p37

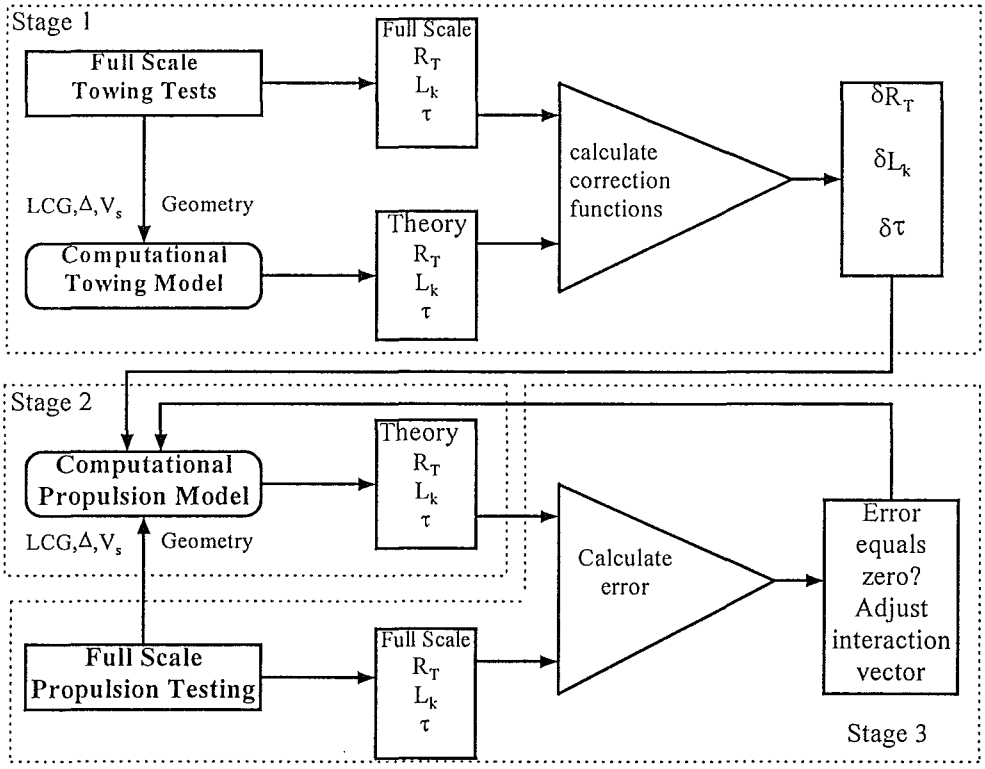

Figure 5.2 Schematic of investigation methodology

map the output onto the full scale data. These were necessary as the test boat deviated slightly from a pure prismatic shape. The hull features an inner and outer chine such that a spray rail approximately 90 mm wide is formed. A delta keel is also provided for fitment of the waterjet intake (see the hull linesplan in the Appendices).

5.2.2 Stage 2

A second computational model was then developed for the self propelled case. This included all known forces acting on the hull. Correction functions found in stage one were then applied to the output data. A key assumption is that the correction functions still hold for small changes in the displacement and LCG. Another key assumption is that is the position of the hull pressure force vector N is unaffected by the waterjet intake. The pressures acting on the afterbody of the hull are known to be small (Savitsky (1964))[1], half of the lift being generated by the forward one quarter of the hull. The intake area accounts for no more than 3.5% of the total

[1] p72, 85

planning area. Hadler (1966) made this assumption in his paper on propeller waterjet interaction which is discussed in section 4.3.4.

5.2.3 Stage 3

Output from the propulsion model is then compared to full scale propulsion data. An error function is calculated. Performance characteristics are recalculated but this time an interaction vector is added at a fixed location x_1 along the hull. The error is then recalculated. The magnitude of the interaction vector is adjusted and the process is repeated over and over until a minimum error is achieved. In this fashion a vector is found of such magnitude that when added to the model at position x_1 a best fit with the full scale data is achieved. The error is recorded.

The process is repeated for positions x_2, x_3 etc and the minimum error recorded for each position. Finally the position with the minimum error is chosen. Therefore at a given speed a vector has been sized and positioned to give the best possible match with the full scale propulsion data.

5.3 Appended Bare Hull Resistance: Computational Model

The following section details the relevant assumptions and calculations used to devise computational towing model. Computer program SAV_CRL.C listed in the Appendices was written in the C programming language by the author to perform the necessary iterations and calculations.

5.3.1 Savitsky Long Form

5.3.1.1 Introduction

The Savitsky Long Form resistance calculation method allows for moments to be taken into account when considering the forces on a planing hull. Hadler, (1966) has expanded on the Savitsky technique to include appendages, and propeller forces in the free body. A similar technique was employed here. The calculation of the magnitudes and positions of each of the force vectors shown in Figure 5.5 must be considered. These calculations and relevant assumptions are summarised in sections 5.3.1.2 to 5.3.2.1.

5.3.1.2 Hull displacement and LCG

The loading condition was calculated by first weighing the empty hull and then calculating the effect of adding various items such as fuel, people and tools. Each item was entered on a loading sheet together with its weight in newtons and its position in the hull longitudinally and vertically. An uncertainty estimate was allocated to each parameter and the final uncertainty also calculated. A sample loading sheet is shown in 6.2.4.

Savitsky and Hadler both assume that the effective weight on the water always remains the same, i.e. equal to the static displacement weight, Δ_0. Once the hull is moving however, there are aerodynamic and propulsor present which serve to change the effective weight on the water. The displacement weight is used to calculate the deadrise surface lift coefficient from which the mean wetted length to beam ratio is obtained (as described in section 3.3.1.1).

In this analysis the displacement is allowed to vary from the static displacement resulting in a new effective displacement called the dynamic displacement Δ. Care must be exercised however when calculating the dynamic displacement so that it includes the forces that were not included in the original test set-up used to find the lift coefficient in the empirical planing lift equation. The exact method should be checked so that forces already included are not added again. Equation 3.3 was found using data collected by Korvin-Kroukovsky et al (1949) using the following procedure:

"For each test run the model was set at a required trim τ, loaded to a required load Δ, and run at specific speed V. The model was free to rise, seeking the position of equilibrium at which the bottom area or the wetted length to beam ratio λ was sufficient to support the load."[1]

Therefore lift forces acting on the model are allowed for as the model finds its own equilibrium. Changes in the displacement due to the vertical component of the viscous drag are accounted for. Any lift force due to appendages, aerodynamic

[1] p6

loadings[1] or the towing force are not present in the towing set up and so must be added. Referring to Figure 5.3, the equation for dynamic displacement for the appended case is:

$$\Delta = \Delta_0 - D_w \sin\alpha + D_a \sin\tau + W\tan\gamma \tag{5.1}$$

where,

D_w = aerodynamic force
α = angle between D_w and horizontal
D_a = appendage drag force
τ = dynamic keel trim measured between the keel and horizontal
W = is the towing force
γ = is the angle between the towing force and horizontal

Note that for the reasons described above the lift component of the viscous drag force is not included.

5.3.1.3 Viscous drag force

The viscous drag force, D_f is estimated using equation 3.8 and is assumed to act in a direction parallel to the keel at a point midway between the chine and the keel. No allowance is made for the delta keel which would only vary slightly alter the position of the viscous drag vector.

5.3.1.4 Position of hull pressure force

The distance of the hull pressure force from the CG, e, is calculated using equations 3.1 and 3.2.

5.3.1.5 Appendage lift and drag forces

The test boat was fitted with only one appendage for the towing tests, a pitot-static tube. The tube was fitted to the transom near the starboard chine protruding 150 mm below the hull. A drag coefficient was found experimentally for the tube so the drag force, D_{ps}, may be calculated using equation (5.2)

---

1 Due to the slower speeds of tank testing due to scaling, aerodynamic forces could be considered to be negligile.

$$D_{ps} = C_D \tfrac{1}{2} \rho A_f V_s^2 \qquad (5.2)$$

where,

C_D = drag force coefficient (= 0.72)
A_f = frontal area (= 0.00205 m^2)
ρ = fluid density
V_s = speed of the planing surface

The drag force vector is assumed to act at a point mid-way along the strut and in a direction parallel to the keel. No allowance is made for the effect of the hull's boundary layer on the pitot-static tube drag which is considered negligible.

5.3.2 Aerodynamic lift and drag

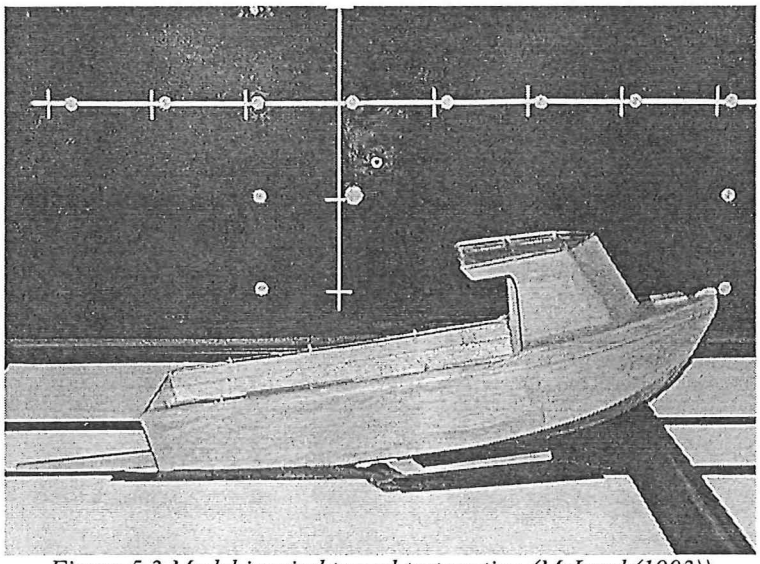

Figure 5.3 Model in wind tunnel test section (McLeod (1993))

An undergraduate student, Mr Andrew McLeod (1993), was engaged to undertake wind tunnel tests on an accurate scale model of the test boat. The model, mounted in the wind tunnel working section is shown in Figure 5.3.

Lift and drag coefficients based on the hull's frontal area were measured along with the moment arm between the centre of aerodynamic pressure and the centre of gravity. It was found that the lift coefficient and the position of the centre of pressure were insensitive to Reynolds number over the speed range. The drag

coefficient showed some variation, although it tends to 0.6 at the higher end of the speed range which is a commonly accepted value at CWF Hamilton and Co. Ltd.

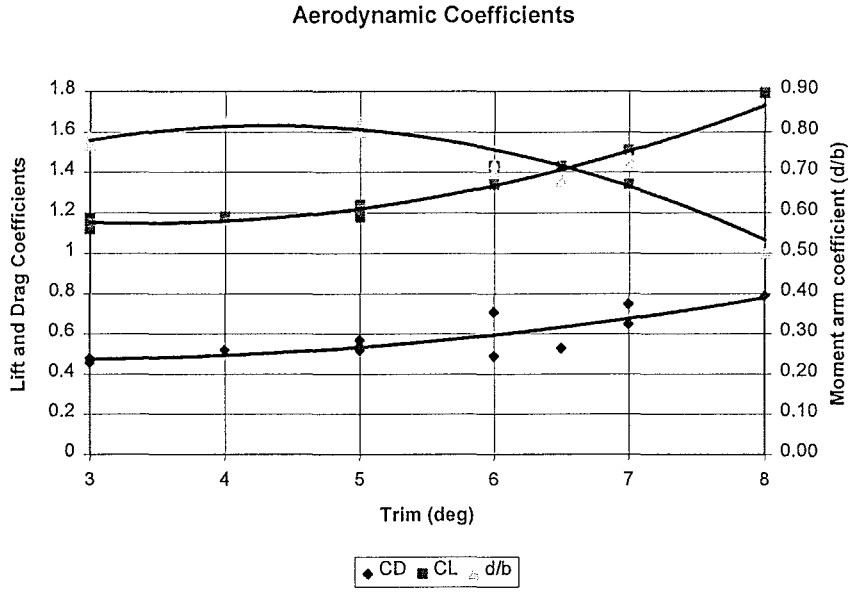

Figure 5.4 Aerodynamic coefficients for varying trim angles

Figure 5.4 shows the lift and drag coefficients and a moment arm coefficient based on the beam, b as a function of the trim angle. The lift coefficient was found to lie between 1.2 and 1.6 depending on the trim angle which is in the range zero to 2 reported by Wikeby (1990) for offshore racing power boats. All coefficients were found to be insensitive to changes in displacement which is to be expected as related frontal area changes are small. Curves were fitted through the points using an equation of polynomial form and the least squares method.

5.3.2.1 Point of application of towing force

The position and direction of the thrust vector or towing force, W, must be known so that it may be added to the computational model. In the case of the towing tests, the towing load was always applied at a known position at the front of the boat. However the angle of tow to horizontal could be set in the program to a specified angle.

5.3.3 Equations of Static Equilibrium

Equations of static equilibrium are written to allow a moment equation to be found using the variables already calculated. Considering the free body diagram shown in

Figure 5.5, three equations of static equilibrium can be written which take into account all forces and moments.

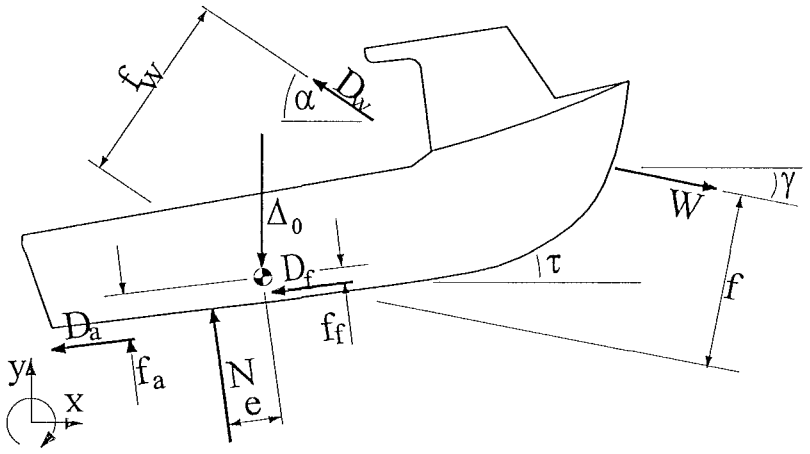

Figure 5.5 Free body diagram (towing case)

Vertical forces:

$$0 = N\cos\tau - (D_f + D_a)\sin\tau + D_w \sin\alpha - W\sin\gamma - \Delta_0 \tag{5.3}$$

Horizontal forces:

$$0 = W\cos\gamma - (D_f + D_a)\cos\tau - N\sin\tau - D_w \cos\alpha \tag{5.4}$$

Moments

$$0 = Ne + D_f f_f - D_w f_w + D_a f_a + Wf \tag{5.5}$$

Combining equations (5.3) and (5.4), eliminating N and solving for W,

$$W = \frac{D_w \cos(\tau+\alpha) + D_f + D_a + \Delta_0 \sin\tau}{\cos(\tau+\gamma)} \tag{5.6}$$

Combining equations (5.3) and (5.4), eliminating W and solving for N,

$$N = \frac{(D_f + D_a)\sin(\tau+\gamma) + \Delta_0 \cos(\gamma) + D_w \sin(\gamma-\alpha)}{\cos(\tau+\gamma)} \tag{5.7}$$

Substituting equations (5.6) and (5.7) into equation (5.5),

$$\begin{aligned} 0 = {} & \Delta_0(f\sin\tau + e\cos\gamma) + (D_f + D_a)(e\sin(\tau+\gamma) + f)... \\ & + D_w(f\cos(\tau+\alpha) + e\sin(\gamma-\alpha))... \\ & + (D_f f_f + D_a f_a - D_w f_w)\cos(\tau+\gamma) \end{aligned} \tag{5.8}$$

Moment equation (5.8) is now in terms of variables which are either given or can be calculated. The trim can be varied and each parameter recalculated until equation (5.8) is satisfied.

5.3.4 Blount and Fox Modification Factor

The Blount and Fox modification factor, M, which is discussed in greater detail in section 3.3.2, is applied only to the pressure and viscous drag components of the resistance. It was found that this improved the prediction method. Almeter (1991)[1] reports its common usage as is also the case at CWF Hamilton and Co. Ltd.

The total resistance can be calculated using equation (5.6) and including M as follows.

$$R_T = \frac{\cos\gamma}{\cos(\tau+\gamma)}\left[D_w \cos(\tau+\alpha) + D_a + M(\Delta_0 \sin\tau + D_f)\right] \tag{5.9}$$

5.3.5 Correction Functions

The computational model outlined above was compared with full scale towing tests which are described in chapter 6. Small non-dimensional correction functions of the ship speed were then calculated to map the computation model onto the full scale data. These were used to allow for changes in performance due to the hull deviating from the pure prismatic form as described in section 5.2.1.

For example,

[1] p13

$$\delta R_T(V_s) = \frac{R_{T\,Full\,Scale}(V_s)}{R_{T\,Model}(V_s)} \tag{5.10}$$

Similarly, correction functions $\delta\tau(V_s)$ and $\delta L_k(V_s)$ were also calculated.

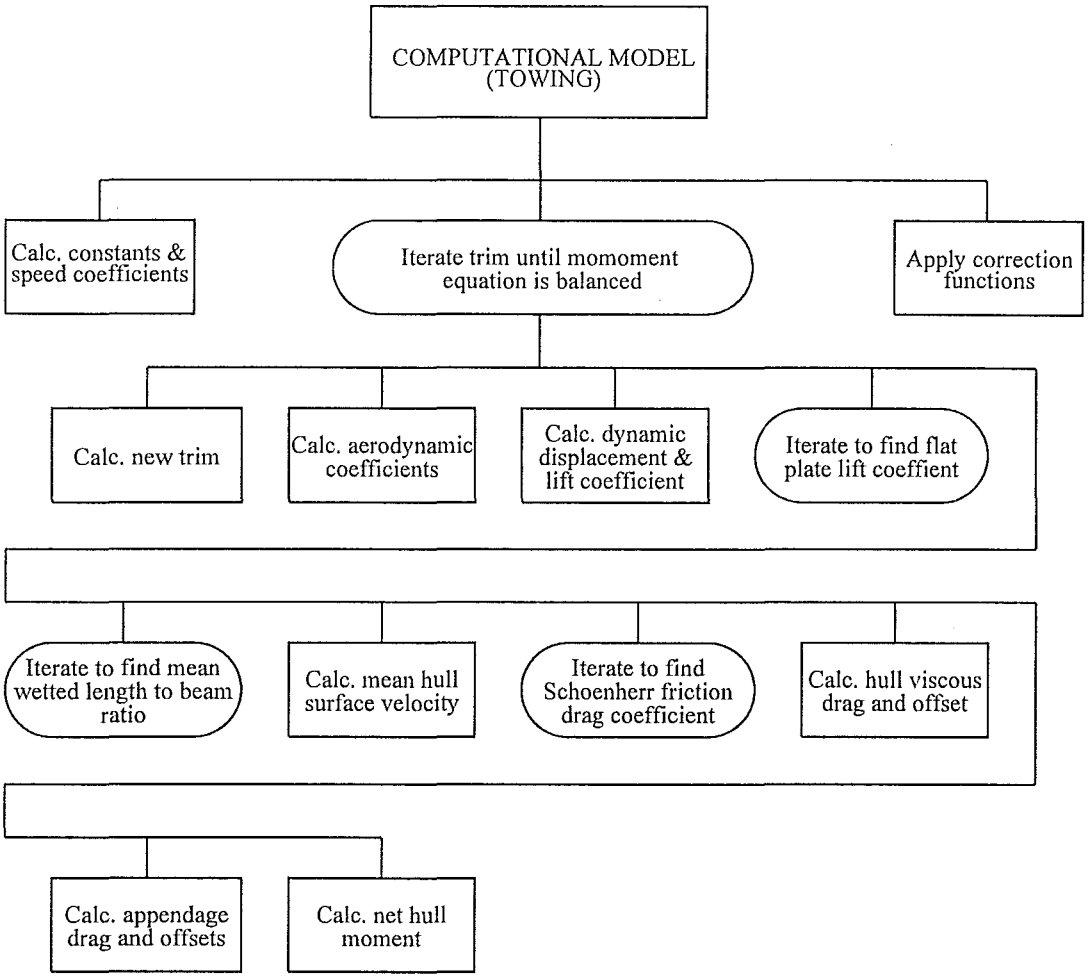

Figure 5.6 Computational structure diagram (towing case)

5.3.6 Computational Procedure

Figure 5.6 shows the calculation steps and general calculation routine of the computational program in the form of a structure diagram. Structure diagrams are read from left to right until a leg with subsidiary tasks is encountered. It is then read down until the leg is completed. Boxes refer to a distinct one off task while loops refer to an iteration or repeated task.

5.4 Self Propelled Hull: Computational Model

The following section details the relevant assumptions and calculations used to devise computational towing model. Computer program SAV_CIR.C listed in Appendix A-7.2 was written in the C programming language by the author to perform the necessary iterations and calculations.

5.4.1 Savitsky Long Form

5.4.1.1 Introduction

In a similar fashion to the theoretical towing model, a theoretical propulsion model has been constructed which accounts for forces acting on the hull when self-propelled. An important distinction is that the hull is no longer being towed from a fixed position but rather propelled by the waterjet system. Forces acting on the waterjet are estimated and a net thrust vector, which is not necessarily horizontal, calculated and then added to the model. Some extra appendages have also been added, namely a rudder and some exposed support brackets.

5.4.1.2 Hull Displacement and LCG

The hull displacement is calculated as described in section 5.3.1.2. There are small changes due to different equipment, fuel load and crew. The weight of entrained water in the waterjet is added to the hull displacement.

The fuel is steadily burnt so the fuel load slowly decreases over time. The fuel loading was measured at the start and end of each days testing so that by assuming a linear rate of consumption, the loading at a given time can be estimated. The precise time of any single test was then used to estimate the fuel load on board for that particular run.

The fuel is also free to move in the fuel tank. In this case the tank is long and rectangular which allows significant movement fore and aft depending on the trim condition at the time. Computer program, FUEL.C included in Appendix A-7.4, was written to calculate the volume and position of the centre of gravity of the fuel given a trim angle and a dipstick measurement.

The change in fuel loading due to consumption was found to be minimal. The engine burns approximately 15 kg of fuel per hour.

5.4.1.3 Viscous Drag Force

Equation 3.8 is again used but an allowance is made for the small decrease in drag due to the hull area removed at the horizontal intake plane. It is assumed that a new boundary layer is "re-grown" from the cut-water and extends the short distance to the transom.

5.4.1.4 Appendage Lift and Drag Forces

5.4.1.4.1 Rudder

A rudder was used to steer the boat during the propulsion tests. This was necessitated by the extension of the nozzle insert which rendered the steering deflector inoperable. It was not possible to directly measure the drag force on the rudder so Hoerner's method as quoted by Hadler (1966)[1] is used. The drag for a non-ventilated rudder can be expressed as follows:

$$D_r = \rho/2\, S_r V_s^2 \left[2C_f \left(1 + 2t/c + 60 (t/c)^4 \right) \right] \qquad (5.11)$$

where

S_r = planform area of rudder
C_f = Schoenherr frictional drag coefficient if $Re > 5\times10^5$
t/c = thickness to chord ratio

The drag force is assumed to act at the centre of area of the rudder and in the direction of the flow which is parallel to the keel. Hoerner[2] also provides a formula for spray induced drag which occurs when the rudder penetrates the surface.

$$D_r = 0.24\, 1/2\, \rho V_s^2 t_w^2 \qquad (5.12)$$

where

t_w = maximum rudder thickness at water surface

---

[1] p572
2 pp10-13

5.4.1.4.2 Miscellaneous

There are several other parts of the vessel which strike water. Two brackets which brace the rudder laterally are partially submerged when planing. A drag coefficient was estimated for the brackets so the drag force, D_b, may be calculated using equation (5.2)

$$D_b = C_D \tfrac{1}{2} \rho A_f V_s^2 \tag{5.13}$$

where,

C_D = drag force coefficient (= 0.6)
A_f = frontal area (= 0.0012 m^2)
ρ = fluid density
V_s = speed of the planing surface

The drag force vector is assumed to act at a point 50 mm above the keel and in a direction parallel to the keel. No allowance is made for the effect of the hull's boundary layer on the pitot-static tube drag which is considered negligible.

5.4.1.5 Aerodynamic lift and drag

The same aerodynamic theory and coefficients described in section 5.3.2 are applied to the self-propelled case.

5.4.2 Waterjet Forces

5.4.2.1 Control volume analysis

A waterjet system is shown in Figure 5.7 for the purposes of a more detailed analysis. The fluid enters and leaves the control volume horizontally. The hull has sufficient surface behind the cutwater such that streamlines are horizontal and parallel at the transom. Vectors are indicated with bold type. Where the same vector is written in normal type, this indicates a scalar quantity. The control volume begins at face of the protruding stream tube which is located at the ramp tangency point between the delta keel and the beginning of the intake roof. The control volume continues through the waterjet just inside the waterjet surface and ends at the nozzle exit plane.

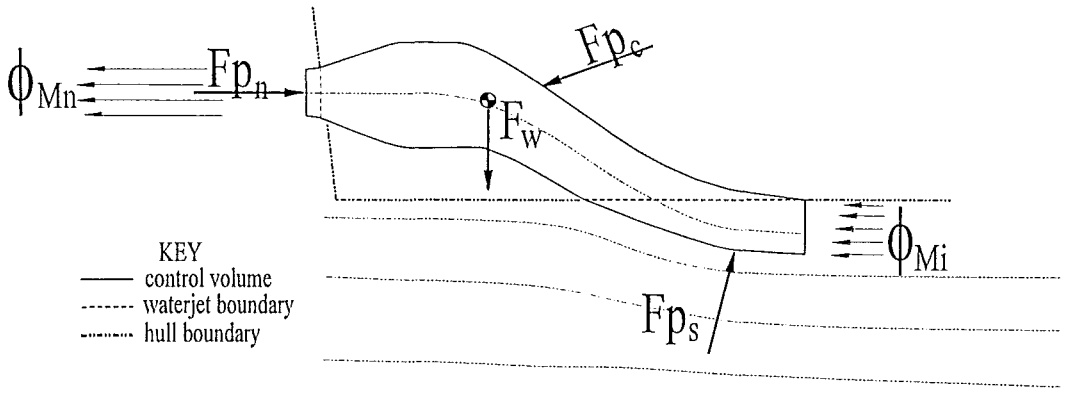

Figure 5.7 Waterjet control volume 1

Only momentum crossing and pressures acting at the control volume boundaries need be considered. Applying control-volume theory to the waterjet system, the following vector equation can be written such that the resultant force on the fluid in a given direction equals the rate of increase of momentum through the control volume in that direction so that,

$$\phi_{Mn} - \phi_{Mi} = \mathbf{Fp_c} + \mathbf{Fw} + \mathbf{Fp_s} + \mathbf{Fp_n} \qquad (5.14)$$

where,

ϕ_{Mn} = nozzle momentum flux
ϕ_{Mi} = intake momentum flux
$\mathbf{Fp_c}$ = pressure force exerted by the waterjet casing on the fluid
$\mathbf{Fp_s}$ = pressure force exerted by the surrounding fluid on the stream tube fluid
$\mathbf{Fp_n}$ = pressure force exerted by the surrounding fluid on the nozzle exit plane
$\mathbf{Fw}$ = force due to gravity acting on the fluid

If the streamlines at the nozzle are parallel then the pressure force $\mathbf{Fp_n}$ can be considered to be one atmosphere or zero.

In order to better understand what is represented by $\mathbf{Fp_s}$ a second control volume shown in Figure 5.8 is drawn around the interface between the waterjet and hull systems. The lower boundary extends down into the fluid sufficiently such that pressure effects due to the intake are negligible and streamlines are horizontal. Buoyancy forces are neglected so **Fw** is not shown.

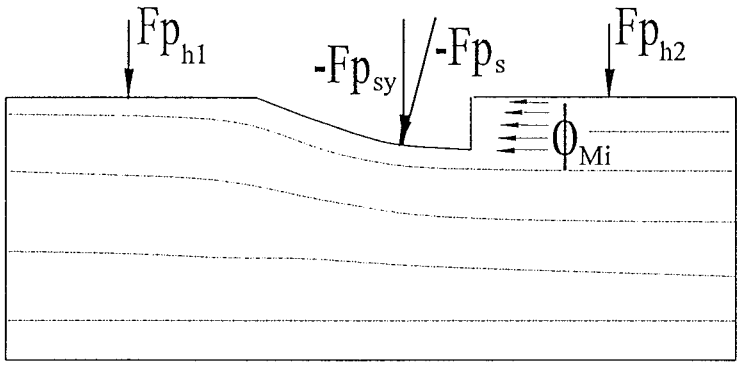

Figure 5.8 Hull/waterjet control volume 1

The stream tube pressure force, $-\mathbf{Fp}_s$ is the force exerted by the stream tube in the waterjet control volume on the fluid and is equal and opposite to $\mathbf{Fp}_s$ in Figure 5.7. The force $\mathbf{Fp}_s$ is required to change the direction of the fluid up into the intake. We are concerned only with forces acting on the hull so will consider momentum flux and pressures acting perpendicular to the hull or as in this case, in the vertical y-direction only. These are designated with a y subscript. If the hull was very large (as shown in Figure 5.8) such that streamlines of the fluid leaving at the transom were horizontal and parallel then it could be assumed that all of $-\mathbf{Fp}_{sy}$ was opposed by an equal and opposite force, $\mathbf{Fp}_h$ which is equal to $\mathbf{Fp}_{h1} + \mathbf{Fp}_{h2}$. Then,

$$\mathbf{Fp}_h = -\mathbf{Fp}_{sy} \tag{5.15}$$

The intake is however not located in the centre of a large flat plate but rather close to the edge of one. In the case of the test boat, the cutwater is 30% of one intake length forward of the transom. A further control volume is shown in Figure 5.9 which has reduced hull surface behind the cutwater such that water leaving at the transom has a vertical component of momentum, ϕ_{Mwy}.

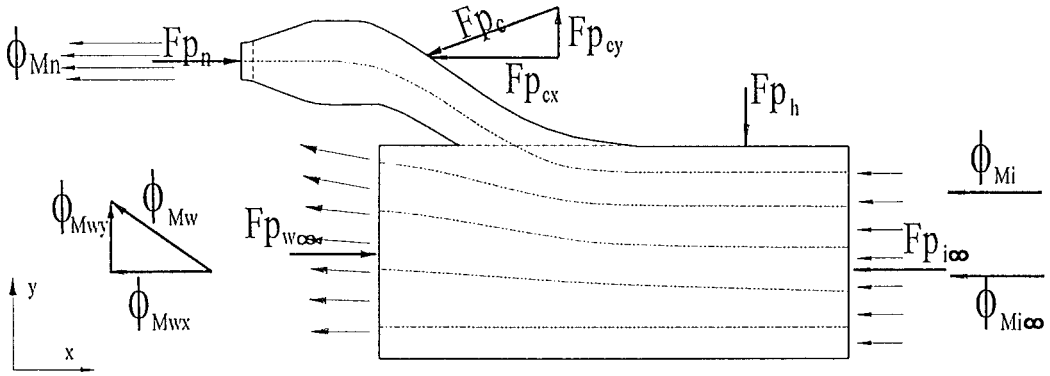

Figure 5.9 Hull/waterjet control volume 2

As Figure 5.9 shows it is likely that not all of $\mathbf{Fp_S}$ is reacted back on the hull but that a component is left as momentum in the wake, so equation (5.15) becomes,

$$\mathbf{Fp_h} = -\mathbf{Fp_{sy}} - \phi_{Mwy} \tag{5.16}$$

where ϕ_{Mwy} is the vertical momentum flux left in the wake due to the stream tube being located near the transom.

Fluid forces can only be felt by the vessel as pressures acting on solid surfaces. Therefore a thrust vector, $\mathbf{T_{ch}}$ is defined as the sum of pressure forces felt by the waterjet casing and the hull. The thrust vector acts on the vessel and is opposite to the pressure forces which act *on* the fluid, so that,

$$\mathbf{T_{ch}} = -(\mathbf{Fp_c} + \mathbf{Fp_h}) \tag{5.17}$$

Now, considering the combined forces acting on the hull and waterjet system shown in Figure 5.9, the following equation can be written.

$$(\phi_{Mn}+\phi_{Mwx}+\phi_{Mwy}) - (\phi_{Mi}+\phi_{Mi\infty}) = \mathbf{Fp_n} + \mathbf{Fp_c} + \mathbf{Fp_h} + \mathbf{Fp_{w\infty}} + \mathbf{Fp_{i\infty}} \tag{5.18}$$

Assuming that the momentum which does not pass through the waterjet system enters and leaves the control volume unchanged (i.e.$\phi_{Mwx} = \phi_{Mi\infty}$) and that Fp_n is equal to 0, then equation (5.18) can be rewritten as:

$$\phi_{Mn} + \phi_{Mwy} - \phi_{Mi} = \mathbf{Fp_c} + \mathbf{Fp_h} + \mathbf{Fp_{w\infty}} + \mathbf{Fp_{i\infty}} \tag{5.19}$$

Substituting equation (5.17),

$$\mathbf{T_{ch}} = -(\phi_{Mn} + \phi_{Mwy} - \phi_{Mi}) + \mathbf{Fp_{w\infty}} + \mathbf{Fp_{i\infty}} \tag{5.20}$$

However the generally accepted definition for thrust acting on the hull, $\mathbf{T_G}$ and that quoted[1] by the ITTC, is in scalar form:

$$T_G = |\phi_{Mn}| - |\phi_{Mi}| \tag{5.21}$$

Clearly this is not the same as equation (5.20). It can be seen that the differences are the vertical component of momentum in the wake and any difference in pressure that may exist between the lower entry and exit planes of the control volume.

If the intake is located some distance from the transom then equation (5.21) could reasonably be considered to account for the forces acting on the waterjet casing. In such a case the streamlines leaving the control volume could be considered parallel and there would be no vertical components of momentum and entry and exit pressures would be the same. However most installations are likely to have the waterjet located near the rear of the hull and the effects described above are likely to occur in these cases. In these instances, if equation (5.21) is used then further forces must be added to account for both the lost lift in the wake and the difference in pressure. It is suggested that these may be significant interaction effects.

In this study no separate attempt has been made to account for the difference in pressure between $\mathbf{Fp_{w\infty}}$ and $\mathbf{Fp_{i\infty}}$. Therefore its effect on the planing hull system is included in the interaction vector.

5.4.2.2 Intake momentum flux

The following theory and assumptions are used to calculate the incoming momentum flux at the front face of the stream tube. For the given stream tube depth the program calculates the fluid velocity, flow rate and momentum flux at heights across the stream tube for a 1 mm strips. By integrating over the face the total flow rate and incoming momentum flux are found.

---

[1] p305

5.4.2.2.1 Hull boundary layer

The hull boundary layer depth and profile was measured using a pitot static tube mounted just ahead of the ramp tangency point. However subsequent analysis found the data to be faulty and insufficient to obtain a reasonable description of the boundary layer. Unavailability of the test boat prevented further investigation causing reliance on the literature and previous experience.

The boundary layer thickness is calculated using Prandtl's equation for a turbulent boundary layer on a flat plate multiplied by an empirical depth coefficient C_{bl}. The coefficient is used to adjust Prandtl's equation for effects such as the favourable longitudinal pressure gradient which serves to reduce the boundary layer depth.

$$\delta = C_{bl} \frac{0.37L}{Re^{0.2}} \tag{5.22}$$

Griffith-Jones (1994)[1] measured the boundary layer on the Hamilton 211 test boat. The test was conducted at a speed of 30 knots. He found that the boundary layer depth was considerably less than that predicted by Prandtl's equation. This result is confirmed by Stephens (1972) and Purnell (1978). Both found δ to be 25% and 40% less respectively than Prandtl for a trim angle of 3 degrees. The explanation for this given by Purnell[2] is the favourable pressure gradient under the hull which suppresses growth of the boundary layer. The boundary layer depth is therefore assumed to be 30% less than that predicted by Prandtl with however, an error band of ±10% so C_{bl} = 0.7±0.1.

The velocity profile in the boundary layer is described as:

$$V = V_s \left(\frac{y}{\delta}\right)^{\frac{1}{n}} \tag{5.23}$$

where n usually takes a value between 5 and 9. Stephens[3] (1972) found n to take a range of values from 6.8 to 7.2 for Re =1-1.7E7.

---

[1] p33
[2] p4
[3] p54

Griffiths-Jones also measured the boundary layer velocity profile at a Reynolds number of 2.6E7. He found n to be 6.8. This falls well into the range of the data collected on the 271 Test Boat(1.5-3.5E7). The hull material for both boats is identical, being bare welded aluminium plate. Therefore the roughness could be considered to be very similar. MARIN, who conducted scale model tests measured a profile which closely fitted a 1/7th power law.

Haglund (1982) uses a 1/9th power law, however Re is considerably higher at 2.2E8. For all cases equation (5.24) used by Purnell[1] gives a reasonable approximation.

$$n = \log_{10} Re \tag{5.24}$$

A ±10% error is applied to n. Combining equations (5.22),(5.23) and (5.24), the velocity within the boundary layer is described as,

$$V = V_s\left(\frac{y\,Re^{0.2}}{0.26\,L_k}\right)^{\frac{1}{\log_{10} Re}} \tag{5.25}$$

The uncertainty on V can be calculated using accepted techniques (Barford (1985)) and is determined by the following equation,

$$\frac{\delta V}{V} = \frac{1}{\log_{10} Re}\sqrt{\left(\frac{\delta Re}{5Re}\right)^2 + 0.1^2 + \left(\frac{\delta L_K}{L_K}\right)^2} \tag{5.26}$$

For example, if the error on Re and L_k is 5% and the error on V_s is 1% then the error on local velocity V is calculated as 1.5%.

5.4.2.2.2 Stream tube shape

The literature contains different suggestions as to the effective width and shape of the stream tube. Some (Svensson (1989), Etter et al (1980)) assume a rectangular stream tube with a width being that of the intake itself.

[1] p4

However Haglund (1982) reports an elliptical shape and a wider width. Discussion in ITTC'87[1] states *"Further analysis of the width to be used in calculations is recommended"*

Griffith-Jones has tested a Hamilton 211 intake in the closed circuit wind tunnel. This waterjet is 20% smaller than the Hamilton 271 used in this project however the

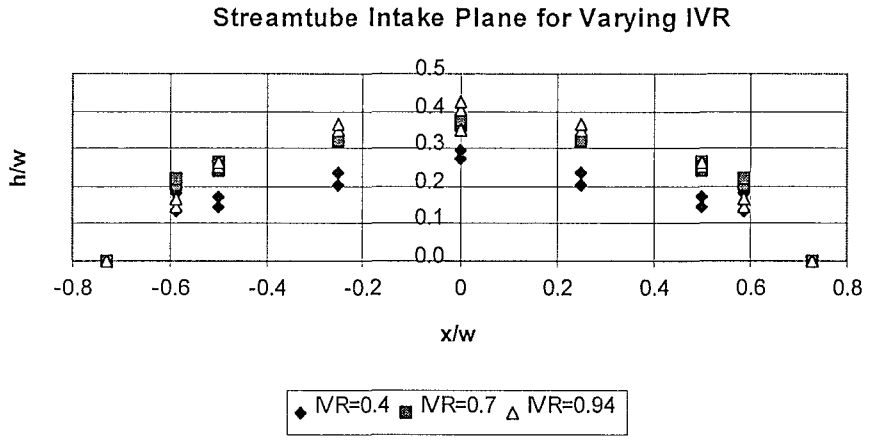

Figure 5.10 Crossection of stream tube at ramp tangency point

intake geometry is similar. Smoke tests were used to determine the shape of the front plane of the incoming stream tube. This plane coincides with the boundary of the waterjet system control volume. The air flow through the waterjet was controlled by adjusting a flap on the outlet side of the waterjet well down stream. At each flap setting the IVR was found by conducting a hot wire velocity traverse of the duct and integrating to find the flow rate.

The intake velocity ratio is considered to have the biggest effect on the stream tube shape. In the study IVR was well matched which would suggest that the reported stream tube shape is realistic. Figure 5.10 depicts the shape (not to scale) of the intake plane measured for a variety of IVR settings. See also Figure 5.1.

[1] p305

It can be seen that the stream tube deepens with increasing IVR. The stream tube remains consistently 50% wider than the intake at all IVR conditions. This is confirmed for one speed setting by data in the JIP report by MARIN (1991)[1].

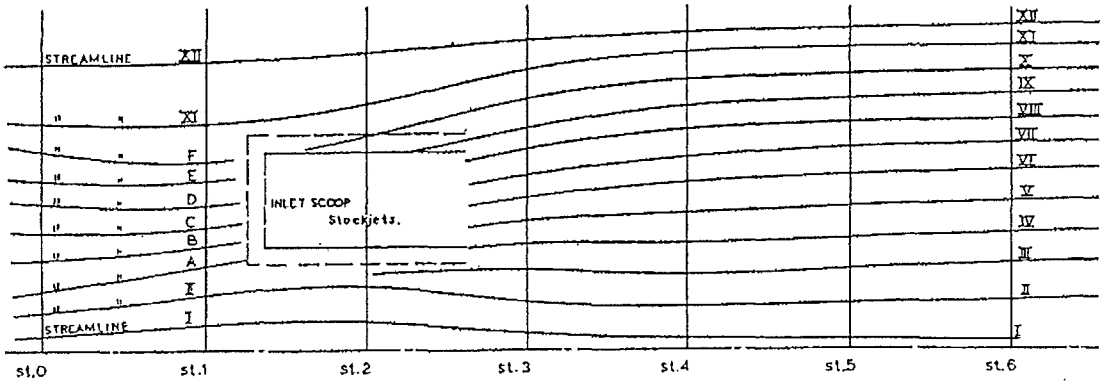

Figure 5.11 Streamlines on hull afterbody (MARIN (1991))

Streamlines on the hull after-body in the inlet region are shown in Figure 5.11 for a speed of 30 knots (F_V= 2.1). The flow is from right to left. Similarly the front face of the ingested stream tube can be seen to be 50% wider than the intake, i.e. from streamline IV to just beyond streamline X. It is not known what the IVR setting was. It should be noted that the vessel had two waterjets fitted, one either side of the keel.

The stream tube intake plane is partially elliptical although rather pointed at the centre. The shape of the intake plane is therefore assumed to be elliptical, such that it conforms to the equation:

$$y = h_S \sqrt{1 - \frac{x^2}{\left(w_S/2\right)^2}} \qquad (5.27)$$

where h_S is the assumed height of the stream tube and w_S is the full width of the stream tube.

[1] pF24

The wider stream tube skims off more of the slower moving boundary layer and therefore gives rise to a higher wake factor. At cruise conditions, the wake factor is approximately 6% for the elliptical stream tube compared with 4% for the rectangular case. Another effect is a movement of the centre of incoming momentum. Since the elliptical stream tube used in the computer program calculations is flatter than the rectangular one, the centre of momentum is moved upwards approximately 20% of the stream tube depth. This has the effect of reducing the bow-down pitching moment of the jet.

5.4.2.3 Nozzle momentum flux

At a given flow rate the nozzle momentum is calculated by assuming a volumetric nozzle velocity, i.e. one found by dividing the flow rate, Q, by the nozzle area A_n. The following equation is used:

$$\phi_{Mn} = C_{\phi M} \rho Q \frac{Q}{A_n} \tag{5.28}$$

where $C_{\phi M}$ is a small momentum correction coefficient based on full scale data. This accounts for the difference between the volumetric average velocity and the momentum average velocity. $C_{\phi M}$ was found by experiment during the propulsion tests to take a near constant value of 1.0015 which is extremely small however the factor is retained for completeness.

5.4.2.4 Thrust vector

The magnitude of the thrust vector is found in accordance with equation 7.1 by calculating the net increase in momentum in the horizontal and vertical directions and then adding each component to find the resultant. The angle of action to horizontal is calculated from the components trigonometrically. The moment arm between the thrust vector and the centre of gravity is also required for the free body model. The total moment caused by the nozzle and intake momentum fluxes are calculated separately with knowledge of the hull and waterjet geometry. The total moment is then divided by the total thrust force to find the moment arm.

5.4.3 Interaction Vector

As described in section 5.2.3, an extra vector is added to the model to account for various interaction effects. This vector will be termed the *interaction vector*. The interaction vector will be used only to represent pressures acting on the hull so therefore can only act perpendicular to the hull. It is positioned near the stern and the moment arm to the centre of gravity is given. There is not sufficient knowledge to calculate the magnitude and position of the interaction vector directly. Therefore it is the aim of the procedures outlined in section 5.2.3 to find this vector. In the computational model the interaction vector was varied until the full scale data was matched as closely as possible.

5.4.4 Equations of Static Equilibrium

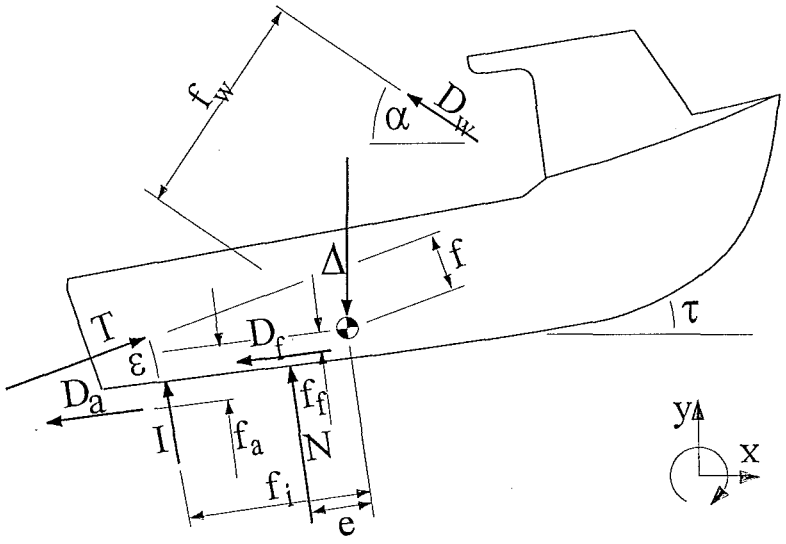

Figure 5.12 Free Body Diagram (Propulsion Case)

The following equations are developed to describe the hull planing in static equilibrium. They differ from the towing case in that the towing force vector **W** has been replaced by the thrust vector **T** which acts at an angle of ε to the keel, and the interaction vector **I** has been added. Assuming that the free body is in a condition of static equilibrium, three equations can be written summing the vertical and horizontal forces and moments to zero:

Vertical forces:

$$0 = (N + I)\cos\tau - (D_f + D_a)\sin\tau + D_w \sin\alpha + T\sin(\tau + \varepsilon) - \Delta_0 \qquad (5.29)$$

Horizontal forces:

$$0 = T\cos(\tau+\varepsilon) - (D_f + D_a)\cos\tau - (N+I)\sin\tau - D_w\cos\alpha \tag{5.30}$$

Moments:

$$0 = Ne + If_i + D_f f_f - D_w f_w + D_a f_a + Tf \tag{5.31}$$

Combining equations (5.29) and (5.30), eliminating N and solving for T,

$$T = \frac{D_w\cos(\tau+\alpha) + D_f + D_a + \Delta_0\sin\tau}{\cos\varepsilon} \tag{5.32}$$

Combining equations (5.29) and (5.30), eliminating T and solving for N,

$$N = \frac{\Delta_0\cos(\tau+\varepsilon) + (D_f + D_a)\sin(\varepsilon) - D_w(\sin(\varepsilon+\alpha)\cos\tau + \cos(\varepsilon+\alpha)\sin\tau)}{\cos(\varepsilon)} - I \tag{5.33}$$

Substituting equations (5.32) and (5.33) into equation (5.31),

$$\begin{aligned} 0 = {} & \Delta_0(f\sin\tau + e\cos(\tau+\varepsilon)) + (D_f + D_a)(f + e\sin\varepsilon)\ldots \\ & + D_w\left(f\cos(\tau+\alpha) - e(\sin(\tau+\varepsilon)\cos\alpha + \cos(\tau+\varepsilon)\sin\alpha)\right)\ldots \\ & + (D_f f_f + D_a f_a - D_w f_w)\cos\varepsilon\ldots \\ & + (f_i - e)I\cos\varepsilon \end{aligned} \tag{5.34}$$

Moment equation (5.31) is now in terms of variables which are either given or can be calculated. As with the towing model, τ can be varied until the moment equation is satisfied.

5.4.5 Correction Functions

The correction functions calculated in section 5.3.5 are applied to the thrust, wetted keel length and trim respectively. The Blount and Fox modification factor is also applied as it was in the towing case.

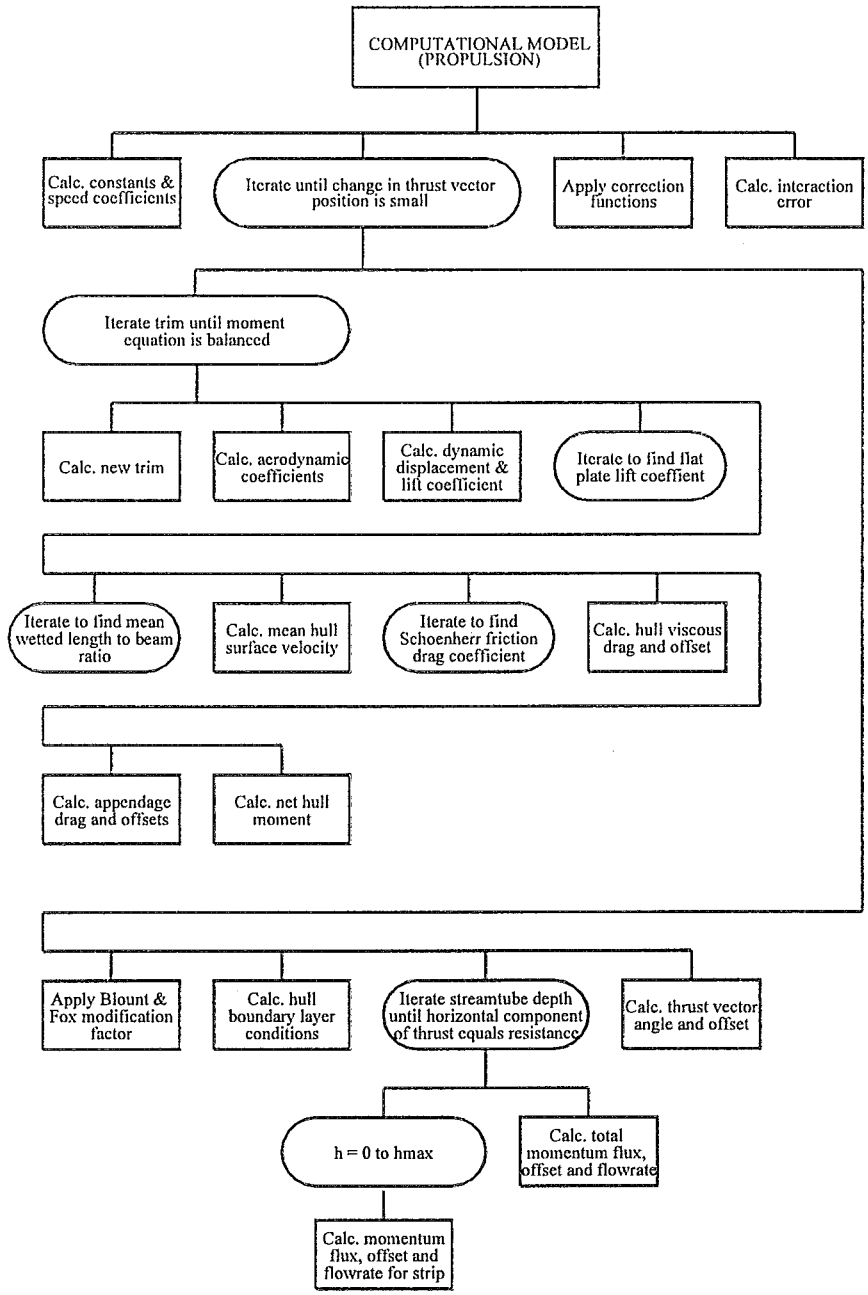

Figure 5.13 Computational structure diagram (self propelled case)

5.4.6 Computational Procedure

Once the self propulsion program has completed a first pass of the hull resistance calculations and an initial estimate of the resistance has been made, the direction and position of the net thrust vector must be calculated. Then the resistance calculations are repeated with the new thrust vector applied to the free body. The entire process is repeated until subsequent iterations fail to produce any significant variation in the

output data. Figure 5.13 shows a schematic structure diagram of the procedures in the computer program.

5.5 Finding Interaction Vector

As previously described in section 5.2.3, the interaction vector is found by comparing the results of the computational model to smoothed functions of the full scale data as shown in the structure diagram in Figure 5.14.

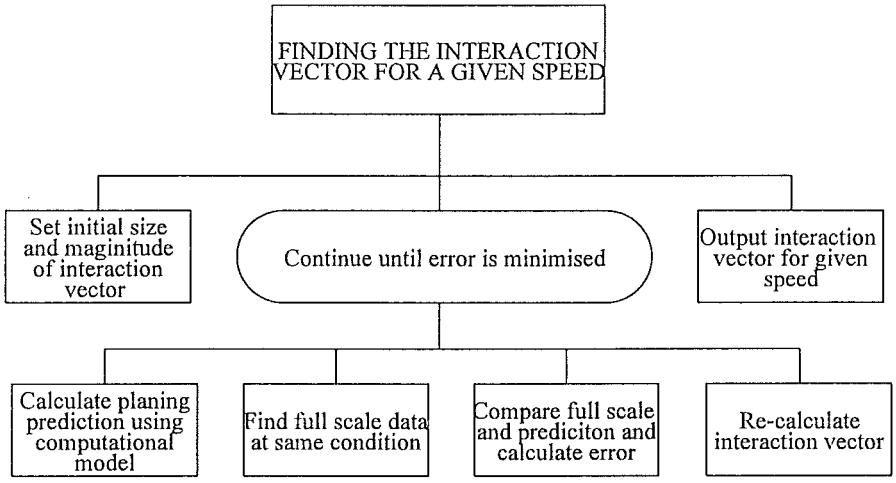

Figure 5.14 Computational structure diagram of the procedure used to find the interaction vector

At a given speed the size and position of the interaction vector is varied until the minimum possible error when compared to the full scale propulsion data is obtained. The parameters which are compared are, resistance, wetted keel length, and the keel trim. The interaction error, i_error, is a *sum of squares type* defined as,

$$i\_error = R_T error^2 + L_K error^2 + \tau error^2 \tag{5.35}$$

where each parameter error is defined as the percentage difference between the parameter for the computational model and the full scale data. For example for the error on resistance is,

$$R_T error = \frac{R_{T\_FS} - R_{T\_COMP}}{R_{T\_FS}} \times 100 \tag{5.36}$$

Once the i_error is minimised the interaction vector magnitude and position is recorded and the program then begins afresh at the next speed setting.

5.6 Conclusions

This chapter is briefly summarised below.

- An interaction vector has been defined which may be added to the existing computational model described by Hadler (1966).
- The interaction vector accounts for all pressure forces acting on the hull not included in the existing model.
- A method for finding the empirical interaction vector has been described where by the theoretical model is compared to the full scale data and interaction chosen to provide the best possible fit.
- A key assumption is that the Savitsky equations for centre of pressure are unaffected by the interaction vector.
- The displacement is allowed to vary in the dynamic condition.
- Three most likely contributors to the interaction vector are considered:
    1. The net momentum increase through the waterjet i.e. consider lift, thrust and moment caused by waterjet.
    2. The loss of planing surface
    3. Lost lift in the wake
- Interaction effects on the water jet performance are limited to the wake factor. The static pressure at the intake is assumed to have a negligible efect on thrust.
- The shape of the ingested stream tube is assumed to be elliptical and a constant 50% wider than the intake.
- Aerodynamic loadings are considered in some detail.

6. Tow Testing

6.1 Introduction

Due to the difficulty of exactly matching test conditions at full scale for both the propulsion tests and towing tests, a theoretical model was required to produce a baseline line planing condition at any specific speed and loading condition. It was decided to use the Savitsky (1964) equations as a base form for the model. Experience at CWF Hamilton and Co. Ltd. has proved the Savitsky method to be reliable as evidenced by its continued used today. The theoretical model is covered in more detail in section 5.3.

In order that the computational model could be checked for accuracy, full scale planing data was required for the bare hull. These data were gathered by conducting full scale and model towing tests. Once complete the data were compared to the computational model and small correction functions of speed calculated to map the computer program more precisely onto the actual data. It is assumed that the correction functions hold for the computational propulsion model.

Two separate test series were performed, model tests conducted at The Marine Research Institute of The Netherlands (MARIN) and a full scale towing test which was conducted in Lyttelton Harbour, New Zealand by the author.

6.2 Full Scale Tests

6.2.1 Introduction

Full scale resistance tests were carried out to better determine the validity of the theoretical model. Tests were conducted on three separate days during the months of September, October and December 1994. An initial shakedown test was required to check the general concept and refine the equipment. Following the shakedown test, some modifications were made to the equipment and then two days of actual testing were conducted.

6.2.2 Towing Site

A site in Lyttelton Harbour near Christchurch was chosen for conducting the full scale towing test. The location is marked on the marine chart excerpt shown in

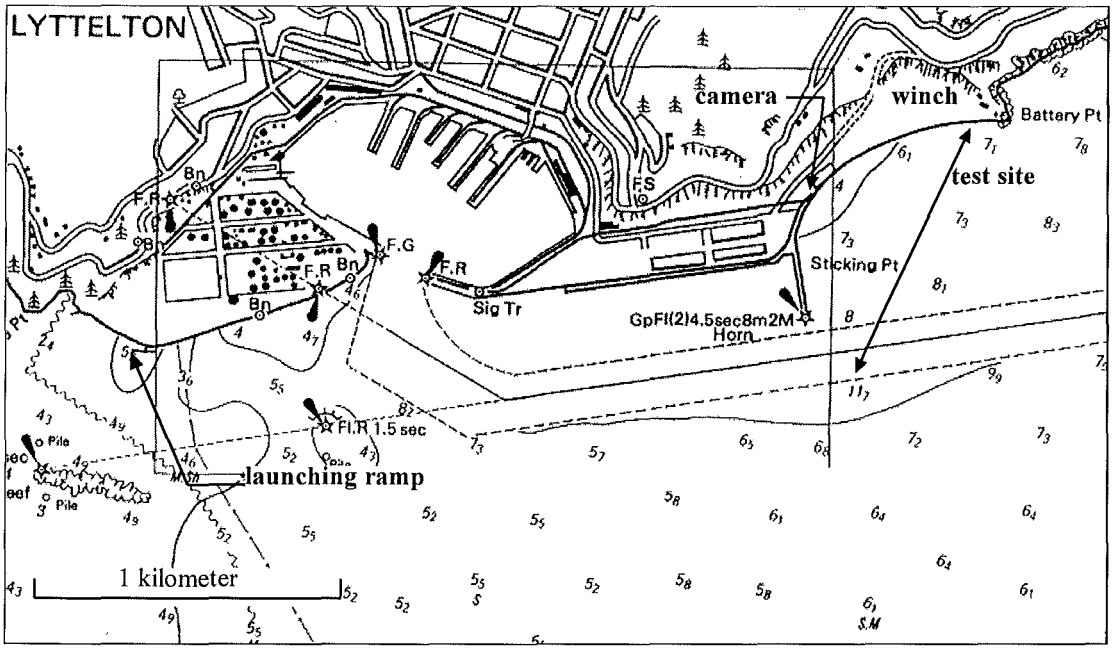

Figure 6.1 Towing test site in Lyttelton harbour

Figure 6.1. There were several requirements for the site. These included, shelter, access, security and reasonable water depth.

Lattore (1982)[1] has shown that as the depth increases beyond that equal to the boat length, the effect on resistance and it is assumed, all other planing characteristics, is small i.e. less than 1-2 percent. As can be seen on the chart, the chosen site is one of the few places in the harbour where the depth exceeds 7 m at low water. To be doubly sure that depth effects were not at issue the propulsion test series were conducted at the same location, any effect will be represented equally and so cancel when assessing differences between propulsion and towing.

The winch site was in fact in a prohibited quarantine area at Battery point, access to which required special permission. This had the benefit of keeping the general public well clear and ensuring security for equipment which was stored at the location for several months.

6.2.3 Winch and chase boat

The boat was towed using a 150 kW winch custom built for launching sailplanes pictured at the test site in Figure 6.2.

[1] pp5-4

Sticking Point break water can be seen in the middle distance. The winch drive line is fitted with a hydrodynamic torque converter which enables a gentle increase in towing force without the need to change gears.

Figure 6.2 Winch and test boat at test site

The winch is fitted with several wires however on day one these proved inadequate. Tensile strength calculations had not allowed for kinks and joins in the wire and it failed several times while trying to accelerate the boat onto the plane. A new cold drawn 4.5 mm diameter wire (ultimate tensile strength 1200 MPa) 1200 m in length was purchased and wound onto the drum. This proved entirely successful, not breaking once during the remaining tests.

The Hamilton 211 Test Boat was used as a chase boat for positioning and manoeuvring the larger 271 Test Boat. The 211 test boat is a small 4.5 m river boat used for development of smaller waterjets.

6.2.4 Hull geometry and loading condition

The hull geometry was identical to that of the subsequent propulsion testing with the exception that the intake was blocked off with a cover plate. This was achieved by removing the intake grill and fitting a specially constructed cover plate as recommended by the ITTC (1987) and specified by Etter et al (1980) and shown in

Figure 6.3. Etter states[1]: *"the inlet portion is blocked by a tare block which extends from the ramp tangency point to the lip step"*

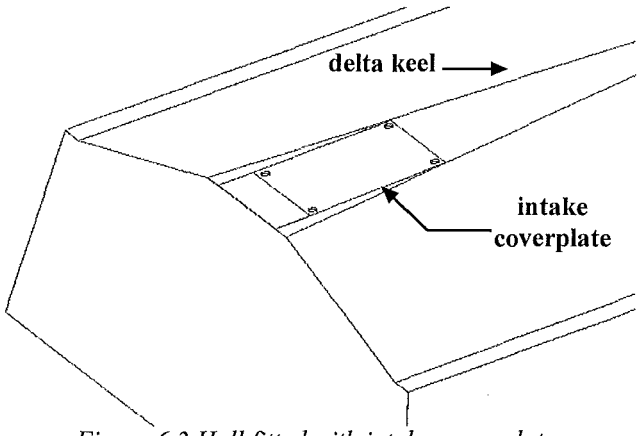

Figure 6.3 Hull fitted with intake cover plate

The hull loading condition was carefully measured and calculated. A sample calculation sheet using the spreadsheet Excel is shown in Table 6.1, in this case run 8 on day 1 of testing.

The empty hull was weighed to determine its unloaded static displacement. This was achieved using a lifting beam attached to lugs welded on the topsides of the hull, the whole arrangement then being lifted by an overhead crane. A load cell built and calibrated by the author, was placed between the hook and beam. The lateral position of the centre of gravity in this condition was determined by adding a known mass at a known distance from the lugs, then measuring the angle through which the hull has rotated. The position of the CG could then be calculated. The loading sheet then accounts for every additional item placed in or on the hull. Every item's position was entered along with an associated estimate of the error. The final hull loading can then be calculated along with its associated uncertainty. The fuel load and any entrained water in the waterjet system required particular consideration.

The fuel load posed a particular problem given its ability to move about at different angles of trim. However draining all fuel from the fuel tank proved a difficult and time consuming process so it was decided to leave the fuel in the tank and calculate the loading. The fuel tank is long and slender and mounted longitudinally under the floor in the middle of the hull just forward of the engine. Computer program

[1] p799

FUEL.C, a listing of which can be found in Appendix A-7.3, was written to calculate the fuel load and the position of its centre of gravity given a dipstick measurement and the hull trim angle at the time. It was found that over the range of trim angles likely to be encountered, the total effect of the moving fuel on LCG was likely to be no greater than ±3 mm which was considered negligible.

It is usual practice to include the weight of entrained water in the calculation of displacement and LCG. In the case of the towing tests however the waterjet is not operating so there is no entrained water. Ideally the system would be completely sealed and made water-tight. However it was felt that small leaks were inevitable so the nozzle was left unplugged to allow any leakage to drain once the wake was separating cleanly around the transom and the hull had attained a reasonable angle of trim.

Table 6.1 Sample loading calculation sheet

Item	*Weight*	*+/-w error*	*x pos*	*+/-x error*	*y floor*	*y pos*	*+/-y error*	*x mom*	*x mom err*	*y mom*	*y mom err*
Units	N	N	m	m	m	m	m	Nm	Nm	Nm	Nm
DELTAoo	19982	52	2.741	0.016	0.641	0.683	0.124	54771	462	13648	2513
Person 1	766	10	4.9	0.03	0.721	0.736	0.01	3753	72	564	15
Person 2	0	10	5.3	0.03	0.736	0.736	0.01	0	0	0	0
Tools	179	0.5	4	0.5	0.688	0.788	0.05	716	92	141	9
Battery	0	1	0.5	0.02	0.558	0.3	0.01	75	4	45	2
xdcr	50	10	6.91	0.01	0.795	0.63	0.01	1037	71	95	8
Wind Mast	31	0.5	4.99	0.02	0.724	3.42	0.01	155	3	106	2
Ballast 1	2300	52	2.153	0.01	0.619	0.913	0.01	4952	135	2100	70
Ballast 2	2280	52	2.153	0.01	0.619	0.913	0.01	4909	135	2082	70
Entrnd W.	0	20	0.3	0.05	0.551	0.25	0.05	0	0	0	0
Man. Tank	170	10	0.8	0.02	0.570	1	0.05	136	11	170	19
-Batt.	-37	0.5	1.07	0.01	0.579	0.679	0.01	-40	1	-25	1
P. Supply	23	0.5	1	0.01	0.577	0.657	0.01	23	1	15	1
Ballast 3	722	1	-0.2	0.01	0.533	0.71	0.01	-144	7	513	8
W y*	0	1	0.63	0.005	0.563	0	0.01	0	0	0	0
W x	0	1	6.91	0.01	0.795	0.63	0.005	0	0	0	0
Fuel	947	10	3.414	0.019	0.666	0.341	0.010	3233	52	323	12
TOTAL	27413	95						73575	521	19776	2515
in kg	2794										

							Calculated Condition	Loading	
		RUN:	8				DISP (N)	27413	+/- 95
							LCGx (m)	2.684	+/- 0.028
	Weight(N)	+/-w err.	xf pos	+/-x err.	yf pos	+/-y err.	LCG (m)	2.494	+/- 0.028
Fuel	947	10	0.702	0.014	0.166	0.003	VCGx (m)	0.721	+/- 0.094

6.2.5 Instrumentation system

A schematic of the instrumentation system designed and built by the author for the Hamilton test boat is shown in Figure 6.4. A critical limitation on the system was

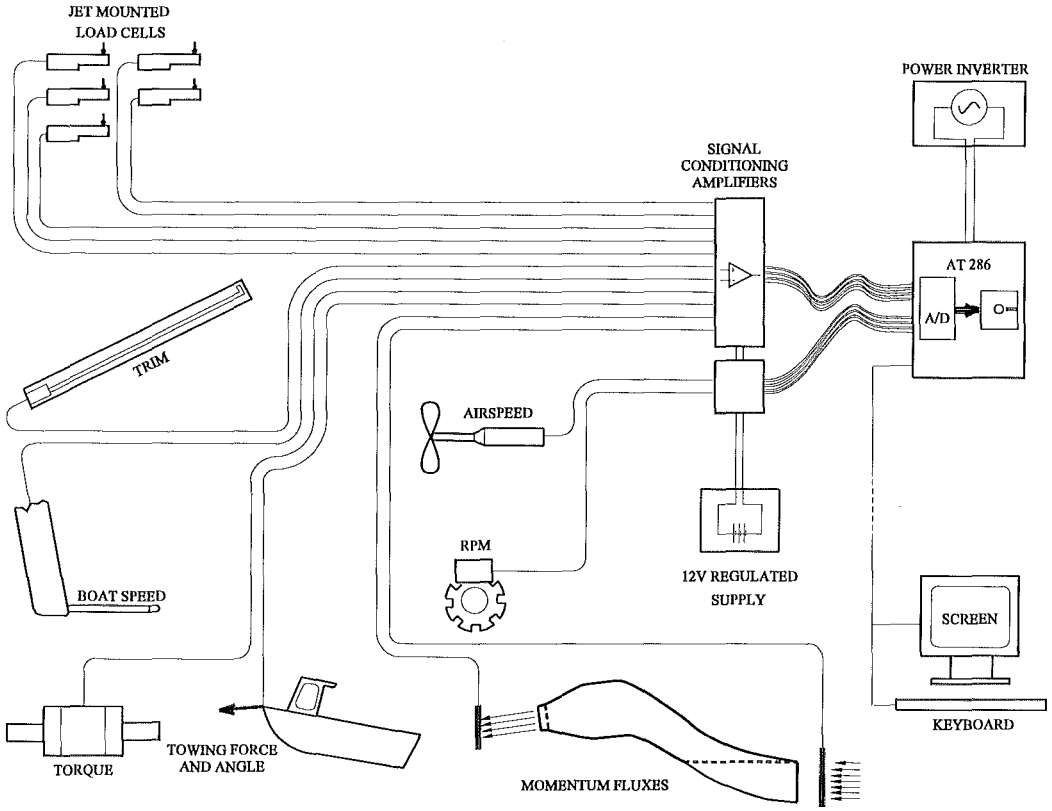

Figure 6.4 Data acquisition system

one of cost. This necessitated the use of a home computer which was a fraction of the cost of "hardened" industrial data loggers. The core of the system is an IBM compatible PC-AT 286 computer fitted with an Advantech PCL812 A/D interface card. Electrical power at 240 volts AC was supplied to the system from the engine's 12 volt system via a quasi sine wave DC/AC power inverter. Earlier in the program a portable generator was used however this proved to be unreliable.

Signal conditioning amplifiers were designed and built at the Department of Mechanical Engineering using an Analogue Devices IB13AN integrated signal conditioning amplifier chip. Only a dozen further components were required to complete the amplifiers to the required specification. Input channels were sampled at 10 Hz, the sampling rate being chosen to provide a reasonable compromise between file size economy and sufficient measurement of the parameters.

Data was displayed in real time on the screen mounted in the cabin. This enabled the monitoring of data collection as it happened and allowed problems to be solved if

they arose during testing. In this way a day's testing could be salvaged if part of the system malfunctioned.

The following parameters could be recorded by the data acquisition system: engine speed, boat speed, intake momentum flux, shaft torque, wind speed, towing load, nozzle momentum flux and the hull's trim angle. Not all of these were relevant to the towing tests. The load cells shown in the diagram were not finally used in the propulsion tests.

6.2.6 Measurements taken

Table 6.2 shows the parameters and the manner in which they were recorded during tow testing. Not all data was recorded using the computer. Some was manually noted while the trim and wetted length were recorded photographically.

Table 6.2 Recorded parameters

Parameter	*Units*	*Computer*	*Photographs*	*Manual*
Time of day	h:m:s.00	√		
Boat Speed, V_s	m/s	√		√
Apparent Wind Speed, V_w	m/s	√		
Total keel trim, τ	deg	√	√	
Towing force, W	N	√		
Towing angle, α	deg	√		
Wetted keel length, L_k	m		√	
LCG	m			√
Static displacement, Δ_0	kg			√

6.2.6.1 Boat Speed

The boat speed was measured using a pitot-static tube and also a hand-held radar gun from within the boat. The radar gun was aimed at a prominent object on the shore and a number of measurements taken and then averaged. This technique yields the ground speed which may not be the same as the speed through the water if a current is running. However tests were conducted at or near slack tide so tidal movements were minimal. The radar gun provided the most reliable measurements.

The systematic error was assumed to be within the level of significance displayed, i.e. ±0.028 m/s. The standard random error was approximately ±0.008 m/s using an average of 6-8 readings. Taking twice the standard error, and adding the systematic

error gives a total error of ±0.044 m/s to a confidence interval of 95% which is equal to ±0.6% on a typical speed of 7 m/s.

6.2.6.2 Wind Speed

The wind speed was recorded using a gill type anemometer mounted on a 4m high mast. The purpose of this was to allow calculation of the aerodynamic forces especially in gusts which may give high momentary apparent wind speeds. However the final testing speeds were not high and the weather generally mild. The change in resistance due to wind gusts was actually very small fraction, of the total thrust, and random so in the final calculations the boat speed over the water was used to calculate the aerodynamic lift and drag.

6.2.6.3 Trim and Wetted Keel Length

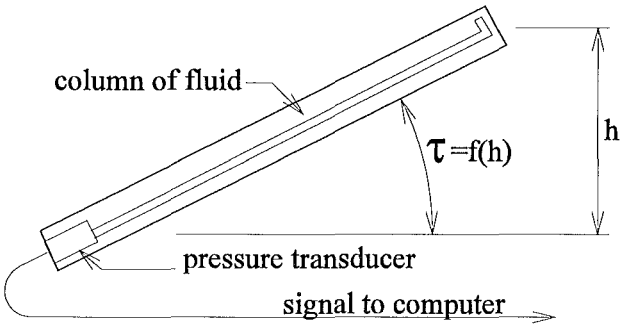

Figure 6.5 Trim meter

Two methods were used for measuring the trim. A device, shown in Figure 6.5, was developed by the author to measure trim in real time, feeding a signal to the computer system. It is based on the principle that the angle of an inclined column of fluid is related to the pressure measured at the bottom, trigonometrically. The system worked reasonably well, however it was found that it was susceptible to accelerations both vertical and horizontal. If the output was averaged over a large number of readings then variations in the signal due to accelerations could be reduced sufficiently. However there were problems. An accelerometer would have been preferable in practice, being less susceptible to thermal drift and more robust.

Finally however, the site permitted still photographs to be taken from the shore and this method was preferred. There were some instances when photographic data was

not sufficient. In these cases data from the trim meter was used to help estimate the missing data points.

The camera position is marked in Figure 6.1. When the boat reached a position abeam of the camera 3-4 photographs were taken in close succession. The exact time would be recorded using a stop-watch synchronised with the on-board computer clock. Later, data from the computer record at that exact time would be matched up with the photographs.

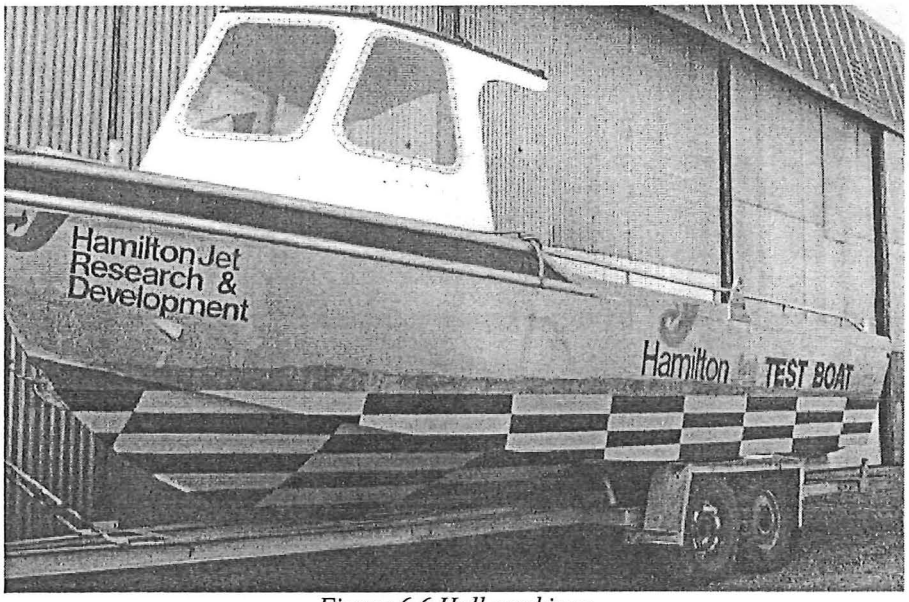

Figure 6.6 Hull markings

Hull markings painted on the side of the boat, shown in Figure 6.6, were then used to measure off the trim angle to the horizon which was considered to be horizontal. The wetted length L_k, also determined in this manner. The block markers were of a known length enabling an easy measurement. The combined readings were averaged to obtain the trim within ±0.3 deg and wetted keel length within ±0.15 m on average.

Earlier in the project it was thought that the testing would take place across a bay on the southern side of Lyttelton harbour where there was no suitable spot to mount a shore based camera. An instrument to measure the draft was developed by the author and is shown in Figure 6.7. The device, in the form of a faired bar, is marked with graduations and penetrates the water at the bow. It is mounted on a vertical

shaft forward of its centre of pressure. In this manner the bar trails. A small plate welded to the back of the ruler at the bottom assists the trailing action.

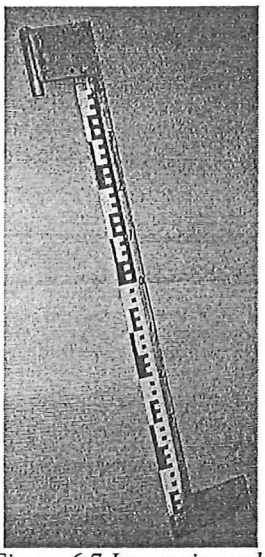

Figure 6.7 Immersion ruler

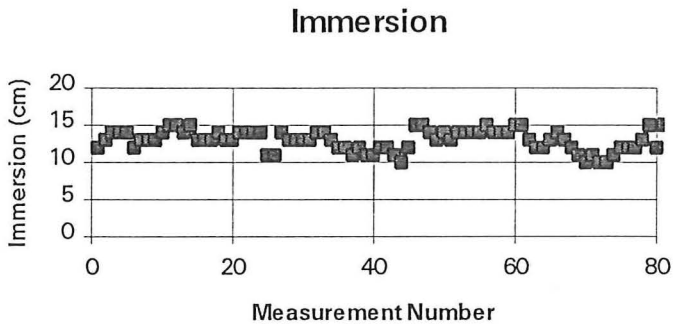

Figure 6.8. Typical immersion recording

A VHS video camera mounted on a bracket on the side of the hull views the ruler. A recording can then be made of the position of the water surface. By advancing the tape frame by frame and recording the immersion over a number of cycles an accurate average may be obtained. Figure 6.8 displays immersion data lifted from a typical recording, in this case at 20 knots.

VHS records at the rate of 24 frames per second, therefore the 80 frame recording is 3.33 seconds long in real time. The average of the 80 immersion recordings is 13.07 cm. The standard deviation is 1.37 cm. The error to 95% confidence is only +/-3 mm indicating that the system may be suitable for further work. However, to measure the draft at the bow and stern, the trim angle is also required to a reasonable degree of accuracy. Given the problems encountered with the trim meter there was some doubt whether this could be achieved so it was with some relief that the alternative site was found and the shore based camera technique proved suitable.

6.2.6.4 Towing Force and Towing Angle

A device was designed and built by the author to measure the towing force and angle. It is shown in Figure 6.9 fitted to the bow of the boat. The device consisted of a strain-gauged aluminium element clamped to a horizontal shaft at one end and connected to the tow wire via a shock absorbing spring and swivel at the other. The

shaft was mounted in ball bearings to allow free movement of the element in a vertical plane. A signal conditioning amplifier was housed in a case attached to one side (far side in photo) of the bearing housing, close to the strain gauge to eliminate noise in the gauge signal. The strain gauged element was re-calibrated before and after each days testing using the lifting load cell to within ±40 N. Averaged signals from the transducer yielded a total average error on the towing load W of ±124 N or ±2.7% on a reading of 4.5 kN.

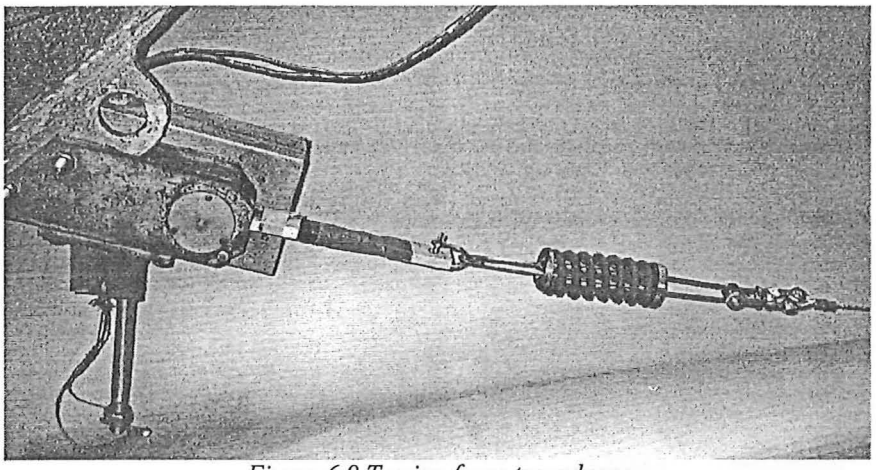

Figure 6.9 Towing force transducer

One end of the shaft also entered the case and was fitted with a toothed quadrant which drove a pinion gear in turn mounted on the shaft of a precision potentiometer. Voltage output from the potentiometer varied linearly with the angle of the element and was calibrated to within ±0.2 deg. The threaded shaft protruding from the bottom of the housing was for the purposes of mounting the immersion ruler which was never used, as discussed earlier.

6.2.7 Daily testing procedure

Testing was conducted in Lyttelton Harbour located approximately 25 minutes drive from the premises of CWF Hamilton and Co. Ltd. A number of variables had to come together at one time for a test to go ahead. The weather was of primary concern, in particular the sea conditions. Testing generally began early, to beat the north east sea breeze that blows up the harbour latter in the day. The following personnel and equipment was required for a days testing:

- 273 Test Boat, trailer and truck
- 211 Test Boat(chase boat), trailer and towing vehicle

- 200 kW glider winch
- winch operator and assistant
- chase boat driver and assistant
- camera man
- the author as 273 Test Boat operator

Upon arrival at the launching ramp marked in Figure 6.1, the computer was started and loaded with the data acquisition software, Labtech Notebook. Date and time settings were checked and reset as required. The boat hull was then prepared, removing the tail-light board and fitting drain bungs, wind anemometer, ballasting, video camera(if required) and towing transducer. The chase boat was then launched, started and prepared to assist in the launching of the test boat. Meanwhile, at the test site the winch crew were moving the winch into position, starting and warming the engine.

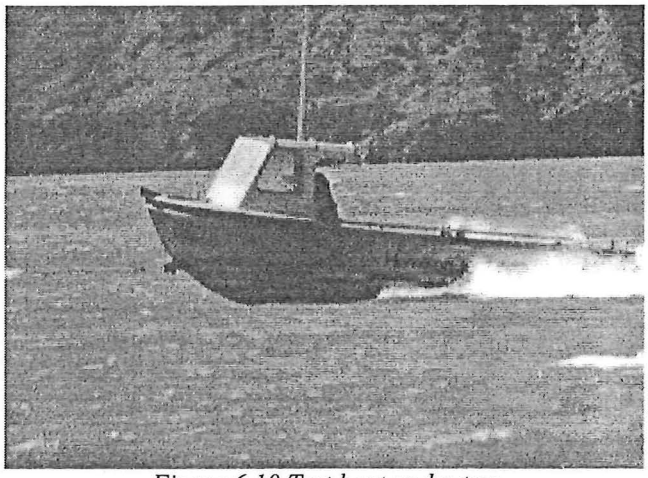

Figure 6.10 Test boat under tow

Initial calibration was then carried out on the slipway, checking the trim meter and towing transducer. A portable load cell was used to calibrate the towing transducer by placing it in series with the transducer and using the launching trailer winch and cable to tension both devices simultaneously. All other transducers were then checked for sensible looking output and if appropriate, their zero values recorded.

The boat was then launched by reversing the trailer into the water rapidly and then applying full braking as no reverse thrust was available due to the blocked intake. The chase boat would then come alongside and a line would be fixed between the two boats. The chase boat would then tow the test boat to the test site. This task would take approximately 20 minutes.

Upon arrival at the test site the test boat was anchored 100 metres offshore while the chase boat would go to shore where the winch wire would be passed to an assistant. The wire was then dragged out to the test boat and connected to the load cell with a

secondary jumper rope connected several metres along the cable taking the load to protect the load cell from any sudden jerking or snagging during the tow out to the start of the test course.

Once in position at the start of the course, the jumper was released and the winch operator was informed by radio to take up the slack and gently begin the tow. Initially there was generally considerable surging, with the wire sinking and rising off the sea bed like a spring however once a reasonable speed was reached the situation stabilised. The test boat operator (the author) would command increasing power until the desired speed was reached for that run. The tow would continue past the camera position by which time the speed would have stabilised. Once the boat was within 150-200 m of the shore, a command to stop would be issued. The test boat would quickly come to rest, the chase boat would come along side and preparations would then begin for the next test.

6.2.8 Results and data reduction

Data that was collected during the full scale towing tests can be found in Appendix A-1. Dynamic data was collected by the data acquisition system at the rate of ten records per second. Typically a towing run lasted 100 seconds.

The data was held in memory until the end of each run when once vibration had ceased the data was down-loaded onto floppy disk. A typical data set required 50-100 kbytes of disk space. The time that the photographs were taken was noted and only data sampled in a window extending 5 seconds before and after that time considered. The parameters listed in Table 6.2 were then averaged over that 10 second window. If any severe discontinuities were found to be present then the averaging window was moved a little one way to exclude them.

Inevitably the boat was found to be either slightly accelerating or decelerating over the period. The acceleration force was calculated and subtracted from the towing force. Uncertainties on parameters to a 95% confidence interval are shown in Table 6.3. They include a systematic error where appropriate and the random error. A typical percentage error is also shown.

Table 6.3 Full scale measurement uncertainties

Parameter	*Average uncertainty to 95% C.I.*	*Percentage uncertainty on typical reading*
Boat Speed, V_s (radar)	0.036 m/s	0.5%
Boat Speed, V_s (pitot-static)	0.11 m/s	1.5%
Apparent Wind Speed, V_w	0.036 m/s	0.5%
Total keel trim, τ (photo.)	0.28 deg	5%
Towing force, W	117 N	2.5%
Towing angle, α	0.5 deg	25%
Wetted keel length, L_k (photo)	0.152 m	3%
LCG	0.028 m	1%
VCG	0.094 m	13%
Static displacement, Δ_0	9.7 kg	0.35%

6.3 Model Tests

6.3.1 Introduction

During 1992 Mr Tom van Terwisga of MARIN was employed by CWF Hamilton and Co. Ltd. for a period of approximately three months. The prime reason for this visit was to increase the knowledge of Hamilton staff on marine propulsion matters and to forge a deeper relationship with MARIN. Mr van Terwisga has been investigating aspects of hull-waterjet interaction himself and so had more than a passing interest in this project. Favourable terms were offered to CWF Hamilton for a model testing program designed to fit in with this study. The offer was accepted enthusiastically and provided the project with some valuable comparative data. A summary of the tests conducted at MARIN is shown in Table 6.4.

Table 6.4 Review of model resistance tests

Condition	*Speed range tested (knots)*	*Remarks*	*Test No.*
Δ_0, LCG_0	6.5-9.5 15.0-22.0	Baseline condition	50208
		Displacement variation tests	
Δ_1, LCG_0	7.5,18	$\Delta_1=1.05\Delta_0$	50209
Δ_2, LCG_0		$\Delta_2=0.95\Delta_0$	50210
		LCG variation tests	
Δ_0, LCG_1	7.5,18	t_0-1.0 deg	50211
Δ_0, LCG_2		t_0-0.5 deg	50212
Δ_0, LCG_3		t_0+0.5 deg	50213
Δ_0, LCG_4		t_0+1.0 deg	50214
		t_0 is trim angle for baseline condition at speed =0	

6.3.2 Procedures

6.3.2.1 General

An accurate one third scale model of the test boat was constructed from the same linesplan as the full scale vessel. Testing procedures were generally in accordance with the 1987 ITTC recommendations. The following comments are taken from a fax supplied with the data by Mr Van Terwisga.

"The model has been weighted before and after the tests, and the LCG positions have been adjusted on a balancing table which is free to pitch. The adjustment of LCG was checked with draft marks that were calculated for and applied to the model. For the extrapolation of the model results to full scale, the dynamic wetted surface of the hull was used. This wetted surface was obtained from readings of underwater photographs that have been made for the baseline condition."

6.3.2.2 Towing Position

The towing force was horizontal and applied directly above the centre of gravity but on the shaft centre-line as shown in Figure 6.11.

The jet installation was slightly different to that in the full scale boat. The angle between the keel and the shaft was five degrees, being one degree greater than the full scale installation.

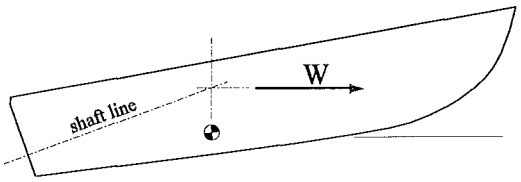

Figure 6.11 Model test towing position

The 1987 ITTC recommend in section 5.3 how the tow rope is to be attached. Specifically: *"The tow rope should be applied close to the final nozzle location and in the direction of the jet to obtain a running trim close to that of the self-propelled model."* Clearly this was not adhered to by MARIN. However towing position can be altered in the computational model to account for this when making comparisons.

6.3.3 Results of model resistance tests

Table 6.5 summarises data from the baseline resistance test, no. 50208. Wetted keel length data was obtained by watching video footage of the tests and manually recording the keel lengths using the hull block markers.

Table 6.5 MARIN resistance test results for test 50208

Speed		*Planing Parameters*		
Knots	*Fv*	*Resistance (N)*	*Lk (m)*	*Trim (deg.)*
6.50	0.90	1578	7.0	1.22
7.01	0.97	2067	6.8	1.94
7.51	1.04	2646	6.7	2.87
8.01	1.11	3252	na	3.84
8.51	1.18	3685	6.6	4.71
9.50	1.32	4028	6.5	5.18
15.01	2.09	4574	4.9	6.83
16.01	2.22	4530	4.8	6.80
18.02	2.50	4378	4.7	6.23
20.03	2.78	4257	4.6	5.62
22.01	3.06	4278	4.6	5.09

6.4 Discussion

6.4.1 Full scale tests compared to Savitsky

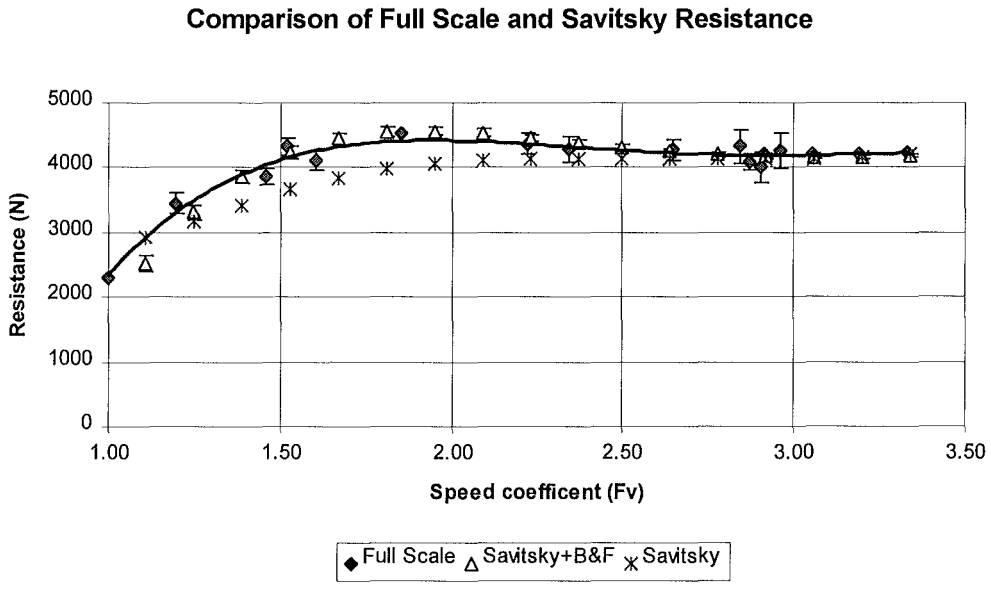

Figure 6.12 Graph showing predicted and full scale resistance

Figure 6.12 shows both the full scale resistance and the predicted Savitsky resistance using the computational model described in section 5.3. graphed against the volumetric Froude number. Two sets of Savitsky data are shown, one including the

Blount and Fox (1976) modification factor, the other not. It can be seen that the full scale data is better approximated by including the Blount and Fox modification factor.

The full scale results include error bars which can be seen, generally to increase with increasing speed. The error on resistance is due to two components, the systematic error and the random error. The random error increased with speed due to increasing pitching and heaving of the hull which caused greater variation in the towing force transducer signal. There are also error bars shown on the predicted resistance. These were found by running the program using all possible envelopes of LCG, and displacement allowing for uncertainties.

A fourth order polynomial was fitted through the points using the least squares method and is shown as the solid line. Excellent agreement can be observed from F_∇ = 2.5 to 3.0.

The prediction is high in the hump region by approximately 3%. It is well known that the Blount and Fox modification factor over predicts in this region. This is most likely due to the effect of the bow which at low trim angles causes a considerable deviation from the assumption that the hull is prismatic. (Almeter, 1991[1]) At low speed the prediction is several percent low.

A correction function has been developed to map the prediction onto the full scale.

$$R_{FS}/R_{Comp} = 0.190757 F_\nabla^4 - 1.67079 F_\nabla^3 + 5.4486 F_\nabla^2 - 7.8106 F_\nabla + 5.1138 \quad (6.1)$$

[1] p13

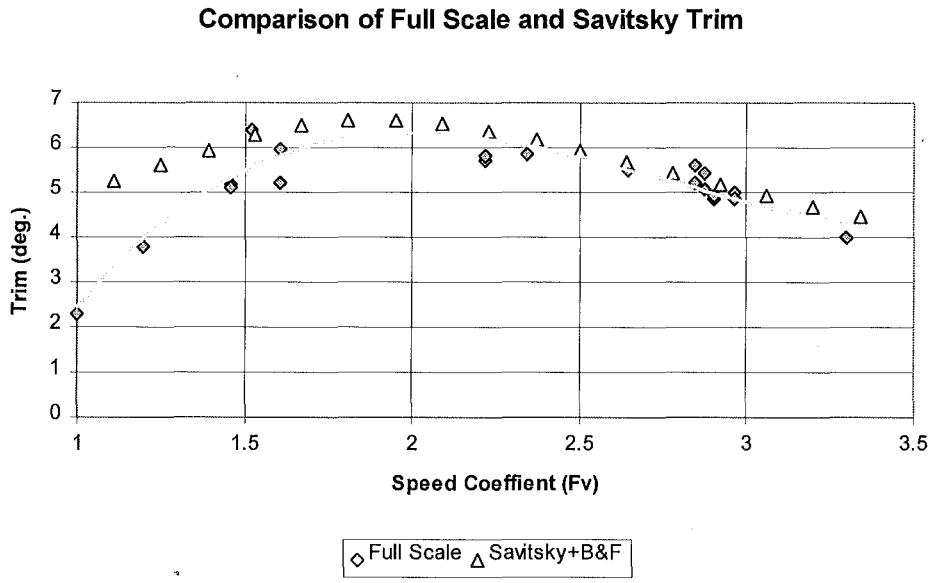

Figure 6.13 Graph showing predicted and full scale trims

Figure 6.13 displays trim data. The trim is over-predicted below the hump. This phenomena was also reported by Hadler (1966), a similar trend can be seen in his graph shown in Figure 4.6. However at speeds above the hump, there is good correlation. The correction function, equation (6.2), is shown below.

$$\tau_{FS}/\tau_{Comp} = 0..29479\,F_{\nabla}{}^{3} - 1.87523\,F_{\nabla}{}^{2} + 3.98979\,F_{\nabla} - 1.8932 \qquad (6.2)$$

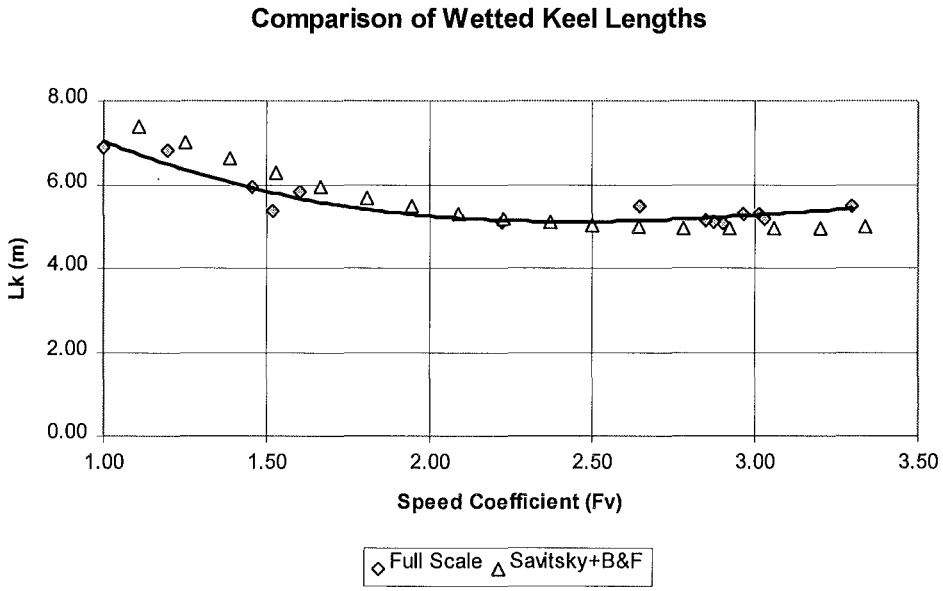

Figure 6.14 Graph showing predicted and full scale wetted keel lengths

Figure 6.14 shows the full scale and predicted wetted keel length data. The wetted lengths are shorter for lower speeds which can be expected due to the rising stem at the bow.

$$L_{KFS}/L_{KComp} = -0.0145F_{\nabla}^{3} + 0.1026F_{\nabla}^{2} - 0.1385F_{\nabla} + 0.9511 \quad (6.3)$$

6.4.2 Model tests compared to Savitsky

Model test results are compared to the prediction program in the three graphs below. The raw prediction is graphed along with the corrected prediction using the speed dependent correction functions presented in section 6.4.1. The prediction program was changed to account for the different model towing position as described is section 6.3.2.2. It is assumed that the correction functions are still valid for the different towing position and slightly different loading conditions.

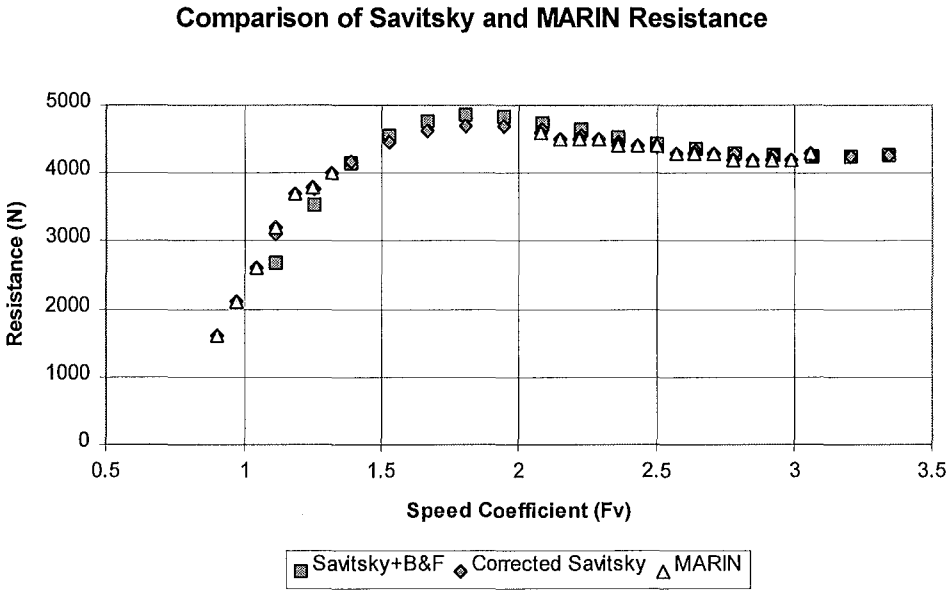

Figure 6.15 MARIN resistance data

A very good correlation is evident between the corrected resistance prediction and the model tests. This suggests that the same characteristics are exhibited by each and that the correction functions can be applied with small changes of loading and to the towing position.

The graphs below for trim and wetted length show similarly good results, the only exception being the wetted length which at high speeds failed to rise as was found at full scale. This may be due to small wavelets present at full scale giving the impression of greater wetted length in the photographs at low trim. The tank testing would have enjoyed dead flat water and are closer to the prediction tending to confirm the explanation.

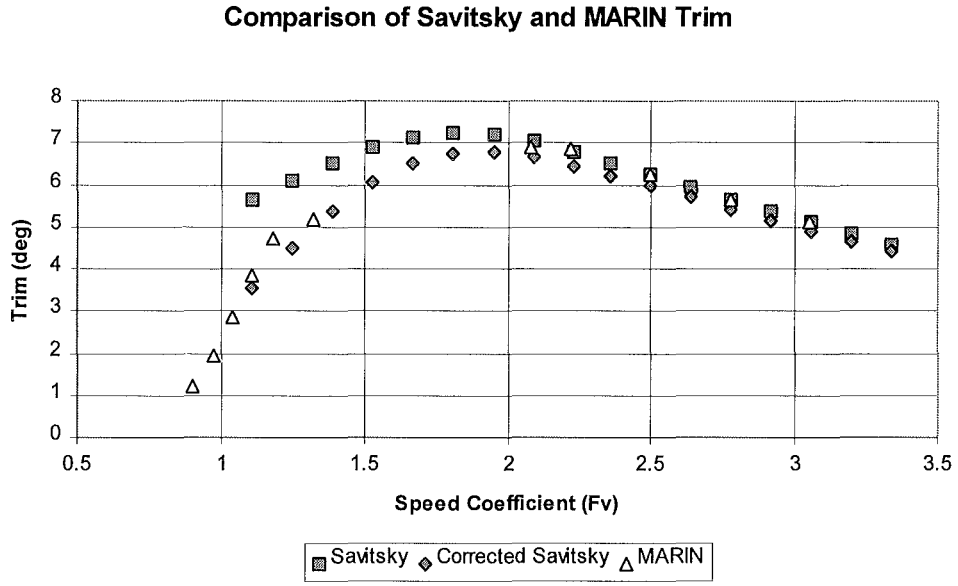

Figure 6.16 MARIN trims

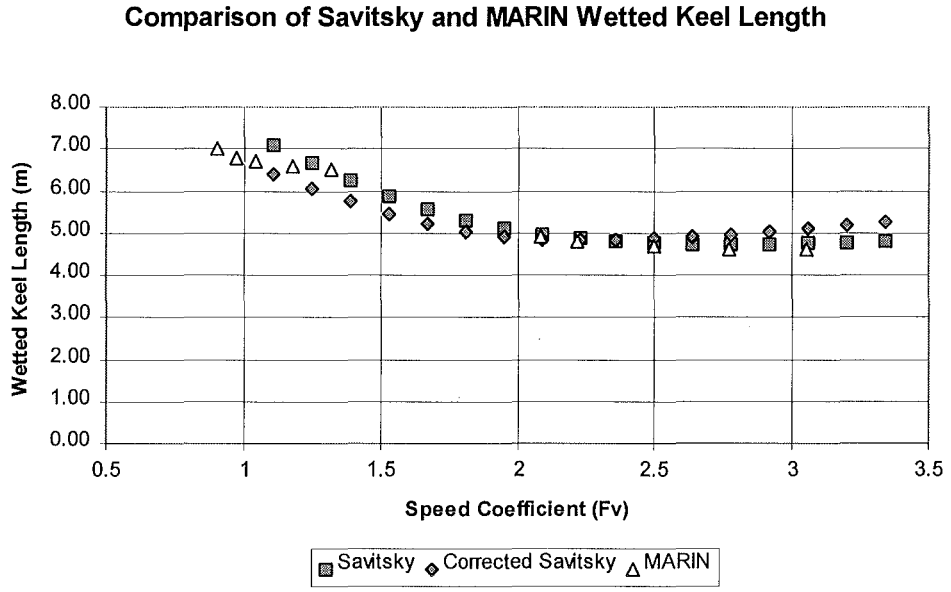

Figure 6.17 MARIN wetted keel lengths

6.5 Conclusions

The following points summarise this chapter.

- The experiments and analysis described above show that the computational model described in section 5.3 can be used to predict the full scale data adequately.
- The hull resistance was generally well predicted by the computational model.
- Trim was over predicted at low speeds however other workers have found the same.
- Wetted length was over predicted at low speed due to the curvature of the bow. The full scale wetted length tended to increase at high speed and low trim however an explanation is offered.
- Small speed dependent correction functions have been developed to account for deviations between the prediction and full scale data for reasons such as that detailed in the point above and the small geometric differences between the test boat and the prismatic hull form used to develop the Savitsky model.
- Using the corrected computational model to predict the MARIN tank test results has proved successful confirming that the correction functions are valid.

7. Propulsion Testing

7.1 Introduction

The following sections summarise key aspects of the propulsion testing that were conducted during the project. Section 7.2 reviews various methods of measuring the all-important intake and nozzle momentum flux on which the calculation of thrust heavily depends. Particular attention is paid to the method MARIN has used to measure the nozzle momentum flux during the model propulsion tests. MARIN have developed a hybrid pitot-static tube which they call an "averaging static pitot" or ASP tube. The author attempted using a similar probe at full scale, however finally adopted a velocity integration method which is also described.

Section 7.2.3 describes some earlier work where an alternative, load cell system was used to measure the thrust. Measurements were also taken of pressures around the waterjet intake. This work is reviewed in section 7.3.8.

The full scale propulsion tests conducted by the author are also described along with the model propulsion tests conducted at MARIN.

7.2 Measuring Momentum Flux and Flow rate

7.2.1 Introduction

The definition of thrust adopted by this project for net thrust, $\mathbf{T_N}$, acting on the combined hull-waterjet system is,

$$\mathbf{T_N} = -(\phi_{Mn} - \phi_{Mi}) \tag{7.1}$$

where ϕ_{Mn} is the momentum flux at the nozzle and ϕ_{Mi} is the momentum flux at the streamtube inlet. These two fluid force vectors are defined as a rate of momentum flux such that $\phi_M = \dot{m}V = \rho QV$.

But Q is equal to VA where A is an area of fluid flowing at constant velocity. In the general case for a varying velocity over an area the momentum flux is:

$$\phi_M = \int_{Area} \rho V^2 da \tag{7.2}$$

There is a three dimensional velocity profile present at both the intake and nozzle so the method used must somehow account for this.

7.2.2 Outgoing Momentum: review of methods

There are numerous variations on the theme of using pitot probes to measure the momentum flux and flow rate however they fall into two basic categories. One uses reference probes which are calibrated against a known flow rate or thrust. The other relies on having enough measurements to integrate the velocity over the area under concern with sufficient accuracy.

7.2.2.1 Reference probes

The basis of this method is to calibrate a probe or set of probes located in the nozzle against either the thrust produced during a static bollard pull test or the thrust calculated from an accurately measured flow rate. This method relies on several assumptions.

1. The reference probe must continue to give a signal which remains proportional to thrust over the entire operating range.

2. The calibrating arrangement must be accurate.

When the boat is moving it is likely that the velocity profile will change compared with that of the static case. It is possible that the skewed velocity profile found at the face of the impeller reported by Griffith-Jones[1] (1994) and Haglund et al (1982)[2] will find its way through to the nozzle as the short internal passages of the waterjet and the nature of the flow are such that there is little mixing.

This phenomena is recorded by Griffith-Jones (1994)[3] at an IVR setting of 0.42 in his Figure 7.5. A variation on the axial flow rate of nearly 9% is evident from one side of the nozzle to the other. The effect is likely to be even more pronounced at very low IVRs. There are also anecdotal reports from the staff of CWF Hamilton and Co. Ltd. of a polished internal surface on waterjets in some high speed river jets leading from behind the cutwater to one side of the nozzle, after passing through

---

[1] pp86-98
[2] p7
[3] p42

some rotation. The suggested reason for this is that sand and gravel entering the bottom of the intake in the high speed region of flow polishes the internal surface. The water at the top of the intake which is slowed by separation and turbulence caused by the shaft and screen rake, does not have so much sand and gravel in suspension.

If this is the case then the probes must return a signal with the same characteristic for all possible values of outgoing momentum regardless of the velocity profile. Therefore a calibration curve constructed for the static case must also hold for the dynamic case (Assumption 1). When the vessel is stationary the IVR tends to infinity and flow into the intake and pump is very much more even resulting in a similarly even nozzle velocity profile.

For example, in the case of the single total pressure probe, the vessels movement may produce a zone of high velocity which just happens to occur in the region of the probe. The rest of the nozzle area may experience a slightly lower velocity and so overall there is negligible net change in total momentum flux as compared to the as-calibrated static case. The velocity calculated from the probe however, will be misleading and lead to an over-estimate of momentum flux if it is assumed that this velocity is present over the entire nozzle area. It is clear then that there must be a sufficient number of probes covering the nozzle to provide a reasonable average of momentum flux across the whole area.

Care must be exercised when using a bollard pull to calibrate reference pitots. This technique relies on the assumption that the incoming momentum is zero and all the thrust is due to the outgoing nozzle momentum. However CWF Hamilton staff have found in practice that at a constant power setting, after a several minutes of measuring, the static thrust can be seen to reduce, sometimes considerably. This is most likely caused by a circulation set up under the boat by the action of the jet of water leaving the submerged nozzle. This has the effect of creating a small effective boat speed which creates some incoming momentum at the intake and some skin friction on the hull, which both serve to reduce the measured bollard pull of thrust.

A further effect has been identified by Jon Hamilton of CWF Hamilton and Co. Ltd. He has proposed some theory and conducted experiments which measured a suction effect on the transom when the jet is operating but the boat stationary. This effect is due to water being entrained into the jet which is submerged in the static case. The entrainment process causes a local transverse velocity in the region of the transom which lowers the static pressure and causes a slight, net rearward force on the hull. This effect has been found to be approximately 1% of thrust using typical propulsion parameters.

A better approach which avoids relying on assumption 1, is to calibrate the reference probes with the boat under way. This is achieved by positioning some device to measure the flow rate near the waterjet and carrying out the calibration dynamically as reported by Hoshino and Baba (1984)[1]. This usually requires carrying a large tank or thin plate weir along with the boat. This is quite possible at model scale but difficult to achieve at full scale given size and general arrangement difficulties.

The High Speed Marine Vehicle Committee of the 18th ITTC comments that *"it is of the utmost importance to have accurately calibrated devices for the flow measurements"* and suggests the following equipment:

- venturi pressure taps in the outlet nozzle
- paddle wheels in the outlet nozzle
- collection of the water flow in a tank behind the model

It appears that the first two points refer to reference devices which are calibrated using the tank.

MARIN have developed a device known as an averaging static pitot tube (ASP) for the purposes of measuring nozzle momentum flux, which is worthy of further discussion. It is similar in principle to an adaptation of the pitot-static tube known as the "Pitometer" presented by Massey (1984)[2]. The general arrangement is shown in Figure 7.1 and a sectioned view of the tube in Figure 7.2.

---

[1] p6
[2] p100

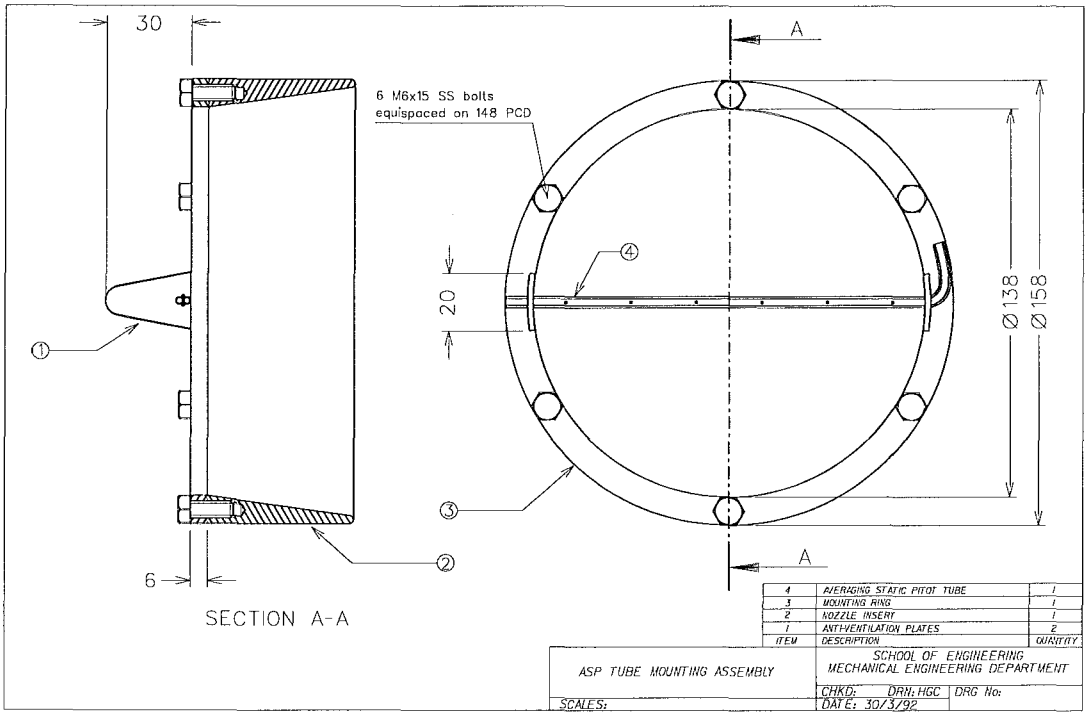

Figure 7.1 ASP tube and mounting plate

It consists of two similar tubes welded together side by side. There is a series of holes in each tube, one set facing forwards, the other backwards. MARIN positioned their probe inside the tail pipe. MARIN calibrate the differential pressure measured by this device against a flow rate measured through a Thompson barge (notch weir). The advantage of this type of device is that it may yield a better average of the total momentum than having a single reference probe.

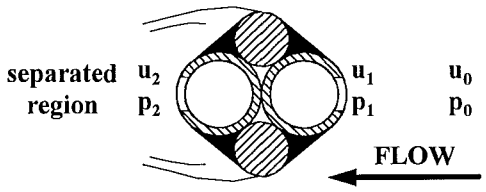

Figure 7.2 Cross-section of ASP tube

Considering Figure 7.2, the principle of operation is as follows. Assume that the energy loss caused by the ASP tube is equal to $\zeta \frac{1}{2} u_0^2$, where ζ is a constant, an energy equation can be written such that:

$$\frac{1}{2}\rho u_2^2 + p_2 + \zeta\frac{1}{2}\rho u_0^2 = \frac{1}{2}\rho u_1^2 + p_1 \qquad (7.3)$$

but $u_1 = u_2 = 0$ so equation (7.3) simplifies to:

$$p_1 - p_2 = \zeta \frac{1}{2} \rho u_0^2 \tag{7.4}$$

which can be rearranged to yield the upstream velocity so that,

$$\therefore \; u_0 = \sqrt{\frac{2(p_1 - p_2)}{\zeta \rho}} \tag{7.5}$$

There are six holes along the ASP so the pressure reading from a transducer coupled between each side is assumed to be equal to the mean of six pressures p_1, minus the mean of six pressures p_2.

There are several critical assumptions upon which the validity of the ASP readings depend. ζ is assumed to be constant along the tube. This may not be so especially at higher jet velocities where cavitation is likely to occur. Massey (1984)[1] comments, that *"Such an instrument requires calibration to determine the correction factor which may not be constant over more than a limited range of velocities"*. It is also likely that some dynamic vibration of the tube will occur which may well change the nature of the separated region along the tube.

A further, but probably more critical assumption is that the tube returns a true average of pressures. As the pressures at each hole will be different, fluid will flow from a high pressure hole to a low pressure hole. There will be energy losses in the tube. It is difficult to say whether a true average of pressures would be achieved in such a case. Some experimental work would reveal this. There is also a potential problem with venting on the low pressure side. Venting prevention plates were incorporated in the design shown in Figure 7.1. It is not known whether they work.

The ASP tube must be calibrated against a known momentum average velocity rather than a volumetric average velocity. The MARIN approach and one attempted by the author is to use the inherently accurate thin plate weir as a flow rate reference.

[1] p100

The weir method is summarised as follows:

1. At a nominal RPM setting record a dimensionless velocity profile across the nozzle. Measure the profile over a range of orientations to build up a three dimensional profile. The RPM reading can be used as a reference parameter to scale individual readings if the pump loading changes as from the pump laws, flow rate is proportional to pump speed.
2. At the same rpm setting measure the volumetric flow rate and the ASP pressure signal.
3. Scale the velocity profile found in 1 to achieve the same flow rate.
4. Using the scaled velocity profile calculate the momentum average velocity.
5. Repeat over a range of RPM settings to construct a calibration function that maps the ASP output to momentum average velocity.

The pitot pressure transducer is only required to hold accuracy over the short time interval of the traverse. The only significant source of systematic error will be in the accuracy of calibration of the weir and error in interpolating between points on the velocity traverses.

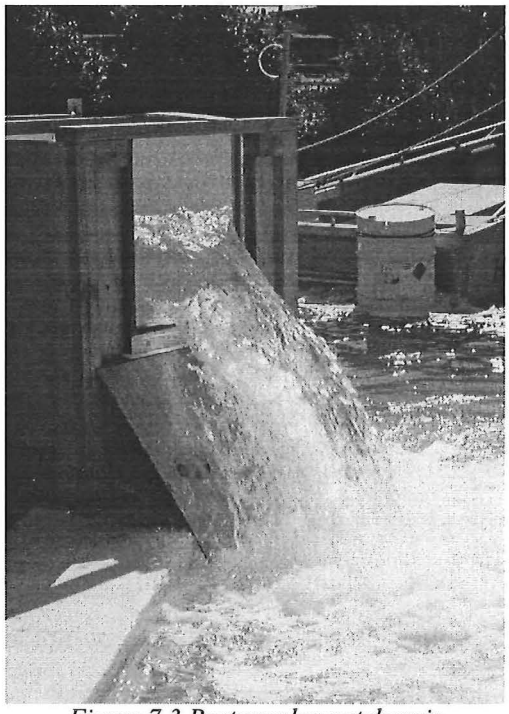

Figure 7.3 Rectangular notch weir

It was decided to embark on the technique developed by MARIN and attempt to use it at full scale. Replication of as much of their technique as possible would be beneficial when comparing results.

A rectangular notch weir, shown in Figure 7.3, was built and calibrated by the author in the civil engineering fluids lab at the University of Canterbury using accurate calibration pits. A relationship exists between the height of water in the weir and

the flow rate. A hook-gauge well is connected to the side of the weir via pipe (i.d. 25 mm) and used to measure the height of water in the weir box. The calibration yielded an excellent average accuracy on flow-rate of +/-0.2%. A photograph of the weir and test boat set up in the CWF Hamilton staff swimming pool is shown in Figure 7.4.

A piping system was constructed to carry water from the waterjet to the weir. This included a valve so that the back pressure on the jet could be varied and a pivot to allow relative movement between the boat and the pipe. Diffusion in the pipe system meant that pressure at the nozzle would fall below zero (1 atmosphere). The valve could then be closed down to bring the pressure up to atmospheric and so simulate nozzle conditions that would be present in practice.

Figure 7.4 Weir test set up

An ASP tube was constructed using the MARIN design and fitted to the nozzle at the nozzle exit plane. Attempts to calibrate the ASP tube revealed two significant difficulties. First the weir flow rate readings were found to be inflow dependent. This was discovered by changing the position of the inflow pipe carrying water from the waterjet to the weir while holding the rpm constant. Variations on recorded flow of 7% were found. This was thought to be due to swirl in the weir caused by the way in which the water flowed in from the pipe giving false readings. Significant modifications including extending the weir box, adding more baffling and manifolding several pressure tappings together would have been needed to be made to the weir to eliminate this dependency. It would also have needed re-calibrating.

A second difficulty was that the ASP tube was very easily damaged and needed repair on several occasions. It became clear that it required redesign and stronger construction.

Finally, development of the weir method was shelved. It was becoming increasingly clear that a large amount of work was still required to develop the technique at full scale. Practicalities of calibrating the system at full scale added considerable pressure and difficulty to the development process. Also questions were being raised with respect to the reliability of the ASP tube. As a consequence the method was dropped in favour of a more direct velocity integration.

7.2.2.2 Integration method

A potentially more rigorous approach and that finally adopted, is to take sufficient readings over a range of positions and then use these to build up a picture of the flow conditions over the entire nozzle. This data can then be integrated over the whole nozzle area to obtain the nozzle momentum flux and the flow rate. Several researchers have used this method with success. Haglund et al (1982) describe their method as follows:

"For a number of conditions, the velocity (ahead of the impeller) was measured by means of pitot tubes. The velocities were plotted and the actual flow rate, Q, was found by numerical integration. As a check, static pressures in the outlet nozzle were also measured. By applying the equation of continuity and Bernoulli's equation ... the flow rate could be calculated. The two methods gave practically the same result." [1]

It was decided to use a pitot rake in the nozzle to gain sufficient readings to enable an accurate integration of the velocities over the entire area. By coincidence the method proved nearly identical to that used by Burtness (1987)[2] at the Stevens Institute of Technology which is summarised in a paper that became available after testing was complete. Burtness used a rake of six Prandtl tubes inserted into a circular part of the ducting following the intake. These could be rotated into three

---

[1] p7
[2] p2

different angular orientations giving a total of eighteen recording positions. The integration method assumed that the velocities measured at each pitot was constant over the area it represents. Burtness's calculated flow was compared to the actual flow by attaching a pipe to the pump exit and recording the time to fill a know volume. The error between the integrated average flow rate and the actual flow rate is quoted as 2.2% on the higher flow rates. The following comment is made with respect to the comparison:

"The close agreement between measured and computed flow rates indicates that the method chosen to integrate the pressure distribution within the test section is valid."[1]

7.2.3 Measurement of Thrust Using a Load Cell System

This project began as a Masters project before it was changed into a PhD a year later. The original project was to involve commissioning and then using a system of load cells mounted between the waterjet and the hull to measure the thrust loads on the waterjet system.

The concept is very similar to that used by Koops (1986) where the waterjet system is supported on a force balance and flexible seals used to isolate the system from the

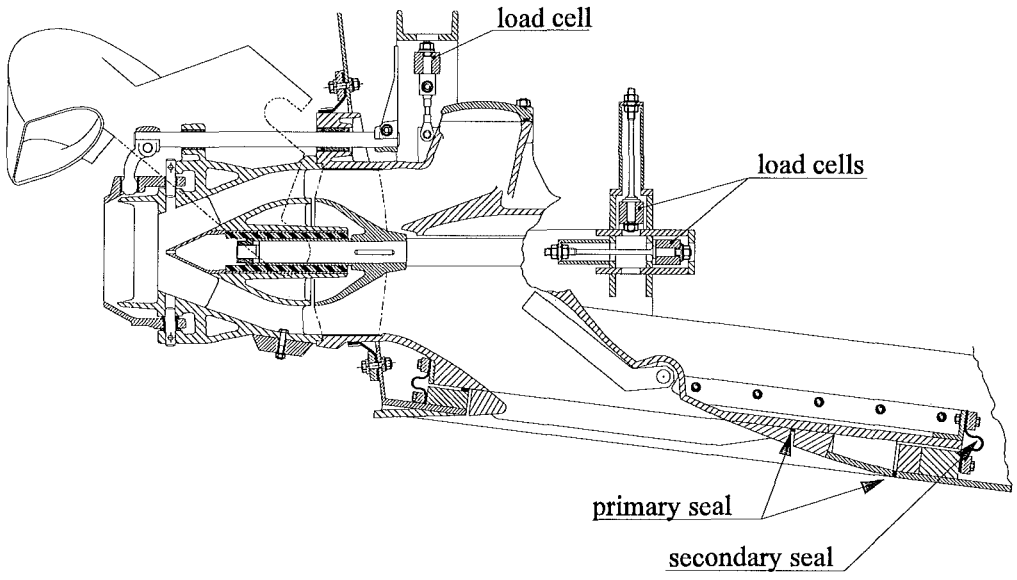

Figure 7.5 Sectioned view of 273 waterjet with load cell and seal arrangement

[1] p5

ducting. The resulting force measured by the system is equivalent to the force vector $-\mathbf{Fp_c}$, , that is the force exerted by the fluid on the waterjet casing (see section 5.4.2). This force has particular significance to Hamiltons as it is the force at the contractual boundary between the waterjet manufacturer and the boat builder.

The sectioned view in Figure 7.5 shows the arrangement used on the Hamilton 271 test boat. The waterjet system was mounted on five load cells, R_1, R_2, ..., R_5. Two tie rods constrained the waterjet laterally, leaving four degrees of freedom: translation fore and aft, translation up and down, rotation about an axis parallel to the shaft and rotation about an axis parallel to the transom. These enabled the measurement of thrust, lift, pitching moment and torque reaction on the waterjet casing.

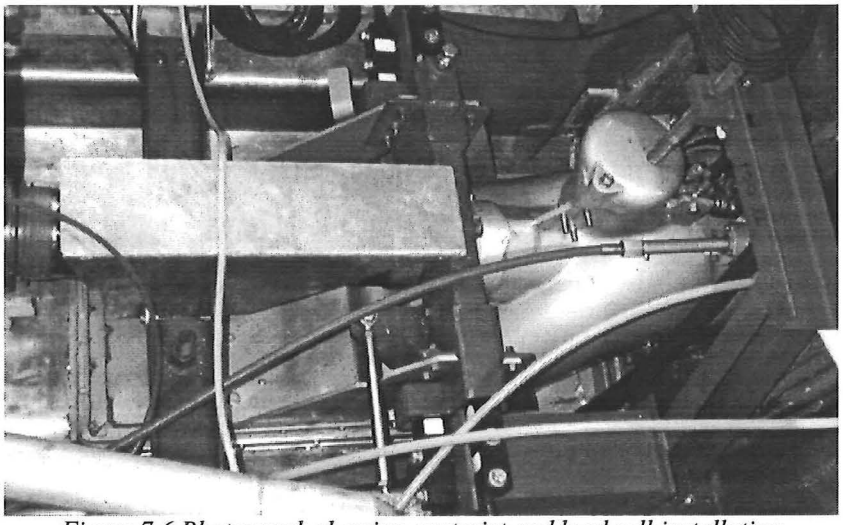

Figure 7.6 Photograph showing waterjet and load cell installation

Four load cells can be seen in the middle of the photograph shown in Figure 7.6 as the black rectangular objects. The fifth load cell is located under the channel section to the right of the inspection hatch cover at the right of the photograph.

The drive shaft to the waterjet (at centre left) was an especially chosen proprietary item incorporating constant velocity joints at each end to eliminate any longitudinal force transmission through the shaft.

The load cells were mounted on a sub-frame and connected to the waterjet by slender rod elements approximately 200 mm in length. The rods were chosen to

transmit forces parallel to their axis while being compliant in a direction perpendicular to their axis. The resisting force in the perpendicular direction is linear and can be accounted for during calibration. An earlier system consisted of sliding contacts between the load cells and waterjet. However friction between the sliding surfaces was unpredictable and resulting errors were too high. The author redesigned and refitted the system to incorporate the rod connections.

Referring again to sectioned view (Figure 7.5), isolation of the waterjet casing from the hull required a physical separation to ensure that forces were transmitted only through the load cells. This required a system of two seals to prevent the ingress of water. A primary seal consisted of a strip of closed cell foam packed into the space made by the separation. The foam was held in place with a water proof flexible sealant. A secondary, backup seal was also installed. It took the form of a flexible rubber skirt around the perimeter of the intake flange.

Calibration of the system was a complex process. The boat was positioned such that the load cell system was level. The thrust load cells were calibrated using a known horizontal force from zero to 7 kN applied to the centre of the tailpipe. This was achieved by hanging a tray containing known weights to one end of a 90° bell crank (radius 1.5 m) that was pivoted to a column inside the workshop. A push rod was connected between the tail pipe and the bell crank to transmit the horizontal calibrating force. This system enabled accurate loads to be imparted as the calibrating weights could be weighed quite accurately.

The remaining three load cells measured forces acting in a vertical plane and required calibration using a vertical force. This was achieved using the same tray and weights used previously. The tray was hung from one end of a beam hung over the boat and pivoted midway along its length. A chain was then connected from the other end of the beam down to the waterjet casing. A complicating factor was that it was impossible to impart a load into each load cell independently without affecting the others. This was because the waterjet was not mounted at discrete points as it had connections to the hull through the primary seal. As a result the lift load cells were calibrated simultaneously. This was achieved by shifting the position of the applied load so that three independent equations could be written of the form:

$$Volts_1R_1 + Volts_2R_2 + Volts_3R_3 = Applied\ Load \tag{7.6}$$

The three equations of this form could then be solved simultaneously to find the calibration coefficients R_1, R_2, and R_3.

Some measurements were taken with this load cell system but the uncertainties were estimated as being too high (≈10%) for an accurate estimate of the magnitudes of hull waterjet interaction. A useful outcome of the load cell measurements was however the high vertical component of measured thrust using this technique (≈40%). This highlighted the fact that the load cells were only measuring the pressure force on the casing and that the downward force on the hull, $\mathbf{Fp_h}$, was not being accounted for.

Quite some months were spent trying to refine the load cell system but finally the problems were found to be too many and too serious. Some are summarised below. The system was then removed and the jet refitted by the author in preparation for the momentum flux measurements that have been already described.

- There were too many connections between the waterjet and hull which caused hysteresis that increased the measurement error.
- Calibration was a difficult process.
- The load cell readings were seen to drift (25-50 N) as people walked around the hull. This fact suggested that the supporting frame was not rigid enough to isolate the load cell system from hull deflections. It was not known what the effect was with the hull planing .
- Inevitably water leaked through the primary seal and pressurised the space between the hull intake block and the intake flange. This space was later vented however the magnitude of remaining effect was not known.
- It was difficult to prevent the seals leaking and inevitably the bilges became quite full.
- As the hull increased trim the self weight of the waterjet system, which was considerable and previously calibrated out, would begin to manifest itself as a

reduction in the thrust readings and an increase to the lift readings. This had to accounted for and increased the overall error.

- The load cell system could only measure the internal force $\mathbf{Fp_c}$ as discussed above.

7.2.4 Measuring Momentum Fluxes: Chosen Method

7.2.4.1 Nozzle momentum flux

As stated, the method finally chosen was very similar to that used by Burtness described above. A Prandtl rake was positioned at the nozzle exit plane to measure the total pressure. The probes were positioned using the tangential method described by Ower and Pankhurst (1966)[1] which apportions the tubes at radial positions such that they represent segments of equal area. The rake was constructed by sandwiching the stainless steel pitot tubes between two halves of aerofoil shape. The pitots extended 13 diameters forward of the supporting strut so that the ends were exactly at the nozzle exit plane. The strut then was well outside the nozzle in the free jet and it is assumed that it had no effect on the pressure readings at the nozzle. A photograph of the completed rake mounted on an attachment ring is shown in Figure 7.7. A copy of the manufacturing drawing can be found in Appendix A-3.

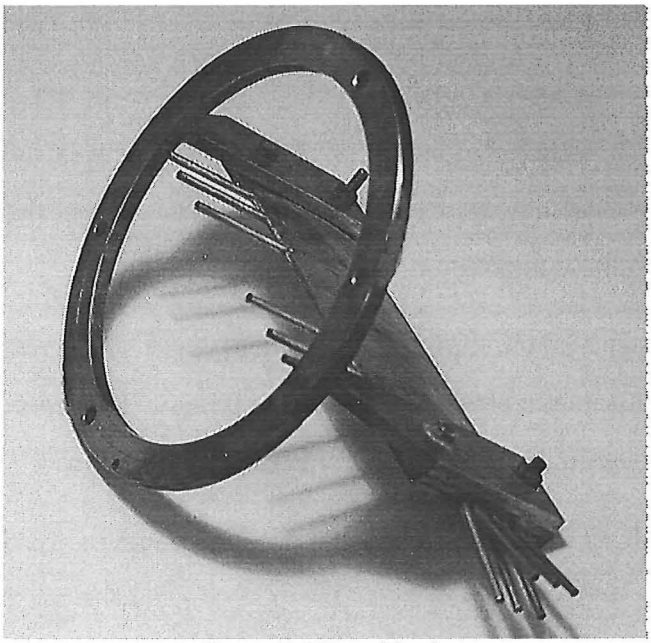

Figure 7.7 Prandtl rake

[1] p115

The probes were bent from one continuous length of tube to prevent leaks. Each probe could be independently connected to the same single pressure transducer (Data Instruments, model SA) to ensure conformity between probes. The pressure transducer was calibrated using a deadweight calibrator which is known to be accurate with less than 0.02% error.

The theory requires measurement of the outgoing momentum at a point at or beyond the nozzle but also where the streamlines are straight and parallel. This occurs at the vena contracta. Griffith-Jones (1994) highlights[1] the importance of considering the pressure on the nozzle plane area if the vena contracta occurs elsewhere and the gauge pressure can not be considered to be zero:

"The nozzle flow data applied to the 211 test boat at cruise conditions gives a mean pressure over the nozzle of 26 kPa which when multiplied by the nozzle area gives 250 N of thrust or 8% of the thrust as calculated from the momentum alone. Whilst this value will be highly dependent on the nozzle design, it is clearly essential to include the vena contracta effects in thrust calculations."

If the total pressure is measured at the nozzle exit plane and it is incorrectly assumed that there is no static pressure then the force at the control volume boundary at the nozzle will be incorrectly calculated as follows. The total pressure will be assumed equal to $p_{dyn} + p_{static}$ which will be treated as if it were dynamic pressure alone. If a constant velocity is assumed across the nozzle, the velocity will then be calculated as,

$$V^2 = \frac{2}{\rho}(p_{dyn} + p_{static}) \tag{7.7}$$

The force on the control volume boundary will be equal only to the nozzle momentum flux which is given by $\dot{m}V$ since the pressure at the boundary is assumed to be zero. The mass flow rate, $\dot{m}$ is equal to $\rho Q = \rho VA$. Therefore,

$$\dot{m}V = \rho AV^2 \tag{7.8}$$

[1] p171

Substituting equation (7.7) into (7.8),

$$\text{Force on CV} = \dot{m}V = 2Ap_{dyn} + 2Ap_{static} \tag{7.9}$$

If however the static pressure is included in the calculations correctly, force on the control volume boundary is equal to,

$$\begin{aligned}\text{Force on CV} &= \dot{m}V + Ap_{static} \\ &= 2Ap_{dyn} + Ap_{static}\end{aligned} \tag{7.10}$$

Comparing equations (7.9) and (7.10) it is apparent that the effect of incorrectly assuming the static pressure to be zero, is to make an error in calculating the force on the control volume of Ap_{static}.

Steps were taken to remove the vena contracta completely by extending the nozzle to ensure straight parallel flow in the jet. An extra straight section two nozzle diameters in length, shown in Figure 7.8 was added to the tail pipe.

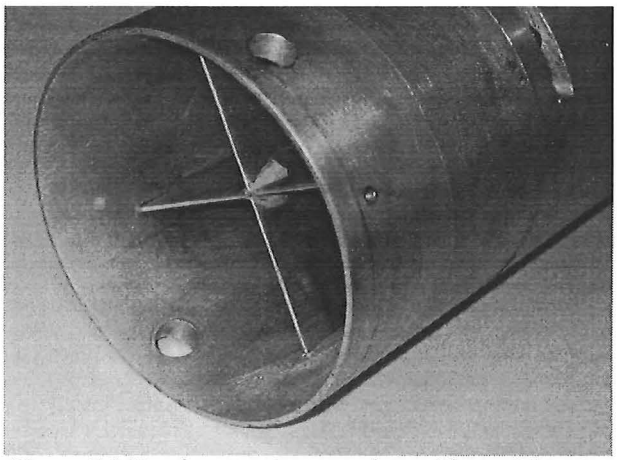

Figure 7.8 Nozzle extension complete with straightening vanes

Static pressure tappings were incorporated to allow a check to be made on whether the static pressure at the nozzle was tending to zero. They confirmed that this was the case with pressures of approximately or less 100 mm H_2O which is equivalent to a force of 13 N which is considered negligible (0.3% of thrust).

Pitot tubes will tolerate a degree of miss-alignment to the axial flow direction of the fluid. This means that if there is some swirl (rotational component) to the jet velocity then it will be measured by the pitot tube and be construed as being part of the purely axial flow. Therefore it has to be assumed that there is no swirl present, or steps taken to ensure that the effect of swirl is negligible.

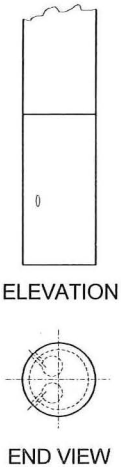

Figure 7.9 Swirl probe

The swirl in the jet was measured using a device from Hamiltons especially built for this purpose. It consisted of a probe fitted with two small static holes drilled perpendicular to its axis and at 60 degrees to one another. Inside the tube two smaller pipes carried pressure to the other end of the probe where the two pressures could be measured and compared. The concept is shown in Figure 7.9. and a photograph of the device being used in Figure 7.10.

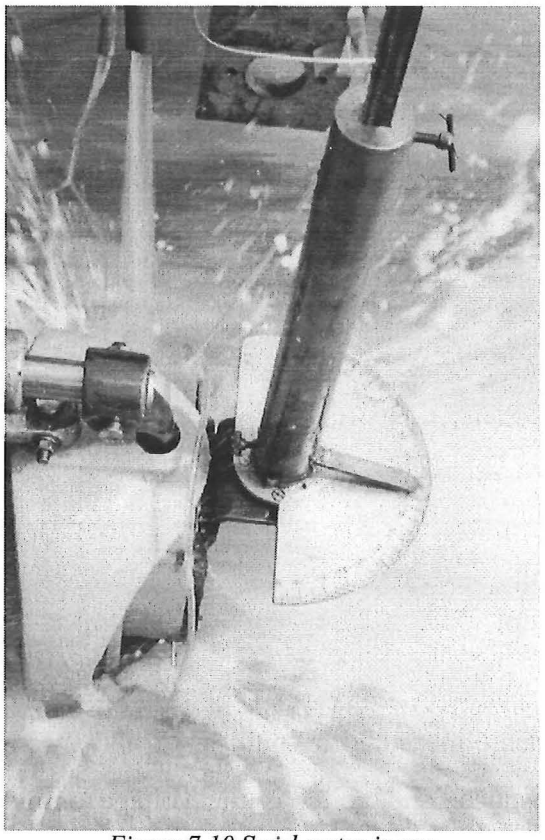

Figure 7.10 Swirl meter in use

Measurements were taken at 3000 rpm and a boat speed of approximately 16 knots. Initial readings revealed an average swirl of nearly six degrees which would lead to an over reading of axial nozzle velocity of 0.5%. The average swirl angle was reduced to three degrees with the addition of four straightening vanes approximately 100 mm in length located in the forward part of the extended nozzle section shown in Figure 7.8. This reduced any tendency to over read to 0.2% (1-cosine3.8) which can be considered negligible. Figure 7.11 displays the swirl data with and without the straightening vanes.

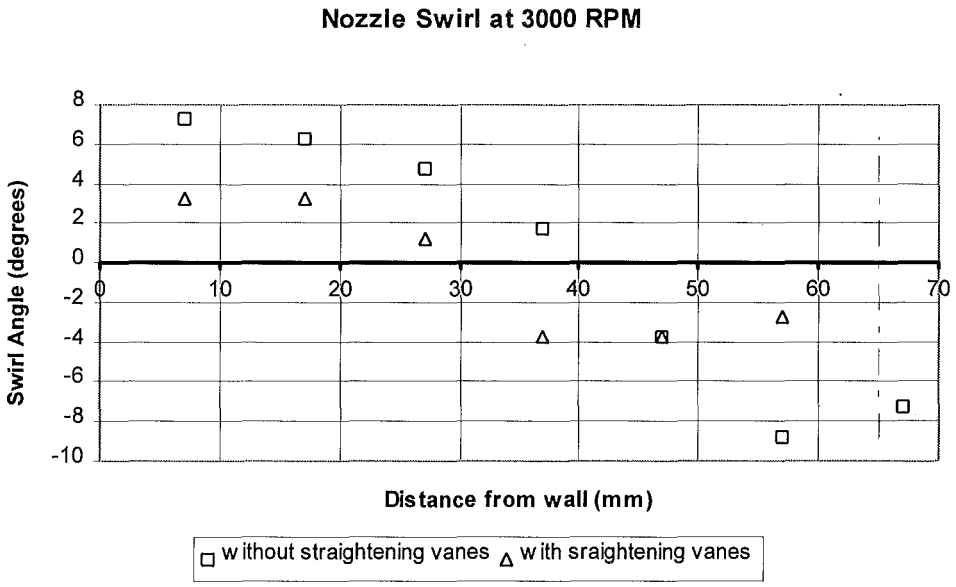

Figure 7.11 Swirl data

The total nozzle momentum flux, $\dot{m}v$, is calculated by summing the momentum calculated over equal areas, each represented by one of the six total head pitot tubes.

$$\dot{m}v = C_3(\rho A_1 v_1^2 + \rho A_2 v_2^2 + ... + \rho A_6 v_6^2) \tag{7.11}$$

where ,

$\dot{m}v$ = momentum flux
ρ = fluid density
A = area of segment
v = average velocity in the segment
C_3 = a correction factor

The square of velocity, v_n is defined as,

$$v_n^2 = \frac{2(C_1 volts_n + C_2)}{\rho} \tag{7.12}$$

where the term in brackets is the total pressure measured by pitot n. C_1 and C_2 are calibration constants for the pressure transducer and $volts_n$ is the voltage output recorded for pitot n.

The pitots are placed so as to represent radial segments of equal area, and the fluid density is assumed to be constant with no air entrainment, so combining equations (7.11) and (7.12),

$$\dot{m}v = C_3 \frac{A_n}{3} \sum_{n=1}^{6} \left(C_1 \text{volts}_n + C_2 \right) \tag{7.13}$$

A more detailed survey of the nozzle velocity was conducted utilising the other two rake orientations at two planing conditions: 2800 rpm, 10.3 knots; 2300 rpm, 6.8 knots. At each condition smooth curves were fitted through the data and a "law of the wall" boundary layer used to approximate the velocity near the walls of the nozzle. A ninth law profile gave the best fit. These curves are shown in Figure 7.12 and Figure 7.13. The momentum flux contribution represented by each rake position was then calculated by integration using the piece-wise velocity functions. The total momentum flux was then found by summing the three contributors.

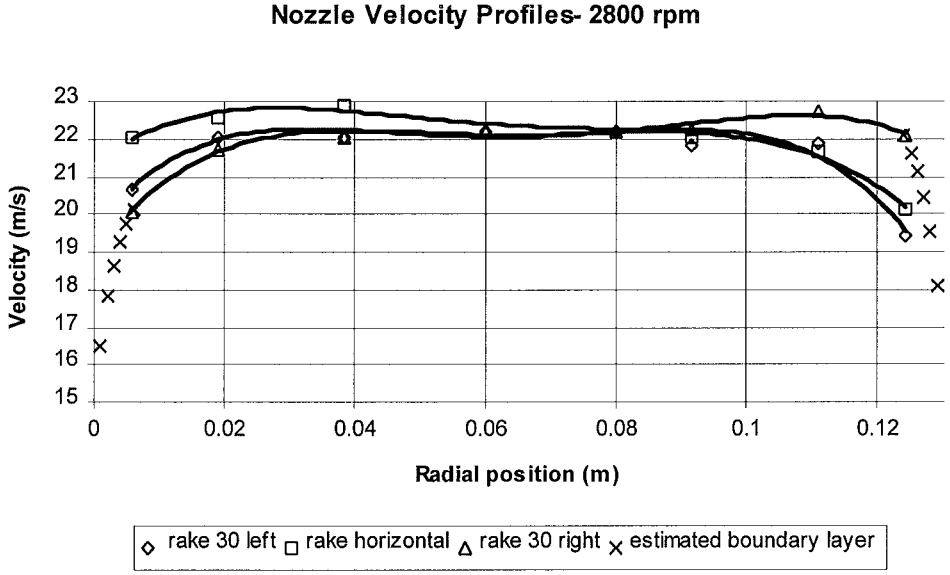

Figure 7.12 Nozzle velocity profiles (2800 rpm)

The momentum flux found by this method was then compared with that found using the single rake position and discrete points assuming constant velocity over each segment. The single position method was found to be consistently 0.95% low at both 2300 and 2800 rpm. This can be attributed to the fact that the other two rake positions gave slightly higher readings at each side of the nozzle as shown in Figure 7.13. This can be observed for both speed cases.

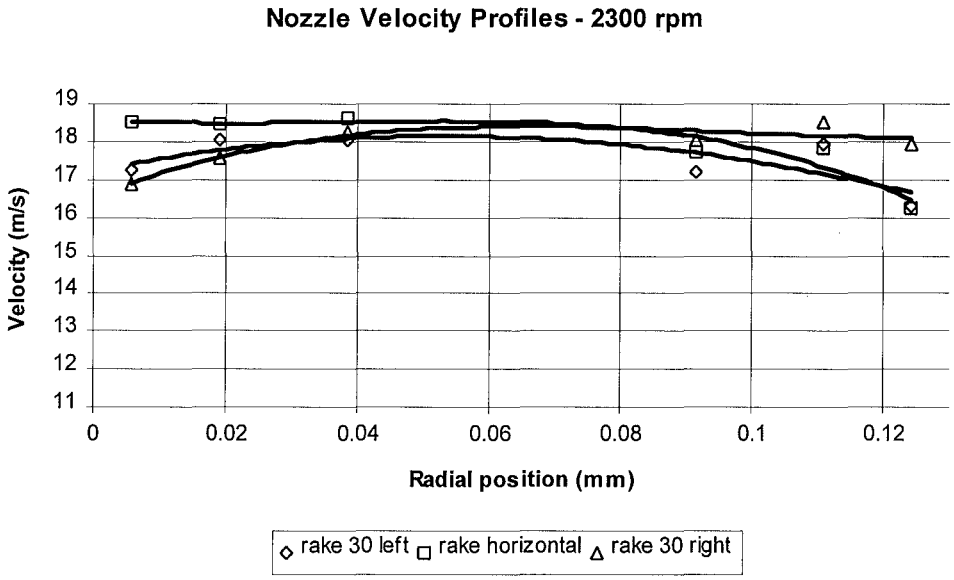

Figure 7.13 Nozzle velocity profiles at 2300 rpm

A graph of the velocity profiles from the "30 deg. left" setting for a whole range of engine speeds is shown in Figure 7.14. The general shape of the profiles can be seen to vary very little with speed so a constant value of 1.0095 was used for the correction factor C_3 introduced earlier. A systematic error of 0.5% was assumed on the correction factor.

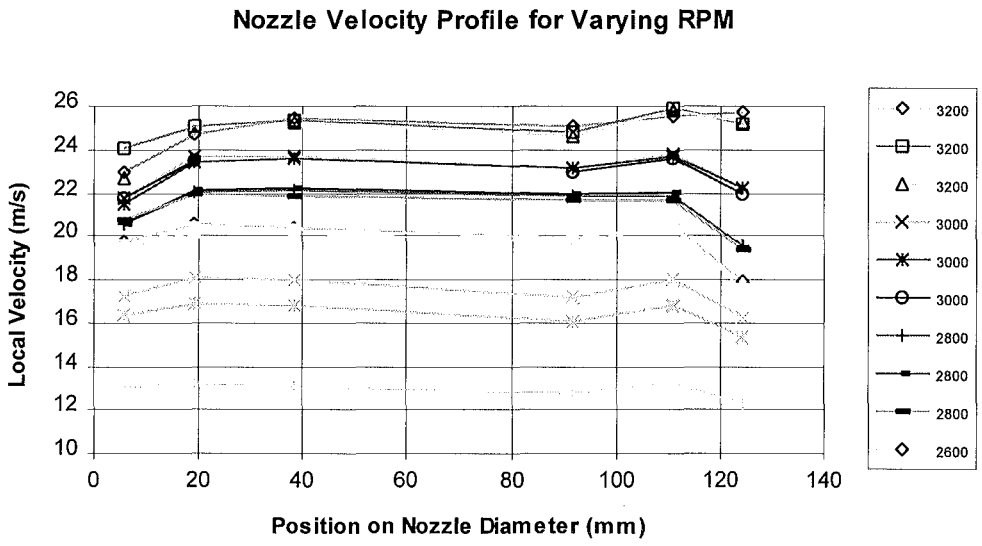

Figure 7.14 Nozzle velocity profiles for a range of rpms

7.2.4.2 Flow rate

As discussed in chapter 5 the flow rate is also required so that the extent of the front plane of the protruding stream tube can be determined. The nozzle velocity data used to determine nozzle momentum flux is again used to determine the flow rate. The flow rate is defined by equation (7.14) where C_4 is a correction factor similar to C_3.

$$Q = \frac{C_4 A_n}{6} \sum_{n=1}^{6} V_n \qquad (7.14)$$

Using equation (7.12),

$$Q = \frac{C_4 A_n}{6} \sum_{n=1}^{6} \sqrt{\frac{2(C_1 volts_n + C_2)}{\rho}}$$

$$= \frac{C_4 A_n}{6} \sqrt{\frac{2}{\rho}} \sum_{n=1}^{6} \sqrt{C_1 volts_n + C_2} \qquad (7.15)$$

7.2.4.3 Intake Momentum

The incoming momentum flux is calculated rather than directly measured as is the nozzle momentum flux. This is because the incoming fluid is not contained in a duct when it passes the water jet control volume boundary. The volume of incoming fluid is described as the "protruding stream tube", the front face of which lies on the waterjet system boundary. The flow rate which was measured using the method described in the previous section, is used to find the incoming momentum. A computer program, INTAKE.C, was written to calculate the momentum flux, the centre of incoming momentum and the uncertainties on each. Further discussion of the assumptions and equations used can be found in section 5.4.2.2.

The uncertainty on intake momentum flux was calculated using the sequential perturbation technique described by Moffat (1985)[1]. The technique involves calculating the required parameters using all possible combinations of the input parameters with their associated uncertainties. This has the effect of producing a

[1] p175

"bell shaped" distribution of the output parameters. The standard deviation is then calculated and used to determine the output uncertainty to the desired level of confidence. Input parameters are listed in *Table 7.1*.

Table 7.1 Input parameters for program "INTAKE.C"

Value		*Uncertainty*
Boat speed,	V_s	δV_s
Wetted keel length,	L_k	δL_k
Ingested flow rate,	Q	δQ
Boundary layer constant,	C_{bl}	δC_{bl}
Stream tube width,	b	δb
Boundary layer exponent uncertainty		δn

The program outputs the intake momentum flux and an associated error along with the position of the centre of momentum and its associated error all of which can be found in Appendix A-2. The error values entered are in general, twice the standard error plus an estimate of the systematic error for the parameter giving a confidence interval of 95%.

7.2.5 Uncertainties

7.2.5.1 Uncertainty on nozzle momentum

The total uncertainty on the nozzle momentum flux measurement is calculated as follows in equation (7.16) using methods described by Barford (1985) which are based on the least squares method. The uncertainty on the nozzle area and the fluid density are considered constant. The net nozzle area was calculated from two components, the gross area less the area taken by the six pitot tubes. The uncertainty also considers these two components. Accurate and repeated measurements of the diameters concerned resulted in a low uncertainty on the net nozzle area of 0.065 %.

Samples of seawater were taken from the site and accurate analysis performed to find the density. This was found to be 1024 kg/m^3 ±0.1%.

The relevant parameters and their associated uncertainties are tabulated in *Table 7.2*. Uncertainties are quoted to a 95% confidence. The calibration constants C_1, C_2 and associated uncertainties δC_1 and δC_2 were found from a linear regression analysis of the calibration data. C_3 is an interpolation correction factor described above.

Table 7.2 Variables and uncertainties

Parameter	*Best Estimate*	*Uncertainty (δ)*
C_1	136.206 kPa/volt	0.223 kPa/volt
C_2	-181.292 kPa	0.724 kPa
C_3	1.0095	0.005
C_4	1.0047	0.0025
δvolts (typical)	3	0.01 volts
Nozzle Area, A_n	0.013228 m^2	8.6E-6 m^2
Fluid density, ρ	1024 kg/m^3	1 kg/m^3

The average uncertainty on nozzle momentum flux found from equation (7.16) was ±0.83% however uncertainties for individual measurements can be found in the Appendix A-2.

$$\frac{\delta \dot{m}v}{\dot{m}v} = \sqrt{\left(\frac{\delta C_3}{C_3}\right)^2 + \left(\frac{\delta A_n}{A_n}\right)^2 + \left(\frac{\delta \sum_{n=1}^{6}(C_1 volts_n + C_2)}{\sum_{n=1}^{6}(C_1 volts_n + C_2)}\right)^2} \tag{7.16}$$

where,

$$\delta \sum_{n=1}^{6}(C_1 volts_n + C_2) = \sqrt{\sum_{n=1}^{6}\left(C_1 volts_n \sqrt{\left(\frac{\delta C_1}{C_1}\right)^2 + \left(\frac{\delta volts_n}{volts_n}\right)^2}\right)^2 + \delta C_2{}^2}$$

7.2.5.2 Uncertainty on flow rate

The uncertainty on flow rate, Q, is defined as in a similar fashion by equation (7.17).

$$\frac{\delta Q}{Q} = \sqrt{\left(\frac{\delta C_4}{C_4}\right)^2 + \left(\frac{\delta A_n}{A_n}\right)^2 + \left(\frac{\delta \rho}{2\rho}\right)^2 + \left(\frac{\delta \sum_{n=1}^{6}\sqrt{C_1 volts_n + C_2}}{\sum_{n=1}^{6}\sqrt{C_1 volts_n + C_2}}\right)^2} \tag{7.17}$$

where,

$$\delta\sum_{n=1}^{6}\sqrt{C_1 volts_n + C_2} = \sqrt{\sum_{n=1}^{6}\left[\frac{\sqrt{\left(\left(\left(\frac{\delta C_1}{C_1}\right)^2 + \left(\frac{\delta volts_n}{volts_n}\right)^2\right)^{0.5}(C_1 volts_n)\right)^2 + (\delta C_2)^2}}{2\sqrt{C_1 volts_n + C_2}}\right]^2}$$

The average uncertainty on flow rate was ±0.5%. Uncertainties for individual measurements can be found in the results table in Appendix A-2.

7.2.5.3 Uncertainty on intake momentum flux

The uncertainty on intake momentum flux was calculated using the sequential perturbation technique described in section 7.2.4.3. Uncertainties were entered along with data for each specific run. A table of typical uncertainties is shown in Table 7.3. The average uncertainty on the intake momentum flux was 29 N for an average momentum flux of 1565 N which is 1.8%.

Table 7.3 Intake momentum calculation uncertainties

Value		*Uncertainty*
Boat speed,	V_s	0.6%
Wetted keel length,	L_k	3%
Ingested flow rate,	Q	0.5%
Boundary layer depth constant,	C_{bl}	10%
Stream tube width,	b	10%
Boundary layer exponent,	n	10%

7.2.5.4 Uncertainty on thrust

The uncertainty on thrust is calculated using equation (7.18). It is assumed that the effect of the angle of the incoming and outgoing fluxes to horizontal and errors in calculation of appendage drag and the wind resistance have a negligible effect on the calculation of the uncertainty on thrust. Therefore,

$$\delta T \cong \sqrt{\delta\phi_{Mi}{}^2 + \delta\phi_{Mn}{}^2} \qquad (7.18)$$

For example, at a boat speed of 24 knots (ϕ_{Mn}=8313 N; ϕ_{Mi}=3867 N) and using the average uncertainties calculated above,

$$\delta T = \sqrt{70^2 + 69^2} = 98\,N$$

The horizontal component of thrust is 4377 N. The average uncertainty to a 95% confidence is therefore 2.2%.

7.3 Full Scale Tests

7.3.1 Introduction

Full scale propulsion tests were conducted over three days during the month of March 1995. Several preliminary tests were required to develop techniques for the measurement of thrust. Equipment was modified and procedures refined during this development phase.

7.3.2 Site

The same site as that used for the towing tests was again used for the propulsion tests. As discussed previously the depth was sufficient to consider depth effects negligible.

7.3.3 Hull geometry and loading condition

The hull geometry was unchanged from the towing tests. The intake cover plate was of course removed. Extension of the nozzle rendered the steering deflector inoperable so a rudder was attached to the bottom of the deflector. The deflector was machined to allow movement. Drive to the rudder was still maintained through the existing system. The rudder was constructed as small as possible to minimise drag.

The boat displacement and LCG changed a little from the towing test condition. Some of the ballasting was moved forward and an extra person taken on board. The weight of entrained water (35 kg) was included in the displacement and LCG calculations.

7.3.4 Instrumentation

The instrumentation for the propulsion tests was the same as that used during the towing tests with the exception that the towing force transducer and towing angle potentiometer were removed and the nozzle pressure transducer added.

7.3.5 Measurements taken

Boat speed, wind speed, wetted keel length and total keel trim were all measured in the same manner as that described for the towing tests.

For the bulk of the tests the nozzle pressures were measured with the rake in one fixed orientation, at 30 degrees to vertical. The six pressures were measured consecutively while maintaining the engine rpm and boat speed constant.

7.3.6 Daily testing procedure

The following personnel and equipment was required for a days testing:

- test boat, trailer and truck
- camera man
- the author as test boat operator
- an assistant on the test boat

Upon arrival at the launch ramp the computer was started and the data acquisition software loaded. The computer date and time settings were checked and reset as required. The boat hull was then prepared, removing the tail-light board and fitting drain bungs, wind anemometer and ballasting. All transducers were then checked for correct zero readings. The fuel level and the angle of the fuel tank was recorded.

The boat was then launched by reversing quickly and applying full braking. The reversing deflector was removed due to the nozzle modifications so no reverse thrust was available. The boat was therefore man-handled from the trailer and brought alongside the wharf. The assistant would then come aboard, the engine started and brought up to operating temperature. The boat was then the motored to the test site.

The test procedure consisted of bringing the boat up to speed, maintaining that speed for a time to allow the planing condition to stabilise, and then recording data. The test run would be started in a position such that the steady state would be achieved abeam of the camera. The photographs were taken as described in the section on towing tests. While the boat maintained the constant test speed, the hose for each pitot probe in the rake was independently connected to the pressure transducer for a period of approximately four seconds. Speed was measured using a radar gun from within the boat. Wind speed was measured using a Gill type anemometer.

At the end of each run the data set was down-loaded onto diskette and latter transferred to hard disc on another computer.

7.3.7 Results of full scale tests

Appendix A-2 contains the measured and calculated data arising from the propulsion tests. The uncertainties on each measurement are also shown in the adjacent column and prefixed with a δ. The symbol **h** symbolises the distance from the hull to the centre of incoming momentum flux. The probe orientation was either 30 degrees left or right or horizontal as signified by the designations L, R and H. A volumetric Froude number is also shown. The wetted keel length and total keel trim were found from photographs.

As discussed earlier in the chapter, all momentum fluxes and the flow rate were determined from the Prandtl rake measurements and then the computational programs. The bank of pitot tubes and their supporting frame work were exposed to the jet and so experienced a drag force. This force was calculated and subtracted from the thrust force measured at the nozzle.

The thrust, T, was calculated according to the ITTC recommended formula (7.1) but only the horizontal component is shown.

7.3.8 Hull static pressure measurements

Measurements of static hull pressures (relative to atmosphere) were taken at two boat speeds. Three rows of pressure tappings were drilled in the hull near the intake at distances of 0.25, 0.5 and 1 times the intake width from the hull centre line. Further tappings were positioned behind the cutwater and beside the keel, ahead of the intake.

Small flanged brass fittings, 30 mm in diameter were glued to the inside of the hull plating, in line with the tapping holes to facilitate the connection of tubes to carry pressure to a pressure transducer. A single pressure transducer was connected to the seventeen tubes via a rotary valve which is shown in the photograph in Figure 7.15. The pressure transducer can be seen mounted on the base plate. As the valve was located up on the deck negative gauge pressures at the valve allowed the ingress of air into ports that were not connected to the pressure transducer. The rotary valve

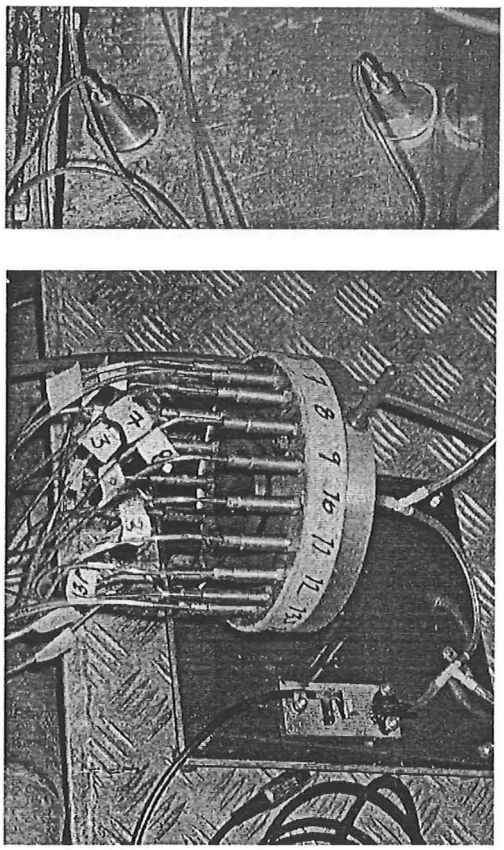

Figure 7.15 Tapping fittings (above) and rotary valve (below)

was subsequently immersed and operated in a tank of water to keep air from entering the lines.

Pressure measurements were conducted at constant speeds of 3.6 m/s and 10.3 m/s. During each test run the computer recorded the transducer signal continuously while the rotary valve was slowly indexed through all 17 ports. Later the signal for each pressure tapping was extracted from the data recording.

Voltage signals were converted to pressures using calibration constants found by calibrating the transducer using a 1 m, (9.81 kPa) column of water on the day. The height of the transducer above each tapping was calculated separately and a correction made to the reading. Several test runs were conducted at each speed and the results averaged.

The pressures (p_{0A}) were then converted to dimensionless coefficients using equation (4.5) which is re-stated below. This has the effect of removing the buoyancy pressure ($\rho g h_I$). The submergence of each tapping site was calculated trigonometrically from trim and wetted keel length data.

$$C_p = \frac{p_{0A} - \rho g h_I}{\frac{1}{2}\rho V_s^2} \qquad (4.5)$$

The results are presented in Figure 7.16 for both speeds, the slower speed results are mirrored onto the port side. A comprehensive error analysis was not conducted. The pressure transducer was found to be quite accurate but data recordings exhibited a high standard deviation due to the boat pounding.

Significance should not be attached to isolated tapping measurements but rather an average gauged from several measurements in a region of interest. Although considerable care was taken to remove burrs, static tappings are known to be unreliable.

At the lower speed, pressure coefficients can be seen to be negative which indicates that the water is being accelerated to a speed greater than that of the hull. The area of greatest "speed up" is at the front of the intake.

In the case of higher speed, coefficients are more positive indicating a slowing of

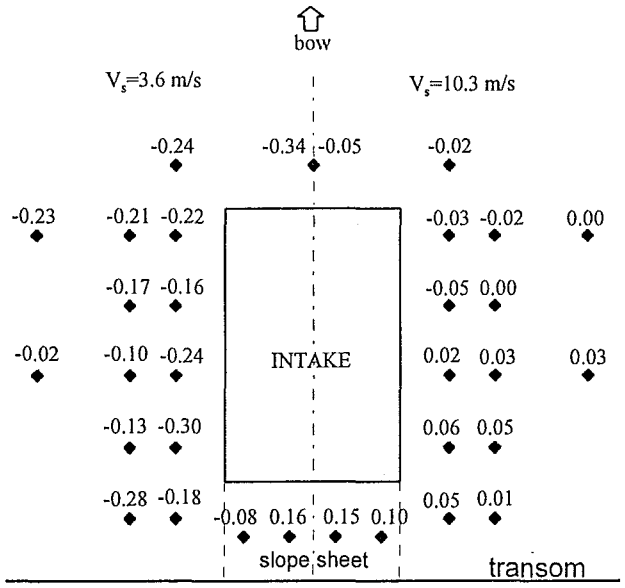

Figure 7.16 Results of pressure tapping measurements. (Pressure coefficient C_p)

water relative to hull speed. Similarly the lowest pressures are occurring at the front of the intake while higher pressures are occurring toward the sides and rear of the intake.

There is certainly evidence of higher pressures behind the cutwater however it should be noted that in this instance a 5 degree slope sheet was in place directly behind the cutwater and running back to the transom. This was present to model the usual installation. Subsequent analysis has revealed that it would have been better to have had the slope sheet set at 0 degrees to the keel as this is the case in the bare hull installation.

7.4 Model Tests

Propulsion tests were also conducted MARIN using the same model as for the towing tests. The model was scaled to represent a full scale loading condition of 2800 kg and LCG equal to 2.5 m.

7.4.1 Model Test Procedures

The hull was re-ballasted to achieve the same displacement and LCG as for the towing tests. The model was fitted with a small waterjet (d_n= 0.042 m) manufactured by Hamiltons. The intake was scaled accurately to represent the full scale version in the test boat. A drawing of the installation is shown in Figure 7.17. The following is a description of how the JIP model tests were conducted at MARIN, MARIN(1991).

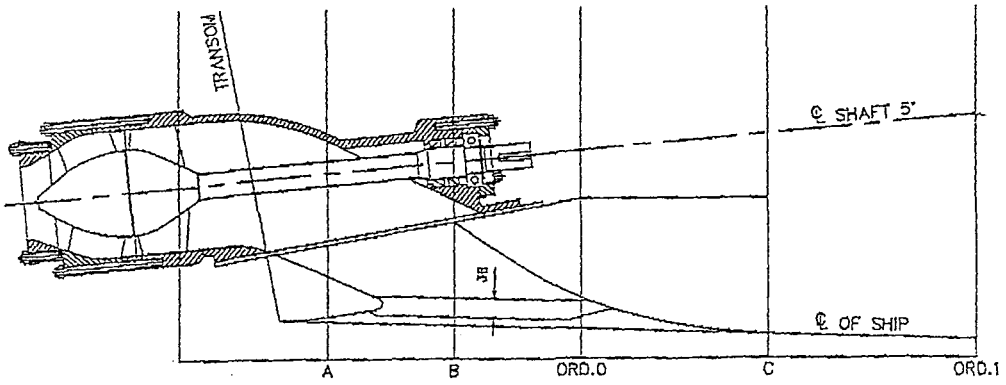

Figure 7.17 Waterjet installation for model propulsion test

"At the self propulsion point of ship, care is taken that the propulsor is operating at the full scale point of operation. This means that the thrust coefficient C_T is equal for the model and full scale. Because the frictional resistance at model scale is larger than at full scale, this means that an additional towing force F_D should be applied to the model.

The rate of revs of the stock jets is adjusted in such a way that the approximate self propulsion point of ship is obtained. The correction required to obtain the results for the exact self propulsion point of ship is determined from the load variation tests. The required thrust at the self propulsion point of ship T_s is now determined from:

$$T_s = \left[T_m + (F_D - F)\frac{\partial T_m}{\partial F} \right] \lambda^3 \frac{\rho_s}{\rho_m} \tag{7.19}$$

where,

T_m = *thrust as determined from model tests*
F = *measured longitudinal towing force*
F_D = *towing force correction for viscous scale effects*
λ = *scale ratio*

subscripts s and m denote the ship and the model respectively.

Equation (7.19) appears to be based on laws of physical similarity.

7.4.2 Results of model propulsion tests

Results of model propulsion tests are shown in Table 7.4.

Table 7.4 MARIN propulsion test results for test 50221

Speed		*Planing Parameters*		
Knots	*Fv*	*Thrust (N)*	*Lk (m)*	*Trim (deg.)*
6.50	0.90	1972	6.15	1.71
7.00	0.97	2581	6.07	2.51
7.50	1.04	3088	5.99	3.44
8.00	1.11	3395	5.99	4.16
8.50	1.18	3616	5.91	4.72
9.50	1.32	3829	5.83	5.13
15.00	2.09	4411	5.03	6.39
16.00	2.22	4398	4.87	6.40
18.00	2.50	4326	4.63	5.33
20.00	2.78	4287	4.55	5.42
22.00	3.06	4415	4.47	4.95

7.5 Discussion

Comparison of the propulsion and bare hull data forms the core nature of this work on hull-waterjet interaction and so is discussed in the following chapter. Graphs of full scale and model data are presented here showing thrust, trim and wetted keel length.

Figure 7.18 displays horizontal thrust data for both the full scale and model propulsion tests conducted at MARIN. Considering the full scale data, with the exception of several stray points that have been omitted from the graph, there is generally little scatter. There are however several points that appear to be outside the averaged error band of 3%. These are probably due to another boats wake or more likely sudden steering corrections that have slowed the boat. The model test thrust is generally lower the full scale thrust however the hull loading was approximately 3% less and the LCG 50 mm forward. Both would result in the lower thrust and change the trim. Running the data through the computational model yielded a difference of approximately 200 N throughout the speed range confirming the explanation.

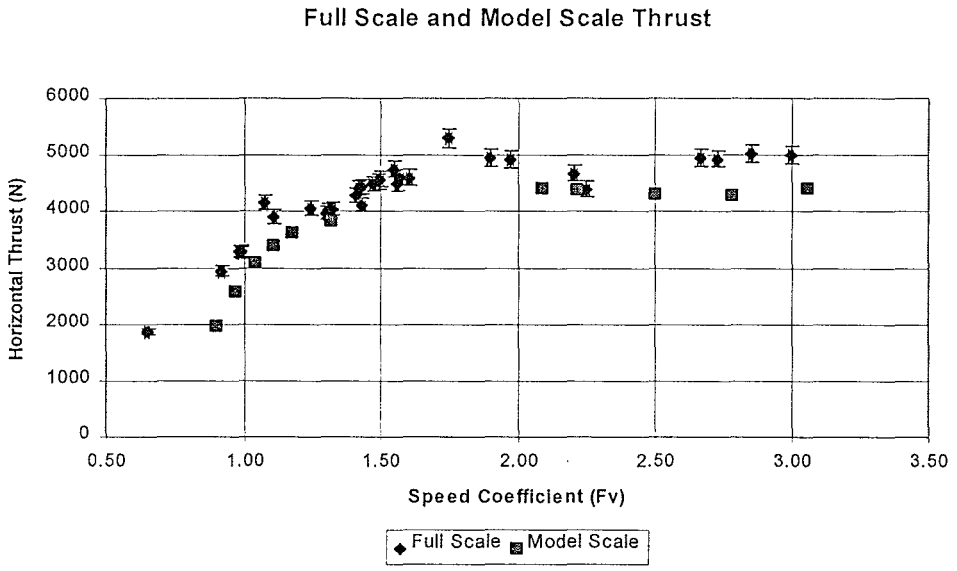

Figure 7.18 Graphs of full scale and model scale thrust

It is unclear what aerodynamic loadings were used in the final preparation of the model data. As discussed in section 5.3.2, the aerodynamic loading not only acted so as to increase the resistance but also had a very considerable component of lift which served to increase the trim and resistance.

The trim readings are shown in Figure 7.19. There appears to be some scatter around the F_∇= 2.75 speed. At higher speeds the boat did tend to pitch slightly which may well have caused a wider scatter of the data than at lower speeds. The model data is again low however the explanation for reduced thrust also applies to the trim.

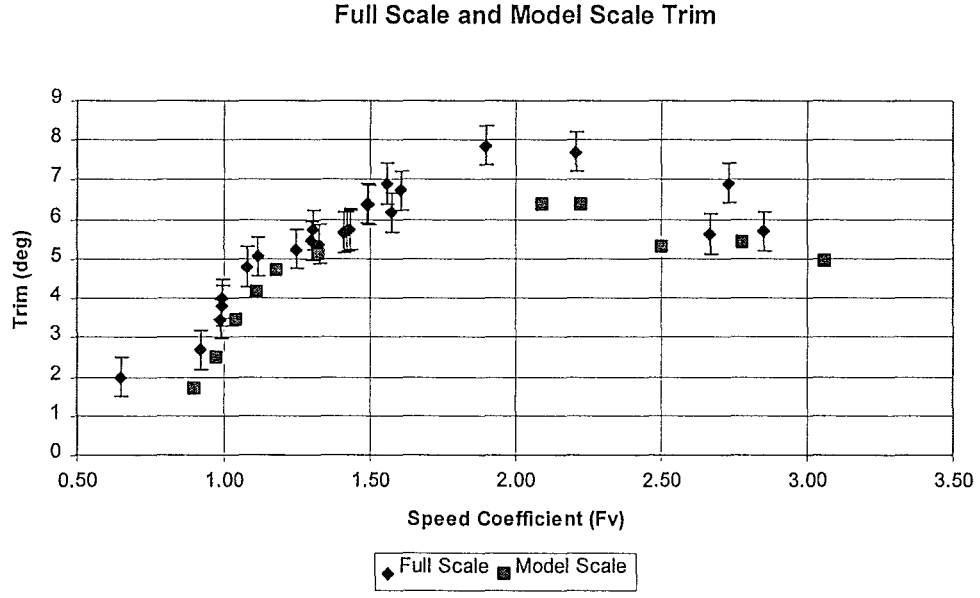

Figure 7.19 Graphs of full scale and model scale trim

It was also noted that an error in transmission of the waterjet installation geometry was made that resulted in the waterjet being mounted incorrectly, at 5 degrees to the keel instead of 3.7. This would have the effect of increasing the bow down moment and so also reduce the trim.

Wetted keel lengths are shown in Figure 7.20. Very close agreement exists. However this is due to the increased full scale displacement acting to lengthen the wetted length while the increased trim serves to shorten the wetted length. The net effect appears to leave the wetted length very similar for both cases.

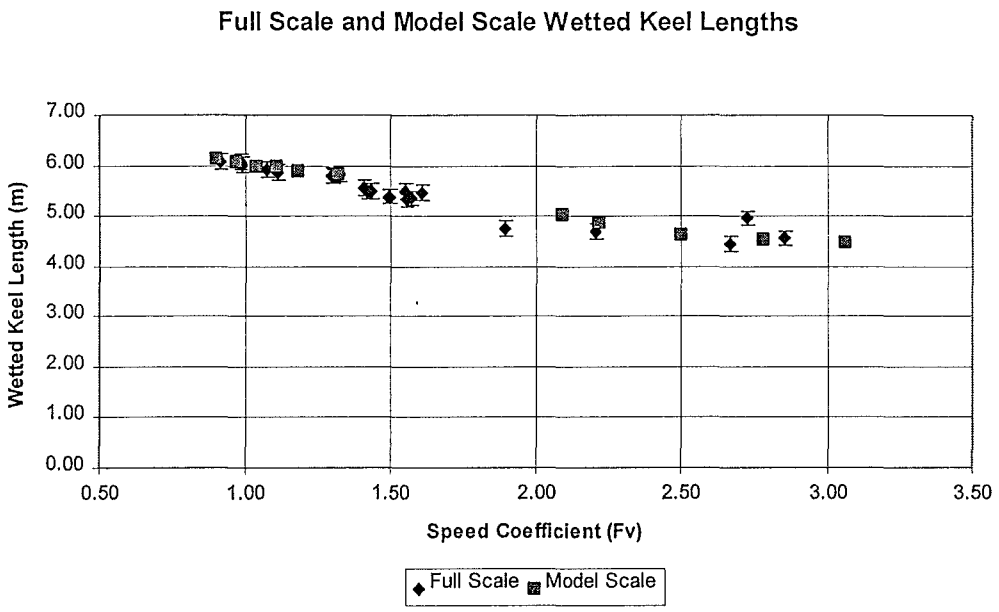

Figure 7.20 Graphs of full scale and model wetted keel lengths

7.6 Conclusions

The following points summarise the work detailed in this chapter:

- Methods of measuring nozzle momentum flux have been reviewed. Two approaches were covered: the use of flow rate calibrated reference probes and velocity profile integration. The averaging static pitot tube used by MARIN was discussed. The integration method was chosen for use in this project.
- The only weakness is the sole reliance on the nozzle integration for the calculation of nozzle momentum flux, flow rate and finally the intake momentum flux. There is no cross check in the procedure by way of an independent measure of flow rate however

previous workers (Burtness 1987) have found that the integration method gives good results.

- The construction of a Prandtl rake to measure the nozzle momentum flux is described. A description of the steps taken to reduce nozzle swirl and static pressure to acceptable levels in presented.
- A method has been presented for the measurement of incoming momentum flux. This method depends on assumptions made about the shape of the stream tube, the type of boundary layer and an accurate measurement of the flow rate. The boundary layer was never finally measured, however many researchers have performed this task before and theory exists to explain its behaviour. Estimates of systematic uncertainty on all assumptions were included in the calculation.
- A detailed uncertainty analysis is conducted on the calculation of momentum fluxes, flow rate and thrust. The average uncertainty on thrust was calculated with a 95% confidence to 2.2%.
- The experimental procedures and results from the full scale and model propulsion tests are reported.
- Earlier propulsion testing using a load cell system to measure thrust are reported as are the reasons why the concept was finally discontinued.
- Experimental work to record hull static pressures around the intake is presented along with the results.
- The full scale and model propulsion test data are compared and found to be in reasonable agreement.

8. Analysis of Results

In this chapter results from the chapters 6 and 7 are studied and analysed further. The first section presents thrust deduction factors for the full scale and MARIN model tests. The second section presents work on finding the interaction vector and discusses its likely causes.

8.1 Comparison of Full Scale Bare Hull and Self Propulsion Tests

8.1.1 Comparison of Thrust Deduction Factor

The thrust deduction fraction is calculated as the ratio of the difference between the net thrust and the bare hull resistance to the net thrust. The question arises however: what line of thrust should be assumed for the bare hull? (or practically, where to apply the tow rope and in what direction to pull) A different towing position effectively changes the LCG and static displacement of the hull so clearly results from resistance tests or Savitsky resistance prediction calculations will differ. This will effect the thrust deduction calculation also.

The ITTC (1987)[1] have recommended using the shaft line. The choice of shaft line no doubt has its origins in conventional propeller practice where the assumption that the thrust force is primarily applied along the shaft certainly holds more true than for a waterjet.

In the case of a waterjet the incoming momentum flux vector is applied some distance from the shaft; below the hull and at angle parallel to the keel. If pressure effects on the intake region are ignored and the thrust assumed to be the difference of momentums then the thrust vector is at a greater angle than the shaft line. In the case of the Hamilton test boat the thrust angle to the keel ranges from 5 to 8 degrees compared to the shaft which is at 4 degrees. The effect of this is to cause a greater pitching moment about the centre of gravity.

Other towing positions can be used. MARIN tow horizontally but at the same distance from the centre of gravity as the shaft. The Savitsky short form method

[1] p307

assumes that all forces pass through the centre of gravity and that thrust is applied horizontally.

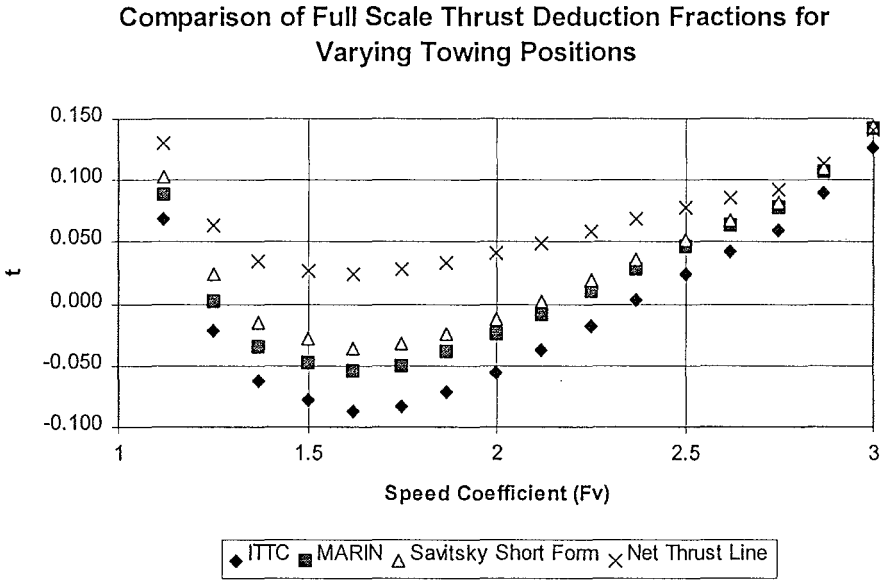

Figure 8.1 Graphs of thrust deduction fraction for varying towing position

Graphs of varying thrust deduction characteristics are shown in Figure 8.1 for the Hamilton test boat as set up for the propulsion tests described in chapter 7. Data for the lower three curves were calculated using the bare hull computational model described in chapter 5. The computer program easily allows a different towing position to be written into the code. Data for the case where the waterjet momentum fluxes are considered uses the self propulsion computational model also described in chapter 5. In all cases appendage drag is included along with aerodynamic loadings. Added resistance due to waves however has been omitted throughout. The thrust deduction curves represent the difference between the Savitsky output and the full scale data.

The importance of carefully considering the towing position is clearly shown as variations in resistance of up to 4% are evident for the bottom three cases. Considering the intake momentum, changes the picture still further. It can be seen in Figure 8.1 that by considering the intake momentum, the bare hull resistance is reduced causing the thrust deduction fraction to be wholly positive. Clearly though this addition to the theory is not sufficient to explain all the interaction effects. If this were the case then the thrust deduction curve would be constant at 0%.

Figure 8.2 displays thrust deduction fractions for the model and full scale data. In this case the full scale thrust deduction is calculated using the MARIN towing position such that the data is compared on the same basis. Error bars are shown on the full scale data to a 95% confidence however no error estimate was supplied with the model data. Very much the same trend is exhibited by both sets of data, both appearing to have a minimum at approximately $F_\nabla = 1.6$ which is in the region of the hump.

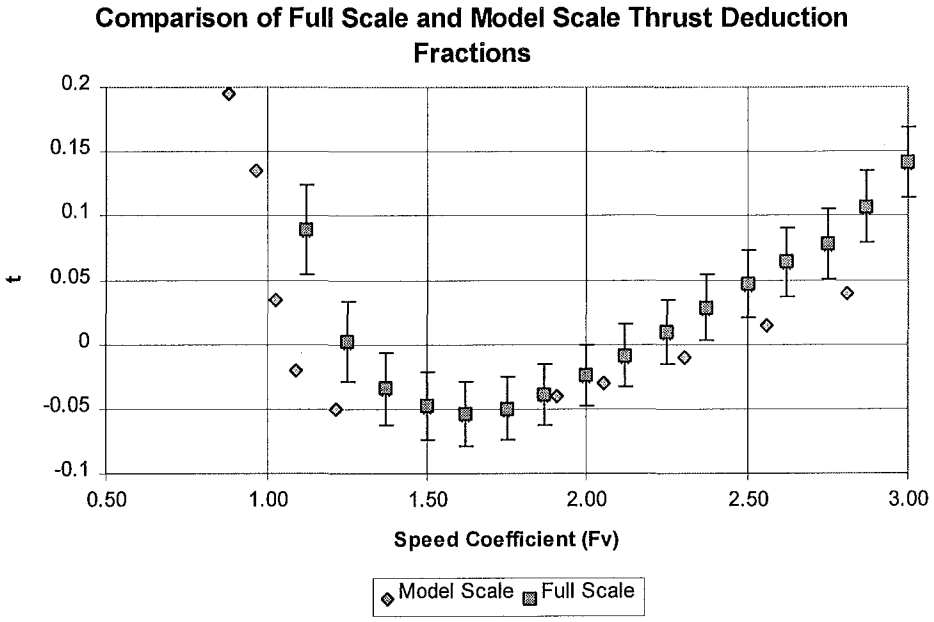

Figure 8.2 Comparison of full scale and model thrust deduction factors

The thrust deduction fraction for the full scale data is consistently several percent higher than the model data. One explanation may be the higher (3%) displacement for the full scale tests. Displacement variation tests conducted by MARIN during the joint industry project (MARIN (1991)) exhibited a 5 to 7 percent increase in t for a displacement increase of 10%. If the effect of increased displacement is assumed to be linear over a small range then in this case a change in t of up to +2% could be expected which would bring the two curves into good agreement.

Considering the different experimental techniques employed, a reasonable degree of confidence can be had in both sets of results.

Negative thrust deduction is evident in the hump region in this case. This is substantially due to the lift effect of the waterjet due to the momentum change which

is created by the net thrust line being at 5 to 8 degrees to the keel rather than the 4° of the shaft line. When the net thrust line angle is added to the keel trim, the net thrust vector may act at 10 to 15° to horizontal producing a substantial lift (sine15° = 0.26). This proposition is supported by the fact that the curve which includes the intake momentum in Figure 8.1 is substantially less negative.

The thrust deduction fraction is seen to be steadily increasing as the boat speed increases to the cruise condition.

Smaller craft operating at higher Froude numbers may suffer from adverse interaction above $F_\nabla = 2$. Larger craft however may enjoy negative thrust deduction. For example a 150 tonne vessel cruising at 25 knots represents a volume Froude number of approximately 1.8. This puts it into the favourable area on the thrust deduction curve, Figure 8.2.

8.1.2 Comparison of full scale trim, wetted length and CG position

Aside from the thrust deduction fraction, other planing parameters are compared below. Following from the discussion above, two cases of towing position were used for the calculation of the bare hull parameters. These were the ITTC recommendation of the shaft line and the net thrust line calculated by considering the nozzle and intake momentum fluxes. To generate reasonably smooth curves for the full scale data, third and fourth order polynomials were fitted through the measured data using the least squares method.

Figure 8.3 displays the difference between thrust and resistance for the two towing positions outlined above. It can be seen that there is a substantial difference between the two as also highlighted by the thrust deduction curves shown in Figure 8.1. The variation is greatest at the hump speed where it is nearly 600 N. This means however that the ITTC convention yields a larger or more conservative resistance prediction than when intake momentum is included. It also results in a more negative t.

The difference between self propelled and bare hull trim is displayed in Figure 8.4. The trim is consistently greater when self propelled throughout the speed range for both towing cases. The ITTC case yields less of a difference as the bare hull trim

calculated using this convention is greater due to a reduced bow down moment than for the net thrust line case.

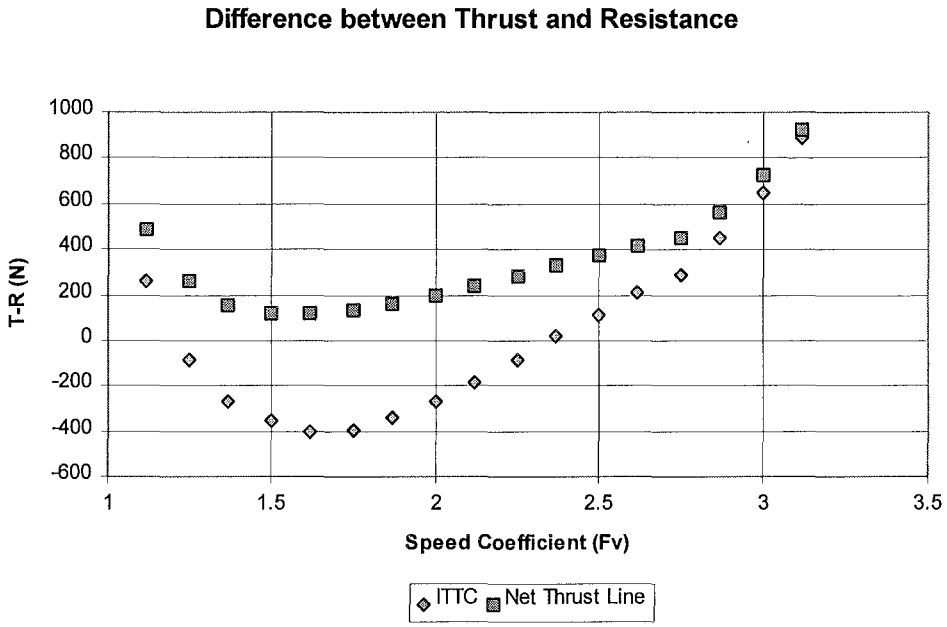

Figure 8.3 Difference between thrust and resistance

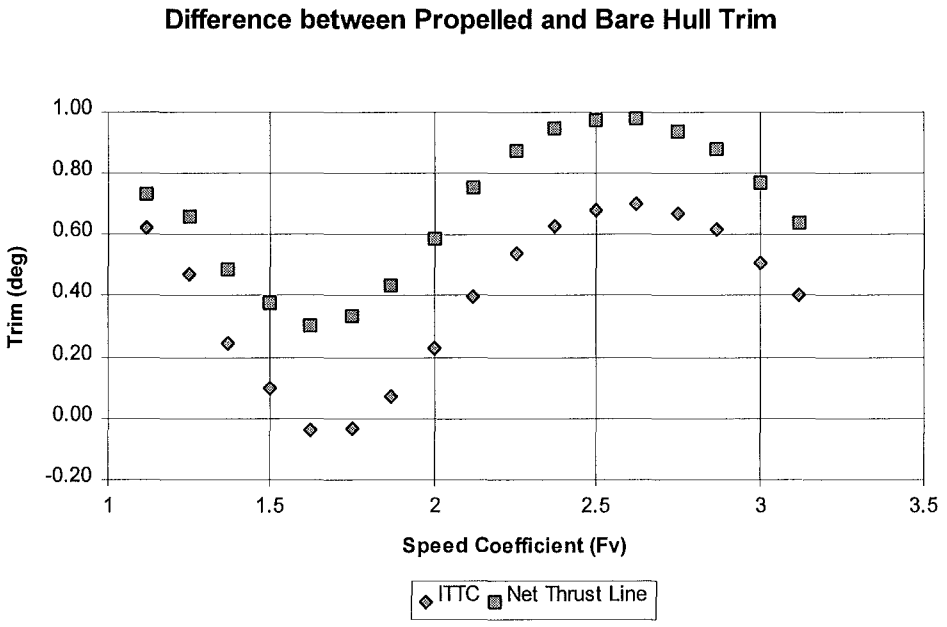

Figure 8.4 Difference between propelled and bare hull trim

shows the difference between propelled and bare hull wetted keel length. Small variations exist between the cases. The wetted lengths show an inverse relationship with trim as would be expected.

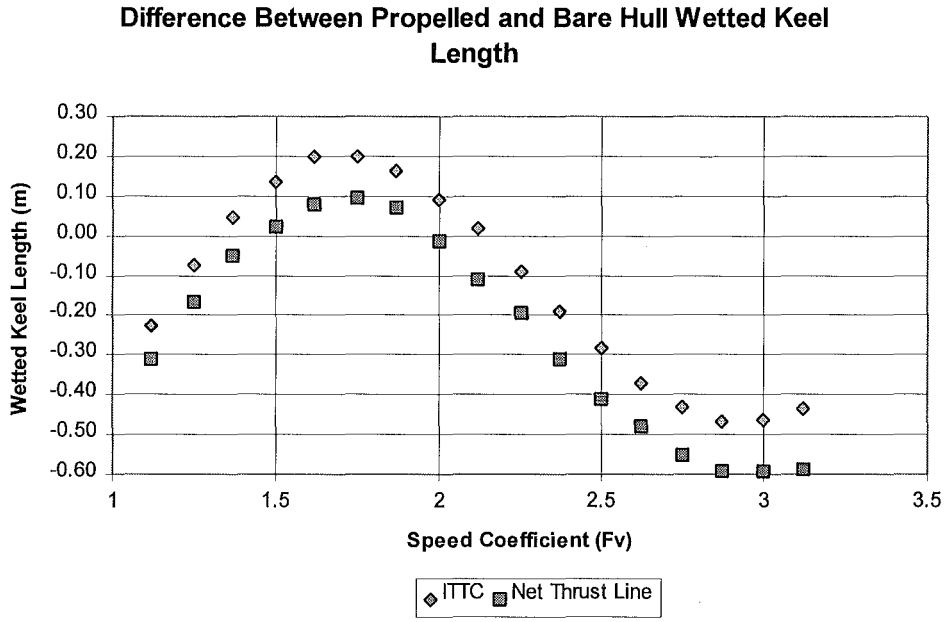

Figure 8.5 Difference between propelled and bare hull wetted keel length

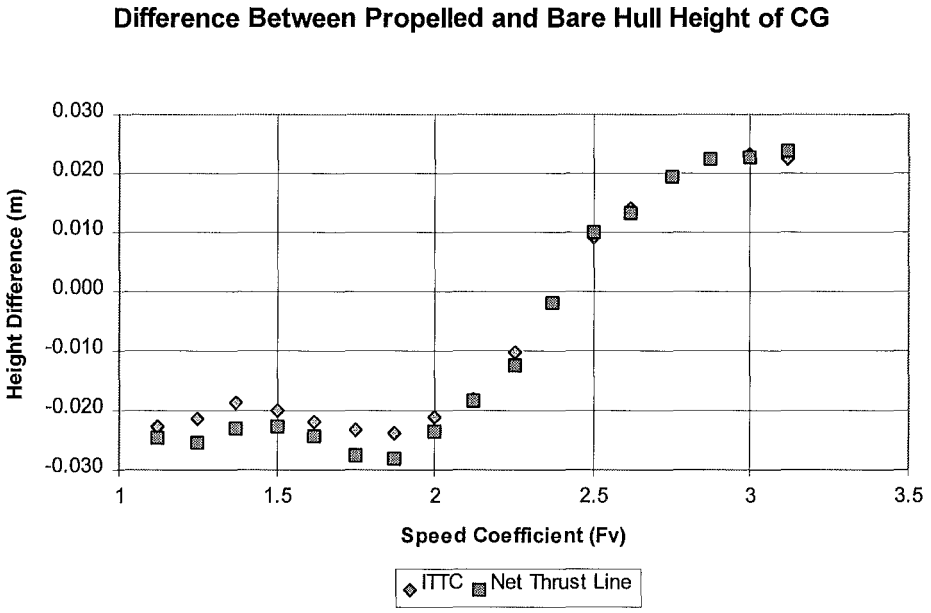

Figure 8.6 Difference between propelled and bare hull height of CG above free surface

For completeness the change in height of the CG is also shown in Figure 8.6. There is little variation between the two cases which given that there is a difference in trim would indicate that hull is rotating about a point close to the centre of gravity.

The next step was to find what forces are causing the differences in planing parameters outlined in the graphs above. This work is covered in the next section.

8.2 Interaction Vector

8.2.1 Review of approach

The interaction vector was designed to be added to the Savitsky model such that the modified model gave correct values. It is timely to briefly review the method by which the interaction vector was calculated. The technique was to apply a vector to the self propelled computational model of such a magnitude and in such a position that the best possible match was achieved with the full scale propulsion results. The self propulsion model thus far includes aerodynamic and appendage forces and the waterjet nozzle and intake momentum flux vectors. It also includes a small correction for the reduced skin friction drag due to the removal of the intake cover plate. It does not account for lost lift in the wake or lost lift on the intake cover plate. The interaction vector will account for these and any other interaction effects.

An error function was calculated as the square root of the sum of the squares of the percentage differences of the resistance, trim and wetted keel length between the model and full scale data. When this error was found to be zero then the hull would be in the same planing position geometrically and have the same resistance. Several iterative loops were required to find the best combination of magnitude and position at a given speed.

8.2.2 Presentation of results

The first attempt at finding the interaction yielded the data shown in Table 8.1. The interaction vector (ivector) is reported along with the its offset from the centre of gravity and the interaction error (i_error). It was found that for the three lower speeds the i_error function did not have a clear minimum so the computational solution would not converge on a best position for application of the vector. In these cases however a moment could be calculated to give a solution.

Table 8.1 Interaction vector results

F_∇	*ivector (N)*	*off_i (m)*	i_error	*Moment (Nm)*
1.11	na	na	3	3488
1.38	na	na	4	2902
1.66	na	na	5	2770
1.94	849	4.3	5	na
2.21	1538	3.7	5	na
2.49	2182	3.7	4	na
2.76	2831	3.0	0	na
3.04	2889	2.1	8	na
3.32	1525	0.0	18	na

The direction of application of the interaction vector was downwards and at right angles to the keel. Overall the stability of the solution was marginal as far as position was concerned. The average offset was found to be 2.8 m which is just behind the transom. However the direction of the interaction vector was as expected from the studies conducted in chapter 5, that is, downwards.

A further computational run was conducted setting the ivector offset constant at 2.8 m and then solving for ivector magnitude. The results of this study are graphed in Figure 8.7. The program converged well with the average error on resistance, wetted length and trim parameters being 2%.

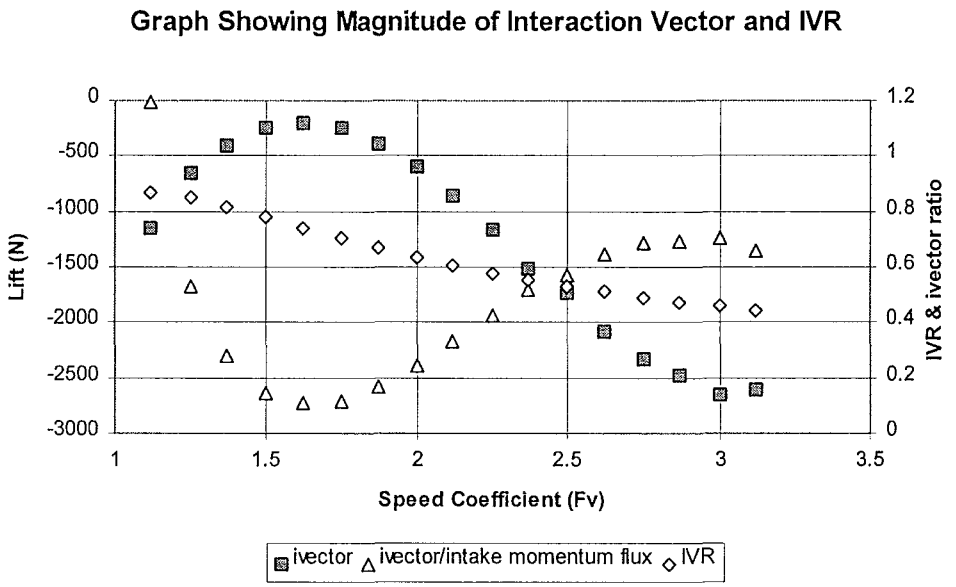

Figure 8.7 Magnitude of ivector at fixed position, IVR and ratio of ivector to intake momentum flux

It can be seen from the graph that the interaction vector increases steadily after the hump before levelling off at $F_\nabla \approx 3$. Also shown are graphs of the intake velocity ratio and the ratio of the interaction vector to the intake momentum flux. The interaction vector shows no clear relationship to the IVR or the intake momentum flux. It was hoped that the magnitude of the ivector may exhibit a simple relationship to the inlet momentum flux but this was not the case.

8.2.3 Possible Contributing Factors to the Interaction Vector

Earlier in the thesis it has been proposed that the lost lift in the wake and lost lift due to removal of the intake cover plate are likely major contributors to the interaction vector.

Referring to the hull static pressure measurements reported in section 7.3.8, pressures in the region of the intake range from approximately 3 to 7 kPa. The range is much the same for both 7 and 20 knots.

Assuming that an average pressure of 5 kPa would have been available to act on the area removed for the intake then the lost lift is equal to 5×10^3 kPa × 0.36 m × 0.66 m = 1190 N.

Considering the drawings of stream tube profiles in Figure 5.1, the approximate entry angle of fluid into the intake relative to the keel can be measured. This was found to be approximately 5 degrees for an IVR of 0.6. If a comparable mass flow to that entering the intake is moving in behind the stream tube to replace it, then the available lift is calculated as sine5 × ϕ_{Mi}. At an IVR of 0.6 the intake momentum flux is approximately 2590 N. It is possible then, if vertical component of this is not recovered that a downwards force of 226 N is present.

Adding both the effects, yields a downwards force of 1190 + 226 = 1416 N. The interaction vector at this IVR is approximately 1000 N so the explanation is certainly feasible.

To take the analysis any further without greater understanding of the hull pressures and the true extent to which lift is lost in the wake is to enter into the realm of

speculation. The techniques employed here have revealed the total interaction force vector but however cannot split this up accurately into its constituent parts.

8.3 Conclusions

The following points summarise chapter 8.

- Thrust deduction data is presented based on varying towing positions and the effect of changing towing position highlighted.
- The ITTC convention of towing along the shaft line is the most conservative approach, yielding the highest bare hull drag and most negative t.
- The thrust deduction fraction is compared with the MARIN results and a good correlation found.
- Negative thrust deduction fractions up to -8% are evident in the hump region for certain towing positions.
- The severity of thrust deduction at speeds other than the hump is clear, tending towards 15% at both lower and higher Froude numbers.
- The change in resistance, trim, wetted length and height of the center of gravity above the free surface is presented.
- The interaction vector concept is re-introduced and the vector calculated and presented. Its position and magnitude is found to be generally consistent with the proposed contributors namely lost planing surface and lost lift in the wake.
- More detailed analysis of the interaction vector is not possible without conducting further experiments.

9. Conclusions

9.1 Contribution to the Understanding of Hull-Waterjet Interaction

The major aim of this project was to gain a better understanding of hull waterjet interaction including explanations of possible causes. The ultimate goal of work in this area is to achieve a full understanding of the mechanisms with a reliable method of predicting interaction for all likely hull and propulsor configurations. This has not yet been achieved, however with this project the following advances have been made.

- The experimental test program has provided some valuable data at both full scale and model scale for a prismatic planing hull. The thrust deduction characteristics have been accurately measured and reported for a prismatic planing hull. Good correlation was found between both model and full scale data giving some credence to the results.
- The feasibility of conducting full scale towing tests has been proved.
- Measuring thrust using a system of load cells has been attempted but found to be too difficult.
- Three major mechanisms have been proposed as causing interaction:

    1. waterjet nozzle and intake momentum flux forces
    2. loss of planing area at the intake
    3. lost lift in the wake

- A method for including the waterjet momentum forces in performance prediction calculations has been presented along with a method for finding the magnitude and position of the combined remaining interaction forces.
- The combined interaction force was calculated and found to be of a magnitude and position consistent with the proposed mechanisms.
- The project has contributed further understanding which will lead to the development of better performance predictions in the future.

9.2 Summary of Conclusions

A summary of the significant findings of each chapter is presented below.

- The thrust deduction and hull wake factors are well established in the existing theory. The wake factor is well understood but the thrust deduction factor is a correction factor which can only be found experimentally.
- Some existing theory includes a pressure coefficient as an extension to the wake factor, however supporting data is lacking.
- Hadler's (1966) work on hull-propeller interaction has provided a useful framework for an analytical method to find the magnitude of interaction effects. As further experimental data and refined analytical methods become available the computational model developed here could form a basis for extension of understanding of interaction between other boat shapes and waterjet configurations.
- An interaction vector has been defined. This may be added to the existing computational model as described by Hadler (1966). The interaction vector accounts for all pressure forces acting on the hull not included in the existing model.
- A method for finding the interaction vector has been described where by the theoretical propulsion model is compared to the full scale data and an interaction vector chosen to provide the best possible fit. The following assumptions were made in developing the theoretical model. The Savitsky equations for centre of pressure are assumed to be unaffected by the interaction vector. The static pressure is assumed to have a negligible effect on thrust. The shape of the ingested stream tube is assumed to be elliptical and a constant 50% wider than the intake.

  The following points were also included in the model. The displacement is allowed to vary from the static condition. Interaction effects on the waterjet performance are limited to the wake factor. The effect of the nozzle velocity

profile on the outgoing momentum is considered. Aerodynamic loadings are considered in some detail.

- The computational model of the towing case predicts the full scale towing data adequately. Small speed dependent correction functions have been developed to account for deviations between the prediction and full scale data. Using the model with these correction functions to predict the MARIN model results has proved very successful.
- Methods of measuring nozzle momentum flux have been reviewed. Two approaches were covered: the use of flow rate calibrated reference probes and velocity profile integration. The averaging static pitot tube used by MARIN was discussed however the integration method was chosen.
- The construction of a Prandtl rake to measure the nozzle momentum flux is described. A description of the steps taken to reduce nozzle swirl and static pressure to acceptable levels is presented. The procedures and assumptions used to calculate the nozzle momentum flux, flow rate and intake momentum flux from the Prandtl rake velocity measurements are presented. A detailed error analysis is conducted on the calculation of momentum fluxes, flow rate and thrust.
- Earlier propulsion testing using a load cell system to measure thrust are reported as are the reasons why the concept was finally discontinued.
- The experimental procedures and results from the full scale and model propulsion tests are reported. The full scale and model propulsion test data are compared and found to be in reasonable agreement.
- Experimental work to record hull static pressures around the intake is presented along with the results for two boat speeds.
- Thrust deduction data is presented based on varying towing positions and the effect of changing towing position highlighted. The ITTC convention of towing along the shaft line is the more conservative approach, yielding the highest bare hull drag.

- Negative thrust deduction fractions up to -8% are evident in the hump region ($F_\nabla \approx 1.5$-2) for certain towing positions. The point is made that many larger craft may be operating in this region and so enjoy the reduction in required thrust. The severity of thrust deduction at speeds other than the hump however is clear, tending towards 15%. The thrust deduction fraction is compared with the MARIN results and a good correlation found. The change in resistance, trim, wetted length and height of the center of gravity above the free surface is presented.

- The interaction vector concept is re-introduced and the vector calculated and presented. Its position and magnitude is found to be generally consistent with the proposed contributors namely lost planing surface and lost lift in the wake. More detailed analysis of the interaction vector is not possible without conducting further experiments.

9.3 Recommendations for Further Work

The problem of hull-water interaction is by no means solved and an unified method for accurately predicting the required thrust for all possible waterjet installations remains to be constructed.

The two mechanisms which require further investigation are the loss in lift in the wake and the lost lift due to the removal of plating in the intake area. It is possible that accurate wake surveys may yield the vertical momentum component in the wake caused by the waterjet intake. Data can be found or collected to better estimate the lost lift at the intake. Further and more accurate pressure measurements over the entire wetted surface would be useful. The best approach however, may well be to use computational fluid dynamics (CFD) to investigate the problem.

Workers should be wary of conducting experiments at full scale as although good data can be collected, the worries and frustrations of coping with a greater range of variables and the sheer logistics of managing people and equipment can be considerable.

There are a number of assumptions in this work which should be tested. In particular the assumption that the intake does not significantly affect the position and

magnitude of the hull fluid force vector. A CFD model could be constructed which includes the intake and hull pressure distribution. The effect of moving the intake could be studied and both mechanisms stated above better understood. In CFD model IVR can also be varied and its influence found. The pressure field acting on the protruding stream tube and its effect on thrust requires further study. It is possible that a potential flow analysis which neglects friction would be sufficient to solve the problem to the required accuracy.

The retention of the existing Savitsky/Hadler type methods should be seen as a goal as they have wide industry acceptance and are straightforward to program and use.

References

ALEXANDER, K.V.; VAN TERWISGA, T.J.C. 1992. Recent work on waterjet-hull interaction effects. *8th International High Speed Surface Craft Conference,* Singapore. 21

ALEXANDER, K.V.; COOP, H.G. and VAN TERWISGA, T.J.C. 1994. Waterjet-hull interaction: recent experimental results. *SNAME,* New Orleans

ALLISON, J.L. 1992. *Marine Waterjet Propulsion.* presented before the Chesapeake Section of the Society of Naval Architects and Marine Engineers, 15 September

ALMETER, J.M. 1991. Resistance prediction of planing hulls. *SNAME Hampton Roads Section,* 13, Feb.

ALRC 1981. *Waterjet Propulsor Performance Analysis.* Prepared by the ALRC Turbomachinery Fluid Mechanics Section. Aerojet Liquid Rocket Company, Sacramento.

BARFORD, N.C. 1985. *Experimental Measurements: Precision, Error and Truth.* 2nd ed., Wiley, New York.

BARNABY, K.C. 1969. *Basic Naval Architecture.* 6th Edititon. Hutchinson & Co. London.

BJARNE, E. 1990. Aspects on high speed craft propulsion. *7th International High Speed Surface Craft Conference.* United Kingdom

BLOUNT, D.L. and FOX, D.L. 1976. Small-craft power prediction. *Marine Technology,* **13**, No. 1, 14-45, Jan.

BOWEN, G.L. 1971. The net thrust relationshiip for waterjet propelled craft. *Hovering Craft and Hydrofoil,* **10**, Jan, 14-15.

BURTNESS, M.N. 1987. *Pressure distributions and losses in a waterjet propulsion system.* Stevens Institute of Technology Report No. SIT-DL-87-9-2566, 4, Sept. New Jersey.

CARNAHAN, B and WILKES, J.O. 1973. *Digital Computing and Numerical Methods.* John Wiley and Sons Inc. New York. 407-414.

COOP, H.G.; BOWEN, A.J. and ALEXANDER, K.V. 1992. Waterjet propulsion - recent applications and research at the University of Canterbury. *Proceed. 1992 IPENZ Conference.* Christchurch.

COOP, H.G. and BOWEN, A.J. 1993. Hull-waterjet interaction mechanisms: theory and validation. *FAST '93*, Yokohama, Japan, December, 855-866.

DYNE, G. and LINDELL, P. 1994. Waterjet testing in the SSPA towing tank. *International Symposium on Waterjet Propulsion - Latest Developments,* London, December, Paper No. 2.

ELLIS, W.E. and SOBOLEWSKI, A.D. 1977. *Propulsion Experiments With A Planing Hull Having Two Flush Inlet Configurations.* DTNSRDC Departmental Report No. SPD-786-01, Nov.

ESDU. 1969. *Introduction To The Measurement Of Thrust In Flight.* Item 69006. Engineering Sciences Data Unit. London.

ETTER R.J.; KRISHNAMOORTHY V. and SCHERER, J.O. 1980. Model testing of waterjet propelled craft. *Proc. of the 19th meet ATTC,*783-806.

FROUDE, R.E. 1886. The efficiency of propellers: a description of a method of investigation. *Transactions of the Institution of Naval Architects,* London.

GRIFFITH-JONES; G.J. 1994. *Investigation Of Incompressible Flow Through An Intake Duct With Applications To Waterjet Propulsion.* University of Canterbury, Christchurch.

HADLER, J.B. 1966. The prediction of power performance on planing craft. *Transactions of the Society of Naval Architects and Marine Engineers.* New York, 10-11 Nov. 563-610.

HAGLUND, K.; SVENSSON, R and BJORHEDEN, O. 1982. Design and testing of a high-performance water jet propulsion unit. *Syposium on Small Fast Warships and Security Vessels*, RINA, London.

HOERNER, S. F. 1965. *Fluid Dynamic Drag*, published by the author, Midland Park, New Jersey.

HOSHINO, T. and BABA, E. 1984. Self propulsion test of a semi-displacement craft model with a waterjet propulsor. *Journal of The Society of Naval Architects of Japan,* **155**, 53-60.

ITTC. 1987. *Report Of The High Speed Marine Vehicle Committee.* ITTC,304-313.

KOOPS, B. 1986. *Waterjet Propulsion System Measurements at MARIN.* Contribution to the High-Speed Marine Vehicle Committee of the 18th ITTC.

KORVIN-KROUKOVSKY, B.V.; SAVITSKY, D. and LEHMAN W.F. 1949. *Wetted Area and Centre of Pressure of Planing Surfaces.* Stevens Institute of Technology. no. SIT-DL-49-9-360, Aug.

LATORRE R. 1982. Analysis of Toro's shallow water Series 62 planing model resistance experiments. *Conference on Behaviour of Ships in Restricted Waters.* Varna, Nov. 5-1 to 5-8

LUKE, W.J. 1910. Experimental investigations on wake and thrust deduction values. *Engineering,* March 25, 392-394.

MARIN. 1991. *Joint Industry Project on Waterjet Application.* MARIN. Wageningen. The Netherlands. Mar.

MASSEY, B.S. 1984. *Mechanics of Fluids*, 5th ed.,Van Nostrand Reinhold, England.

MCLEOD, A.I. 1993. *A Wind Tunnel Investigation into the Aerodynamic Properties of the Hamilton Test Boat.* Bachelor of Engineering Project Report No. 93/9. Department of Mechanical Engineering, University of Canterbury, Christchurch.

MOFFAT, R.J. 1985. Using uncertainty analysis in the planing of an experiment. *Journal of Fluid Engineering, Transactions of ASME,* **107**, June, 173-178.

OWER, E. and PANKHURST, R.C. 1966. *The Measurement of Air Flow.* 4th ed. Pergamon Press, London. 118-122.

PIERSON, J.D. and LESHNOVER S. 1950. *A Study of the Flow, Pressures, and Loads Pertaining to Prismatic Vee-Planing Surfaces.* Report SIT-DL-50-382. Stevens Institute of Technology, Hoboken, New Jersey.

PURNELL, J.G. 1978. *The Performance Gains of using Wide, Flush, Boundary Layer Inlets on Waterjet Propelled Craft,* David Taylor Naval Ship Research and Development Center, Report PAS-75-45, March.

ROBB, A.M. 1952. *Theory of Naval Architecture,* Charles Griffin and Co. Ltd. London, Chap.31.

ROY, S.M. 1994. The evolution of the modern waterjet marine propulsion unit. *International Symposium on Waterjet Propulsion (RINA)*, 1-2 Dec, London, 1-20.

SAVITSKY, D. 1964. Hydrodynamic design of planing hulls. *Marine Technology,* October, 71-95.

SAVITSKY, D. and ROSS, E.W. 1952. Turbulence stimulation in the boundary layer of planing surfaces, part ii, preliminary experimental investigation. *Stevens Institute of Technology Experimental Towing Tank Report No. 44,* August.

SOTTORF, W. 1932 & 1934. *Experiments with planing surfaces.* NACA TM 661 and NACA TM 739.

STEPHENS, L.K., ET AL. 1973 *Waterjet Inlet/Duct Development Phase I, Validation Tests.* Rep. 7244-1, Hydronautics Incorporated, January

STRICKER, J.G.; BECNEL, A.J. and PURNELL J.G. 1993. Development of a waterjet propulsor for the Marine Corps high water speed landing application. *23rd American Towing Tank Conference.* New Orleans, June.

SVENSSON, R. 1989. *Experience with the KaMeWa waterjet propulsion system.* American Institute of Aeronautics and Astronautics, Inc. Report No. 89-1440-CP

SVENSSON, R. 1991. Waterjet Propulsion of High-Speed Craft. *Proc. IMAS '91,*16-1-11.

VAN TERWISGA, T. 1991. On the effects of waterjet-hull interaction on thrust and power requirements. *MARIN Report No. 49918-1-SRD* also *FAST '91,* 1149-1167

VAN TERWISGA, T. 1993. A Theoretical Model for the Powering Characteristics of Waterjet-Hull Systems. *FAST '93,* Yokohama, Japan, December, 975-991.

VAN TERWISGA, T. 1993. On the description of waterjet powering requirements. *Contribution to the 20th ITTC Workshop on Waterjets.*

VARSAMOV, K and LAZAROV, S. 1987. On the performance prediction for ships with waterjets. *18 ITTC,* **2**, 167-169.

VENTURINI, G.N. 1973. Waterjet propulsion dynamics, *Hovering Craft and Hydrofoil,* **13**.

WIKEBY, O. 1990. Aerodynamics of offshore racing powerboats. *Ship and Boat International,* April, 13-16.

WILSON, M.B. 1977. A survey of propulsion-vehicle interactions on high-performance marine craft. *Proc. 18th ATTC.*

Appendices

A-1. *Results of Towing Tests*

DAY1 Run no.	*window start record*	*window finish record*	*window no. records*	*photo start time*	*Towing force W average (N)*	*acceleration (N)*	*corrected (N)*	*95% C.I. (N)*
0	1000	1050	50	na	4237	45	4282	139
2	1121	1231	110	11:43'53"	4082	-86	3996	176
3	719	834	115	12:00'57"	4334	-68	4266	218
4	1107	1164	57	12:16'48"	4247	118	4365	109
5	575	646			na	na	na	
6	1460	1495	35	02:35'37"	4287	-220	4067	73
7	480	529	49	02:44'33"	3779	80	3859	71
8	507	585	78	02:54'56"	4010	99	4109	90
10	860	914	54	03:30'53"	4423	-98	4325	205
11	910	950	40	03:42'28"	4363	-42	4321	77
DAY2 Run no.								
1	500	800	300	0:31'32"	4613	-78	4535	110
2	600	700	100	0:40'38"	3587	-6	3581	97
3	700	775	75	0:55'19"	na	na	na	na

DAY1 Run no.	*alpha ave. (deg.)*	*alpha err. 90%CI (deg.)*	*Vs (pitot-static) ave. (m/s)*	*Vs (pitot-static) err. 95%CI (m/s)*	*Vs (radar) ave. (m/s)*	*Vs (radar) err. 95%CI (m/s)*	*Vw ave. (m/s)*	*Vw err. 95%CI (m/s)*
0	na	0.16	7.63	0.05	8.68	0.036	12.6	0.2
2	-2.7	0.66	9.57	0.16	10.76	0.036	11.8	0.4
3	-1.6	1.64	9.78	0.15	10.99	0.036	13.5	0.3
4	0.3	0.13	7.22	0.08	8.23	0.036	11.2	0.5
5	1.2	0.83	13.29	0.15	14.76	0.036	17.5	0.4
6	-2.6	0.31	9.46	0.08	10.65	0.036	10.3	0.2
7	-0.5	0.26	4.59	0.04	5.41	0.036	4.9	0.1
8	-0.7	0.36	5.10	0.09	5.95	0.036	6.1	0.1
			9.96	0.23	11.18	0.036		
10	-0.5	0.40	9.37	0.10	10.55	0.036	11.5	0.2
11	0.0	0.12	4.80	0.03	5.63	0.036	6.4	0.0
DAY2 Run no.								
1	na	*	9.10	0.27	9.81	0.036	9.8	0.6
2	na	*	4.47	0.05	4.44	0.036	5.0	0.3
3	na	*	10.33	0.10	11.23	0.036	10.4	0.2

DAY1	*Trim (photo)*		*Wetted Length*		*Fuel Loading*		
Run	*ave.*	*err. 95%CI*	*ave.*	*err. 95%CI*	*loading*	*lcg_f*	*vcg_f*
no.	*(deg.)*	*(deg.)*	*(m)*	*(m)*	*(kg)*	*(m)*	*(m)*
0	na	na	na	na	96.53	0.75	0.16
2	4.84	0	5.07	0	96.53	0.80	0.14
3	4.99	0.14	5.31	0.06	96.53	0.81	0.14
4	5.72	0.18	5.11	0.04	96.53	0.75	0.16
5	3.59	0.16	5.41	0.02			
6	5.07	0.36	5.11	0.12	96.53	0.78	0.15
7	5.17	0.46	5.95	0.08	96.53	0.79	0.15
8	5.96	0.06	5.83	0.04	96.53	0.70	0.17
	3.94	0.3	5.31	0.06			
10	5.23	0.24	5.15	0.06	96.53	0.76	0.15
11	6.38	0.64	5.36	0.07	96.53	0.72	0.16
DAY2							
Run no.							
1	5.49	na	5.47	0.1	96.53	0.77	0.15
2	3.78	na	6.83	0.06	96.53	0.87	0.13
3	na	na	5.19	0.21			

A-2. *Results of Propulsion Tests*

Record no.	*File*	*Run*	V_s *(m/s)*	δV_s *(m/s)*	*Fv*	L_K *(m)*	δL_K *(m)*	τ *(deg)*	$\delta\tau$ *(deg)*
1	O3O7	0	2.46	0.030	0.65	na	na	2	na
2	O3O7	2	3.46	0.030	0.92	6.08	0.05	2.69	0.27
3	O324	8	3.67	0.017	0.99	6.08	0.05	3.47	0.87
4	O324	10	3.70	0.024	0.99	6.03	0.00	3.80	0.01
5	O3O7	5	3.74	0.030	0.99	5.20	0.21	4.00	0.31
6	O324	3	4.01	0.047	1.08	5.92	0.05	4.80	0.31
7	O324	4	4.14	0.021	1.11	5.87	0.09	5.07	0.52
8	O3O7	3	4.70	0.030	1.25	na	na	5.25	na
9	O32O	12	4.84	0.038	1.30	5.81	0.14	5.47	0.07
10	O32O	11	4.86	0.018	1.31	5.79	0.09	5.73	0.59
11	O32O	10	4.93	0.018	1.33	5.84	0.11	5.37	0.29
12	O32O	14	5.25	0.022	1.41	5.56	0.20	5.67	0.30
13	O32O	15	5.29	0.026	1.42	5.50	0.20	5.70	0.30
14	O32O	16	5.33	0.045	1.43	5.50	0.20	5.74	0.30
15	O32O	13	5.34	0.017	1.43	5.49	0.20	5.75	0.30
16	O32O	8	5.56	0.024	1.49	5.39	na	6.40	na
17	O3O7	6	5.56	0.030	1.47	6.13	0.05	3.94	0.22
18	O324	9	5.58	0.042	1.50	5.39	0.09	6.37	0.18
19	O324	2	5.77	0.025	1.55	5.49	0.14	5.07	1.19
20	O324	7	5.81	0.022	1.56	5.33	0.21	6.90	0.42
21	O32O	7	5.87	0.026	1.58	5.36	0.11	6.17	0.70
22	O32O	1	5.97	0.033	1.60	5.92	0.46	3.07	0.18
23	O324	1	5.99	0.019	1.61	5.47	0.00	6.73	0.18
24	O32O	6	7.07	0.022	1.90	4.76	0.12	7.87	0.47
25	O3O7	4	7.45	0.030	1.98	5.97	0.11	5.29	0.27
26	O32O	5	8.21	0.040	2.21	4.69	0.05	7.70	0.50
27	O324	6	9.93	0.026	2.67	4.45	0.28	5.63	0.53
28	O3O7	8	10.29	0.030	2.73	4.96	0.28	6.92	1.82
29	O32O	9	10.62	0.026	2.85	4.56	0.38	5.70	1.71

Record no.	V_w *(m/s)*	δV_w *(m/s)*	Q *(m^3/s)*	dQ *(m^3/s)*	ϕ_{Mn} *(N)*	$\delta\phi_{Mn}$ *(N)*	ϕ_{Mi} *(N)*	$\delta\phi_{Mi}$ *(N)*
1	5.21	0.15	0.172	0.0007	2284	18	412	10
2	4.59	0.18	0.219	0.0008	3710	27	742	16
3	4.40	0.22	0.232	0.0008	4160	28	833	14
4	4.54	0.15	0.232	0.0007	4158	24	841	16
5	10.43	0.30	0.232	0.0009	4163	32	854	16
6	2.96	0.13	0.261	0.0015	5237	51	1027	26
7	4.49	0.24	0.255	0.0010	4993	39	1035	18
8	9.91	0.32	0.263	0.0015	5314	52	1201	26
9	8.56	0.41	0.261	0.0011	5258	44	1234	26
10	8.95	0.25	0.262	0.0011	5310	43	1244	22
11	9.82	0.27	0.264	0.0011	5376	44	1271	40
12	9.12	0.26	0.273	0.0012	5746	49	1402	24
13	9.08	0.25	0.277	0.0009	5913	37	1434	24
14	8.57	0.36	0.278	0.0010	5951	40	1445	30
15	10.10	0.29	0.269	0.0012	5591	49	1403	24

16	10.26	0.28	0.282	0.0012	6151	51	1534	26
17	11.40	0.32	0.279	0.0016	6017	59	1510	15
18	6.87	0.29	0.284	0.0010	6210	40	1551	30
19	4.50	0.17	0.288	0.0016	6389	63	1625	30
20	5.02	0.19	0.284	0.0011	6206	45	1613	24
21	10.10	0.28	0.286	0.0016	6326	62	1639	30
22	4.63	0.16	0.218	0.0010	3657	31	1247	30
23	10.50	0.31	0.287	0.0016	6370	62	1680	32
24	10.36	0.34	0.306	0.0014	7194	63	2117	36
25	12.14	0.33	0.304	0.0017	7130	70	2191	46
26	10.67	0.28	0.307	0.0013	7252	58	2454	46
27	11.91	0.33	0.326	0.0016	8185	81	3146	60
28	13.81	0.47	0.329	0.0019	8329	81	3271	35
29	14.92	0.39	0.333	0.0013	8563	67	3428	66

Record no.	*T (N)*	*δT (N)*	*h (m)*	*δh (m)*	*Probe*	*Displmnt. (kg)*	*LCG (m)*	*VCG (m)*
1	1862	20	0.082	0.006	L	na	na	na
2	2948	31	0.073	0.005	L	2910	2.478	0.705
3	3299	42	0.073	0.01	H	2876	2.463	0.71
4	3285	40	0.072	0.01	R	2869	2.46	0.711
5	3276	36	0.071	0.01	L	2901	2.466	0.707
6	4160	77	0.075	0.01	LE	2891	2.467	0.708
7	3907	57	0.071	0.01	L	2887	2.465	0.708
8	4057	58	0.066	0.005	LE	na	na	na
9	3966	70	0.063	0.008	L	2861	2.455	0.712
10	4004	65	0.063	0.008	L	2864	2.456	0.711
11	4046	84	0.062	0.008	L	2867	2.457	0.711
12	4277	73	0.06	0.008	H	2852	2.453	0.713
13	4410	61	0.061	0.008	R	2850	2.452	0.713
14	4436	70	0.06	0.008	R	2849	2.452	0.714
15	4122	73	0.059	0.008	H	2858	2.454	0.712
16	4534	77	0.059	0.008	L	2873	2.458	0.71
17	4460	61	0.059	0.008	LE	2897	2.471	0.707
18	4576	70	0.059	0.008	R	2873	2.458	0.71
19	4699	93	0.058	0.008	LE	2895	2.468	0.707
20	4501	69	0.057	0.008	H	2880	2.459	0.71
21	4606	92	0.057	0.008	LE	2876	2.459	0.71
22	2388	61	0.044	0.006	L	2892	2.47	0.708
23	4599	94	0.056	0.008	LE	2899	2.466	0.707
24	4953	99	0.05	0.006	L	2880	2.459	0.71
25	4864	84	0.048	0.003	LE	2904	2.471	0.706
26	4679	104	0.044	0.006	L	2882	2.46	0.709
27	4947	141	0.039	0.006	L	2884	2.462	0.709
28	4940	89	0.038	0.005	LE	2894	2.464	0.708
29	5038	133	0.037	0.006	L	2870	2.457	0.711

A-3. *Manufacturing Drawing of Prandtl Rake*

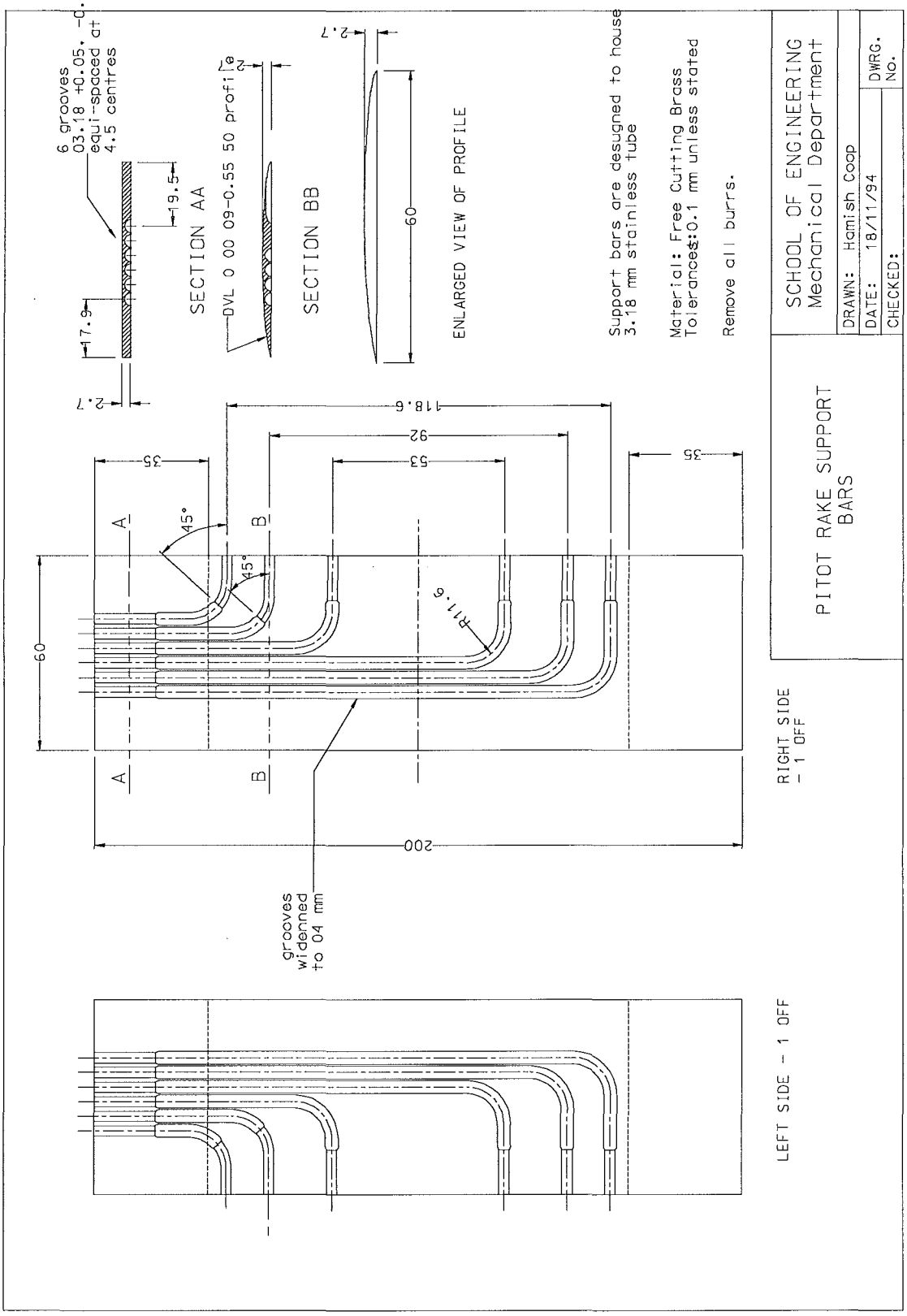

A-4. *Hamilton Test Boat Specifications*

Feature	*Specification*
Hull	• planing work boat • prismatic, constant deadrise, no rocker, no strakes • constant deadrise • hard chine • 13 mm camber between chines and keel •
Construction	Welded aluminium plate
Length	7.4 m
Maximum projected chine beam	2.18 m
Deadrise	15.4°
Nominal LCG	2.5 m
Nominal Displacement	2800 kg
Engine	7.3 l Chevrolet Crusader, (210 kW)
Propulsion system	Hamilton 273 single stage waterjet
Steering	Hydraulic helm pump

A-5. *Hamilton 273 Waterjet Specifications*

Feature	*Specification*
Configuration	Single stage, semi-mixed flow
Direction of rotation	Anti-clockwise looking at flywheel
Casings	Cast LM6 aluminium alloy to BS1490 Q.C.
Mainshaft	70mm diameter SAF2205 stainless steel
Impeller	4 or 5 bladed cast CF8M stainless steel to ASTM A296
Thrust Bearing	Grease lubricated deep groove ball bearing
Tail Bearing	Water lubricated cutless bearing
Corrosion Protection	Cathodic with anodes
Dry Weight	115 kg
Entrained Water Weight	35 kg

A-6. *Hamilton Test Boat Linesplan*

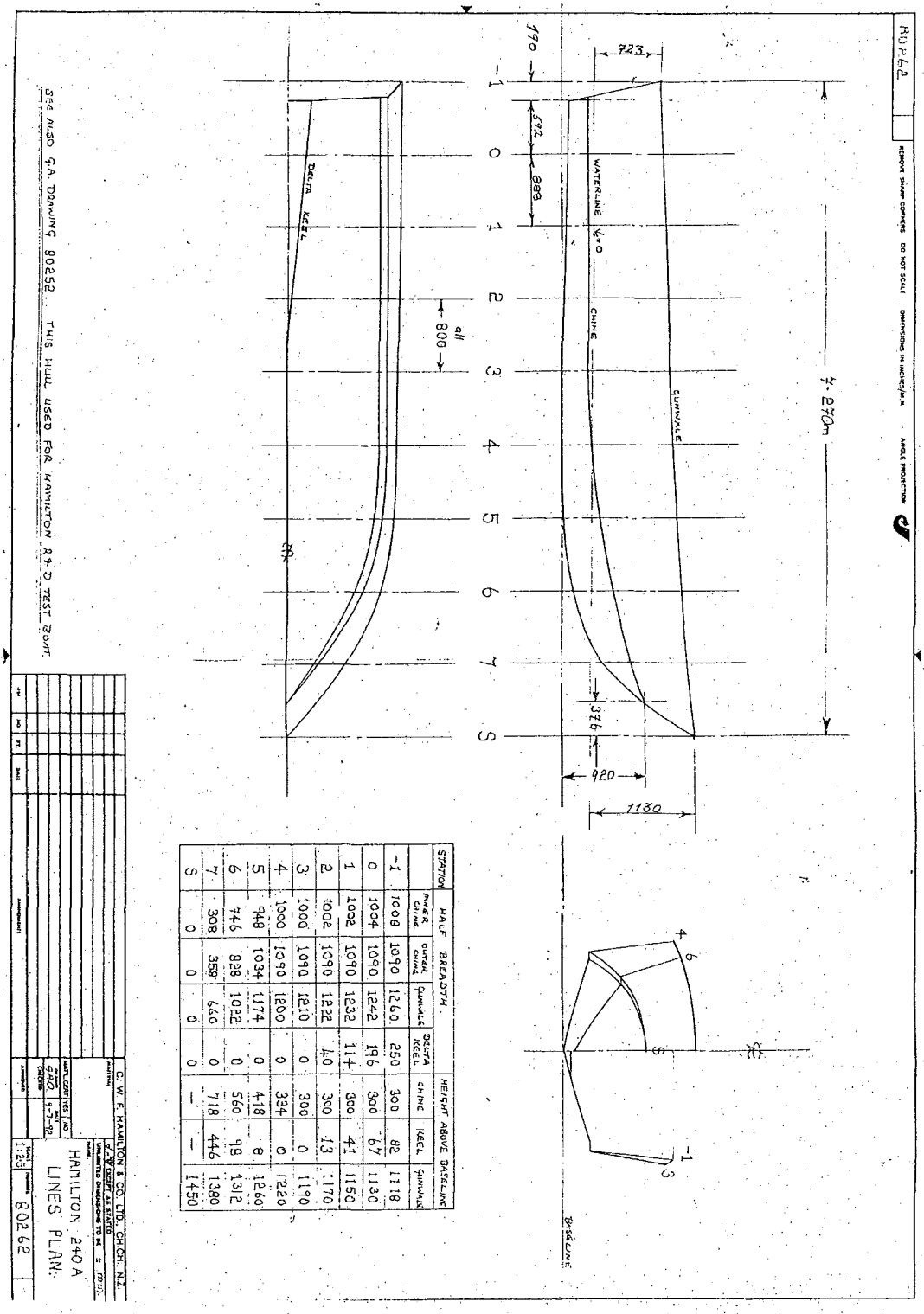

STATION	HALF BREADTH. PAPER CHINE	OUTAK CHINE	SUMMALE	DELTA KEEL	HEIGHT ABOVE BASELINE CHINE	KEEL	SUMMALE
-1	1008	1090	1260	250	300	82	1118
0	1004	1090	1242	196	300	67	1130
1	1002	1090	1232	114	300	41	1150
2	1002	1090	1222	40	300	13	1170
3	1000	1090	1210	0	300	0	1190
4	1000	1090	1200	0	334	0	1220
5	948	1034	1174	0	418	8	1260
6	746	828	1022	0	560	98	1312
7	308	358	660	0	718	446	1380
S	0	0	0	0	—	—	1450

A-7. *Computer Program Listings*

Subroutine calc_resistance listed below performs the main iterations to find the interaction vector. It calls subroutines in the program group sav_cir.c which is also listed. Input and output code is omitted. Programs to calculate the position of the fuel loading and the intake momentum flux are also listed.

A-7.1 CALC_RESISTANCE()

```
{
float
ca,e,gimp,k1,k2,k3,k4,k5,k6,k7,k8,k9,kimp,kl10,nu,
        vol,lcgmax,af,fwind,ba,lgbx,kfv1,kc,v,cb,cv
,aa,limit,
        decr,f1,f0,l5,co,t1,k,vm,re,cf,a;

/*      constants               */
ca=.0004;
e=exp(1);
gimp=32.17;
k1=.75;
k2=5.21;
k3=2.39;
k4=.0065;
k6=.6;
k7=.012;
k8=.0055;
k9=.242;
kimp=1.689;
kl10=log(10);
nu=.0000128;
ro=1.94;

/* eqn 23 volume of water displaced     */
vol=disp/gimp/ro;
/* eqn 26 determination of maximum LCG
lcgmax=lpmax*.46*mtf;*/
/* eqn 27 Calculation of wave allowance at ref. vel.
da=.012*disp*nlb/td;*/
/* estimation of frontal area max beam squared (in sq
ft)        */
af=bpx*bpx;
/*cd[hull_line]=.6;*/
/* wind resistance   */
fwind=cd[hull_line]*af*.00238*pow(1.689,2)/2*nlb/t
d;
/* beta[hull_line] in radians   */
ba=beta[hull_line]/57.29577951;
k5=k4*beta[hull_line];
if(bpx==0)
        return(1);
lgbx=lcg/bpx;
/* eqn 23 min velocity for which the savitsky
prediction is valid*/
a=gimp*pow(vol,.333333);
kfv1 = pow(a,.5)/kimp;
if(kts<kfv1)
        valid=0;
else
        valid=1;
/* eqn 13 part of----?*/
kc=disp*2/ro/bpx/bpx;
v=kts*kimp;
fv=v/pow(gimp*pow(vol,.3333333),.5);
/* main body of calculation*/
/* eqn 13 cb the coef of lift for a plate with a deadrise
of beta*/
if(v==0)
        return(1);
        cb=kc/v/v;
/* eqn 10 coef of velocity      */
cv = v/pow(gimp*bpx,.5);
aa=k2*cv*cv;
/* eqn 20 iterative solution of lambda*/
limit=.001;
lr=3;
decr=2;
f1=k1-(1/(aa/lr/lr+k3))-lgbx/lr;
while(pow(f1*f1,.5)>limit&&pow(decr*decr,.5)>limi
t)
{
        f0=f1;
        lr=lr-decr;
        if(lr==0)
                return(1);
        f1=k1-(1/(aa/lr/lr+k3))-lgbx/lr;
        decr=decr*f1/(f0-f1);
}
/* eqn 20 cp is the ratio of longit'l dist from the
transom to
 the centre of pressure divided by the mean wetted
length*/
//      cp=lgbx/lr;
l5=pow(lr,.5);
/* eqn 11, iterative soln for co the co-eff of lift for a
plate
  with zero deadrise*/
limit=.0002;
co=.5;
decr=.1;
f1=co-k5*pow(co,k6)-cb;
while(pow(f1*f1,.5)>limit&&pow(decr*decr,.5)>limi
t)
{
        f0=f1;
        co=co-decr;
        f1=co-k5*pow(co,k6)-cb;
        if(f0==f1)
                return(1);
        decr=decr*f1/(f0-f1);
}
/* eqn 9 calculation of trim angle      tau is in
radians trim is in degrees*/
if(cv==0)
        return(1);
t1 = co/(k7*l5+k8*pow(lr,2.5)/cv/cv);
```

```
trim = pow(t1,(1/1.1));
tau=trim/57.29577951;
k=k7*pow(lr,.5)*t1;
/* eqn 18 calc of vm the mean velocity over the
planning surface*/
if(cos(tau)==0)
        return(1);
vm=v*pow(1-(k-k5*pow(k,k6))/lr/cos(tau),.5);
/* eqn 17 reynolds number*/
re=vm*lr*bpx/nu;
/* eqn 16 calc of cf the friction drag coeff*/
limit=.001;
cf=.003;
decr=.001;
f1= log(re*cf)/kl10-k9/pow(cf,.5);
while(pow(f1*f1,.5)>limit||pow(decr*decr,.5)>limit)
{
        f0=f1;
        cf=cf-decr;
        f1= log(re*cf)/kl10-k9/pow(cf,.5);
        if(f0==f1)
                return(1);
        decr=decr*f1/(f0-f1);
}
/* eqn 19 resistance of the boat hull calc*/
rbh=((disp*tan(tau)+ro*vm*vm*lr*bpx*bpx*(cf+ca)/
2/cos(ba)/cos(tau))
*nlb/td);
/*eqn 29 wind resistance*/
rwind=fwind*kts*kts;
/* eqn 27 wave resistance*/
//rwave =
da[hull_line]*pow(kts/ka[hull_line],na[hull_line]);

if(bf[hull_line]=='Y')
{
        /* eqn 22 Blount and fox correction factor
relation resulting from
        analytical curve fitting of experimental
results
         (only applies if froude No.<3.7*/
        if(fv<3.7)
        {
                k=fv-.85;

        m=.98+2*pow(lgbx,1.45)*pow(e,-2*k)-
3*lgbx*pow(e,-3*k);
        }
        else
                m=1;
}
else
        m=1;

/* eqn 27 total resistance*/
rt=rbh*m+rwind+rwave;

/* eqn 31 estimated horse power*/
ehp = rt * v/550 * td/nlb;
if (i_flag==2)
        {
        calc_resistance_long();
        }
if (i_flag==1)
        {
        calc_resistance_long();


    //for (off_i=6;off_i<100;off_i=off_i+1)
        /* {
        off_i=8;
        find_interaction_vector();
        jj++;
        if(jj==20)
                jj=2;
        gotoxy(5,jj);
                printf("%4.1f  %4.1f  %5.0f
%4.2f  %4.2f  %4.2f
%6.2f",kts,off_i,ivector,Rerror,Lerror,terror,ierror);
        }*/
     calc_interaction_resistance();
        tdf=(rti_fs-rtl_fs)/rti_fs;
        }
return(0);
}

int find_interaction_vector()
{
extern float ierror,ivector,gr,disp,off_i;
float iv_l,iv_r,ivector_max,ivector_min,ie_l,ie_r;

        // ITERATION FOR I VECTOR
MAGNITUDE
        ivector_min=-1300;ivector_max=0;

        iv_l=(ivector_max-ivector_min)*(1-
gr)+ivector_min;
        iv_r=(ivector_max-
ivector_min)*gr+ivector_min;

        ivector=iv_l;
        calc_interaction_resistance();
        ie_l=ierror;

        ivector=iv_r;
        calc_interaction_resistance();
        ie_r=ierror;
                while(pow(iv_r-iv_l,2)>1)
                {
                        if(ie_r<ie_l)
                                {

        ivector_min=iv_l;

        iv_l=iv_r;ie_l=ie_r;

        iv_r=(ivector_max-
ivector_min)*gr+ivector_min;
                                ivector=iv_r;

        calc_interaction_resistance();
                                ie_r=ierror;
                gotoxy(5,24);
                                printf("ivector
%6.0f",ivector);
                        gotoxy(25,24);
                        printf("ierror
%6.2f",ierror);
```

```
        gotoxy(45,24);
                                printf("off_i
%5.1f",off_i);
                                }
                        else
                                {

        ivector_max=iv_r;

        iv_r=iv_l;ie_r=ie_l;

        iv_l=(ivector_max-ivector_min)*(1-
gr)+ivector_min;
                                ivector=iv_l;

        calc_interaction_resistance();
                ie_l=ierror;
                gotoxy(5,24);
                                printf("ivector
%6.0f",ivector);
                        gotoxy(25,24);
                        printf("ierror
%6.2f",ierror);

        gotoxy(45,24);
                                printf("off_i
%5.1f",off_i);
                                }


                }
return(0);
}
int find_interaction_offset()
{
extern float ierror,off_i,gr,bpx;
float iv_lo,iv_ro,off_i_max,off_i_min,ie_lo,ie_ro;


        // ITERATION FOR I VECTOR OFFSET
        off_i_min=6;off_i_max=12;

        iv_lo=(off_i_max-off_i_min)*(1-
gr)+off_i_min;
        iv_ro=(off_i_max-
off_i_min)*gr+off_i_min;

        off_i=iv_lo;
        find_interaction_vector();
        ie_lo=ierror;

        off_i=iv_ro;
        find_interaction_vector();
        ie_ro=ierror;
                while(pow(iv_ro-iv_lo,2)>0.2)
                {
                        if(ie_ro<ie_lo)
                                {

        off_i_min=iv_lo;

        iv_lo=iv_ro;ie_lo=ie_ro;

        iv_ro=(off_i_max-
off_i_min)*gr+off_i_min;
                                off_i=iv_ro;

        find_interaction_vector();
                                ie_ro=ierror;
                                }
                                else
                                {

        off_i_max=iv_ro;

        iv_ro=iv_lo;ie_ro=ie_lo;

        iv_lo=(off_i_max-off_i_min)*(1-
gr)+off_i_min;
                                off_i=iv_lo;

        find_interaction_vector();
                                ie_lo=ierror;
                                }

                        }
return(0);
}
```

A-7.2 SAV_CRL.C

```
#include<stdio.h>
#include<math.h>
#define PI 3.14159


/*          hull resistance        */
extern float
disp,disp_i[11],epsilon,lpmax,lpmax_i[11],lcg,lcg_i[1
1],bpx,bpx_i[11],beta[11],cd[11],da[11],
          ka[11],kts,na[11],nlb,tau,td,rbh,rti,rtl,rtl_fs,r
wind,rwave,lr,trim,fv,mtf,kglbs,nlbf;
extern char
          bf[11],lu[3],disp_u[4],force_u[4],trm,filena
me[50];
extern int
data_state[11],hull_line,valid,i_flag,mtf_flag;

/* miscellaneous*/
extern char scales[10],wdrag[10],version[5],tog[3];
extern float
epsilon,Lkl_fs,Lkl,taul_fs,taul,l_st,phi,l_in,l_tc,i_widt
h,dj_i,vcg,ivr;


int calc_resistance_long()
{
float
alpha,bl_delta,ca,cf,cfr,CDw,CLw,delta_lr,Dps,DDw,
Da,Db,Dr,Dw,fw,
fv2,fv3,fv4,fv5,gimp,k4,k5,k6,k9,kimp,kl10,lrb,LLw,
nu,off_fa,off_e,off_f,off_fw,off_ff,
off_Dps,off_Db,off_Dr,ro,old_tau,tau_max,tau_min,v
ol,lcgmax,af,fwind,ba,
lgbx,kfv1,v,cb,cv,limit,decr,f1,f0,cpj,cpbh,co,k,vm,re,
rer,a,
nlbi,rho,xi,l_dk,h_dk,Df,dispi,gamma,W,i,m,e,corrf_r
,corrf_t,corrf_l;


/* constants */
ca=.0004;
gimp=32.17;
k4=.0065;
k6=.6;
k9=.242;
kimp=1.689;                    /* knots to feet/sec */
kl10=log(10);
nu=.0000127908;                        // kinematic
viscosity mu/ro of salt water
e=exp(1);
//gamma=0/57.3;                //angle between towing
line and horizontal
                                       //in
ft^2/second from Barnaby pg. 156 */
rho=64.103;                /* density of salt water
lbs/ft^3 */
ro=rho/gimp;                           /* mass
density of water =rho/gimp */
af=0.04*pow((mtf*10),2);       /* from Andrew
McLeod's report */
/* eqn 23 volume of water displaced */
vol=disp/(gimp*ro);

// eqn 26 determination of maximum LCG
//lcgmax=lpmax*.46*mtf;

/* eqn 27 calculation of wave allowance at ref. vel.
da=.012*disp*nlb*/

/* beta[hull_line] in radians */
ba=beta[hull_line]/57.296;
k5=k4*beta[hull_line];
lgbx=lcg/bpx;

if(bpx==0)
          return(1);

/* eqn 23 min velocity for which the savitsky
prediction is valid */
a=gimp*pow(vol,.33333);
kfv1=pow(a,.5)/kimp;
if(kts<kfv1)
          valid=0;
else
          valid=1;

/* speed coefficients */
v=kts*kimp;
fv=v/pow(gimp*pow(vol,.33333),.5);
fv2=pow(fv,2);fv3=pow(fv,3);fv4=pow(fv,4);fv5=po
w(fv,5);
cv=v/pow(gimp*bpx,.5);

/* ITERATIVE SOLUTION FOR TRIM - MAIN
BODY */
rtl=0;Da=0;
//for(i=0;i<3;i++)
{
/* initial settings */
decr=1;
limit=50;
old_tau=0;
tau_min=tau-3/57.3;
tau_max=tau+3/57.3;
f1=50000;

while(pow(f1*f1,.5)>limit||decr>.1)

{
     old_tau=taul;
          taul=(tau_min+tau_max)/2;
          trim=taul*57.3;
     gamma=phi-xi+taul;gamma=-2/57.3;
/*gamma=shaft angle to water*/
          /* wind resistance */
          CDw=0.0105*trim*trim-
0.0541*trim+0.5422;
          CLw=0.0271*trim*trim-
0.1830*trim+1.457;
          DDw=CDw*0.5*af*0.08072/gimp*v*v;
          LLw=CLw*0.5*af*0.08072/gimp*v*v;
/*32.2=gimp*/
          Dw=pow((DDw*DDw+LLw*LLw),0.5);
          alpha=atan(LLw/DDw);
     dispi=disp-
LLw+rtl*tan(gamma)+Da*sin(taul);//ITTC
```

```
        /* deadrise lift coefficient */
        cb=dispi/(0.5*ro*bpx*bpx*v*v);

        /* iterative solution for flat plate lift
coefficient
        -based on equation 16 in Savitsky '64 */
        limit=.00001;
        co=cb;
        decr=.01;
        f1=co-(.0065*beta[hull_line])*pow(co,.6)-
cb;
        while(pow(f1*f1,.5)>limit||pow(decr*decr,.
5)>limit)
        {
                f0=f1;
                co=co-decr;
                f1=co-
(.0065*beta[hull_line])*pow(co,.6)-cb;
                if(f0==f1)
                        return(1);
                decr=decr*f1/(f0-f1);
        }

        /* iterative solution for lamda -based on
        Savitsky equation no. 15 */
        limit=.00001;
        lr=2;
        decr=.01;
        f1=pow((taul*57.2958),1.1)*(0.0120*pow(l
r,.5)+
        .0055*pow(lr,2.5)/cv/cv)-co;
        while(pow(f1*f1,.5)>limit||pow(decr*decr,.
5)>limit)
        {
                f0=f1;
                lr=lr-decr;
        f1=pow((taul*57.2958),1.1)*(0.0120*pow(l
r,.5)+
                .0055*pow(lr,2.5)/cv/cv)-co;
                if(f1==f0)
                        return(1);
                decr=decr*.5*f1/(f0-f1);
        }

        /* vm the mean velocity over the planning
surface */
        k=.012*pow(lr,.5)*pow(taul*57.2958,1.1);
        vm=v*pow(1-(k-
k5*pow(k,k6))/lr/cos(taul),.5);

        /* Reynolds number */
        re=vm*lr*bpx/nu;

        /* Shoenherr friction drag coefficient for
hull*/
        limit=.0001;
        cf=.003;
        decr=.001;
        f1=log(re*cf)/kl10-k9/pow(cf,.5);
        while(pow(f1*f1,.5)>limit||pow(decr*decr,.
5)>limit)
                {
                f0=f1;
                cf=cf-decr;
                f1=log(re*cf)/kl10-k9/pow(cf,.5);
                if(f0==f1)
                        return(1);
                decr=decr*f1/(f0-f1);
                }
        /*spray drag due to delta_lr*/
        delta_lr=0;


        /* resistance components of the boat hull */
        Df=ro/2*v*v*bpx*bpx*(cf+ca)/cos(ba)*((v
m/v)*(vm/v)*lr+delta_lr);

    /* pitot-static drag */
        Dps=0.715*(0.00205*3.281*3.281)*(ro/2)*
v*v;
        off_Dps=vcg-(.3+.13/2)*mtf;

    // drag on rudder support brackets
        Db=0.6*(0.0012*3.281*3.281)*(ro/2)*v*v;
        off_Db=vcg-0.05*mtf;

        /* Shoenherr friction drag coefficient for
rudder*/
        limit=.0001;
        rer=v*.25*mtf/nu;
        cfr=.003;
        decr=.001;
        f1=log(rer*cfr)/kl10-k9/pow(cf,.5);

        while(pow(f1*f1,.5)>limit||pow(decr*decr,.
5)>limit)
                {
                f0=f1;
                cfr=cfr-decr;
                f1=log(rer*cfr)/kl10-
k9/pow(cfr,.5);
                if(f0==f1)
                        return(1);
                decr=decr*f1/(f0-f1);
                }
        Dr=ro*(.066*3.281*3.281)*cfr*1.08*v*v;
        off_Dr=vcg-(-.1*mtf);

        Da=Dps+Db+Dr;
        /* offset of appendage drag */
        off_fa=(Dps*off_Dps+Db*off_Db+Dr*off_
Dr)/Da;

        /* offset of centre of pressure N */

        cpbh=.75-1/(5.21*cv*cv/lr/lr+2.39);
        off_e=lcg-cpbh*lr*bpx;

        /* offset of centre of drag */
        off_ff=vcg-(bpx/4)*tan(ba);

        /* offset of aerodynamic drag force */
        off_fw=(-
0.0208*trim*trim+0.1794*trim+0.4279)*bpx;
        /* offset of towing vetor from CG */
```

```
        off_f=(6.91*mtf-lcg-(vcg-
0.63*mtf)/tan(taul+gamma))*sin(taul+gamma);
    //offset along shaft
        //off_f=-(vcg-l_st-lcg*tan(phi-xi))*cos(phi-
xi);
        //MARIN
        //off_f=-.155*mtf;
    //Savitsky short form
    //off_f=0;
        /* net pitching moment -based on Savitsky
equations */
        f1=
        dispi*(off_e*cos(gamma)+sin(taul)*off_f)

        +(Df+Da)*(off_f+off_e*sin(taul+gamma))
                +(Da*off_fa+Df*off_ff-
Dw*off_fw)*cos(taul+gamma)

        +Dw*(cos(taul+alpha)*off_f+sin(gamma-
alpha)*off_e);

        limit=50;
        if(f1>0)
                tau_max=(taul+2*tau_max)/3;
        else
                tau_min=(taul+2*tau_min)/3;
                decr=pow(pow(old_tau-
taul,2),.5)*57.3;

}

/* END OF MAIN BODY */

if (bf[hull_line]=='Y')
{
/* Blount and Fox correction factor relation resulting
from analytical curve fitting of experimental results
(only applies if Froude no.< 3.7 */

        if (fv<3.7)
        {
        k=fv-.85;
        m=.98+2*pow(lgbx,1.45)*pow(e,-2*k)-
3*lgbx*pow(e,-3*k);
        }
        else
        m=1;
}
else
m=1;

/* total resistance =Tcos(gamma) */
rtl=
        cos(gamma)/cos(taul+gamma)*((sin(taul)*d
ispi+Df)*m
        +Dw*cos(taul+alpha)+Da);
}
// Apply correction factors from tow testing
if(fv<2.75)
        corrf_r=(fv4*0.190757-
fv3*1.67079+fv2*5.4486-fv*7.8106+5.1138);
else
corrf_r=1;
rtl_fs=rtl*corrf_r;
if(fv<2.5)
        corrf_t=(fv3*.29479-
fv2*1.87523+fv*3.98979-1.8932);
else
        corrf_t=0.96;
taul_fs=taul*corrf_t;

corrf_l=(-fv3*0.0145+fv2*0.1026-fv*0.1385+.9511);
Lkl=(lr+tan(ba)/(2*PI*tan(taul)))*bpx;
Lkl_fs=Lkl*corrf_l;

if (force_u[0]=='K')
        nlbi=.2247;
else
        nlbi=1;
rtl_fs=rtl_fs/nlbi;rtl=rtl/nlbi;

gotoxy(10,22);
return(0);
}
```

A-7.3 SAV_CIR.C

```
#include<stdio.h>
#include<math.h>
#define PI 3.14159
//Function Declarations
void flowrate();

/*          hull resistance        */
extern float
disp,disp_i[11],lpmax,lpmax_i[11],lcg,lcg_i[11],bpx,
bpx_i[11],
          beta[11],cd[11],da[11],
          ka[11],kts,na[11],nlb,td,rbh,rti,rti_fs,
          rwind,rwave,m,lr,tau,taui,taul,trim,fv,mtf,kg
lbs,nlbf;
extern char
          bf[11],lu[3],disp_u[4],force_u[4],trm,filena
me[50];
extern int
data_state[11],hull_line,valid,i_flag,mtf_flag;

/* miscellaneous*/
extern char scales[10], wdrag[10],version[5],tog[3];
extern float
l_st,phi,xi,l_dk,l_in,l_tc,i_width,s_width,dj_i,vcg,
ierror,ivector,ivr,off_i,taui_fs,Lki,Lki_fs,tauprop_fs,t
prop_fs,
Rerror,Lerror,terror;

int calc_interaction_resistance()
{
float
a,Ai,af,An,alpha,ba,bldelta,cb,cv,ca,cf,cfr,cpj,cpbh,
co,corrf_r,corrf_l,corrf_t,CDw,CLw,decr,decr2,decr3,
delta_drag,delta_lr,dC,dispi,Dps,DDw,Da,Db,Df,Dr,
Dw,e,ehp,
epsilon,err,f1,f2,f3_0,f3_1,f0,fv2,fv3,fv4,fv5,fw,fwin
d,
gimp,h,hb,h_dk,hlow,hhigh,hmax,i,ii,intakeflux,intak
eoffset,
j,j1,j2,j3,k;

float
kfv1,kk,klow,khigh,k4,k5,k6,k9,kimp,kl10,limit,limit
2,
Lkprop_fs,lrb,LLw,lcgmax,lgbx,mmoment,mm,nbdm
,ibdm,new_epsilon,
new_off_f,nozzleflux,n,nu,nlbi,off_fa,off_e,off_f,off_
fw,
off_ff,off_Dps,off_Db,off_Dr,old_tau,q,Q,QQ,Re,Re
p,re,rer,
rho,ro,step,tau_max,tau_min,TV,TH,T,v,vi,vm,vol,v
w,width,x;

int iter;
     /* constants */
ca=.0004;e=exp(1);gimp=32.17;k4=.0065;k6=.6;k9=.
242;
kimp=1.689;                /* knots to feet/sec */
kl10=log(10);
nu=.0000127908;  /* kinematic viscosity mu/ro of
salt water in ft^2/second from Barnaby pg. 156 */
rho=64.103;                /* density of salt water
lbs/ft^3 */
ro=rho/gimp;        /* mass density of water
=rho/gimp */
af=0.04*pow((mtf*10),2);      /* from Andrew
McLeod's report */
Ai=0.06565*mtf*mtf;
//vw=cd[hull_line]*kimp;
/* eqn 23 volume of water displaced */
vol=disp/(gimp*ro);

/* eqn 26 determination of maximum LCG
lcgmax=lpmax*.46*mtf;*/

/* eqn 27 calculation of wave allowance at ref. vel.
da=.012*disp*nlb*/

/* beta[hull_line] in radians */
ba=beta[hull_line]/57.296;
k5=k4*beta[hull_line];
lgbx=lcg/bpx;

if(bpx==0)
          return(1);

/* eqn 23 min velocity for which the savitsky
prediction is valid */
a=gimp*pow(vol,.33333);
kfv1=pow(a,.5)/kimp;
if(kts<kfv1)
          valid=0;
else
          valid=1;

/* speed coefficients */
v=kts*kimp;fv=v/pow(gimp*pow(vol,.33333),.5);
cv=v/pow(gimp*bpx,.5);
fv2=pow(fv,2);fv3=pow(fv,3);fv4=pow(fv,4);fv5=po
w(fv,5);
decr=1;limit=50;old_tau=0;taui=taul;
/*limit2=.02;*/off_f=0;epsilon=8/57.3;

// Full Scale Propulsion data

tprop_fs=fv3*541.28-fv2*3898.1+fv*9322.2-2528.7;

Lkprop_fs=(fv3*0.2802-
fv2*1.2381+fv*.5045+6.5329)*mtf;

tauprop_fs=(fv3*.7216-fv2*6.9852+fv*19.576-
9.6563)/57.3;


T=0;Da=0;
// ITERATION FOR THRUST
for(iter=0;iter<4;iter++)
{
f1=50000;tau_min=taul-4/57.3;tau_max=taul+4/57.3;
/* ITERATIVE SOLUTION FOR TRIM - MAIN
BODY */
          while(pow(f1*f1,.5)>limit||decr>.1)
          {
          old_tau=taui;
          taui=(tau_min+tau_max)/2;
```

```
        trim=taui*57.3;

        /* wind resistance */
        CDw=0.0105*trim*trim-
0.0541*trim+0.5422;
        CLw=0.0271*trim*trim-
0.1830*trim+1.457;
        DDw=CDw*0.5*af*0.08072/gimp*v*v;
        LLw=CLw*0.5*af*0.08072/gimp*v*v;
/*32.2=gimp*/
        Dw=pow((DDw*DDw+LLw*LLw),0.5);
        alpha=atan(LLw/DDw);
    dispi=disp-Dw*sin(alpha)+Da*sin(taui)
        -T*sin(taui+epsilon)-ivector*cos(taui);
        /* deadrise lift coefficient */
        cb=dispi/(0.5*ro*bpx*bpx*v*v);

        /* iterative solution for flat plate lift
coefficient
        -based on equation 16 in Savitsky '64 */
        limit=.00001;       co=cb;    decr=.01;
        f1=co-(.0065*beta[hull_line])*pow(co,.6)-
cb;

        while(pow(f1*f1,.5)>limit||pow(decr*decr,.
5)>limit)
                {
                f0=f1;
                co=co-decr;
                f1=co-
(.0065*beta[hull_line])*pow(co,.6)-cb;
                if(f0==f1)
                        return(1);
                decr=decr*f1/(f0-f1);
                }

        /* iterative solution for lamda -based on
        Savitsky equation no. 15 */
        limit=.00001;
        lr=2;
        decr=.01;
        f1=pow((taui*57.2958),1.1)*(0.0120*pow(l
r,.5)+
        .0055*pow(lr,2.5)/cv/cv)-co;

        while(pow(f1*f1,.5)>limit||pow(decr*decr,.
5)>limit)
                {
                f0=f1;                  lr=lr-decr;

        f1=pow((taui*57.2958),1.1)*(0.0120*pow(l
r,.5)+
                .0055*pow(lr,2.5)/cv/cv)-co;
                if(f1==f0)
                        return(1);
                decr=decr*.5*f1/(f0-f1);
                }

        /* vm the mean velocity over the planning
surface */
        k=.012*pow(lr,.5)*pow(taui*57.2958,1.1);
        vm=v*pow(1-(k-
k5*pow(k,k6))/lr/cos(taui),.5);

        /* Reynolds number */
        re=vm*lr*bpx/nu;

        /* Shoenherr friction drag coefficient for
hull*/
        limit=.0001;        cf=.003;  decr=.001;
        f1=log(re*cf)/kl10-k9/pow(cf,.5);

        while(pow(f1*f1,.5)>limit||pow(decr*decr,.
5)>limit)
                {
                f0=f1;
                cf=cf-decr;
                f1=log(re*cf)/kl10-k9/pow(cf,.5);
                if(f0==f1)
                        return(1);
                decr=decr*f1/(f0-f1);
                }
        /*spray drag due to delta_lr*/
        delta_lr=0;

        // drag decrement due to loss of intake area
        lrb=lr*bpx;
        if(lrb-(l_tc+l_in)<=0)
                {
                gotoxy(10,24);
                printf("delta_drag failure
d_d=%f4.1",delta_drag);
                }
        else

        delta_drag=.074*.5*ro*vm*vm*i_width*po
w(vm/nu,-.2)
                *(pow(lrb,.8)-pow(lrb-
(l_tc+l_in),.8)-pow(l_tc,.8));

        /* resistance components of the boat hull */
        Df=ro/2*v*v*bpx*bpx*(cf+ca)/cos(ba)*
        ((vm/v)*(vm/v)*lr+delta_lr)-delta_drag;

        /* wave resistance
        rwave=da[hull_line]*pow(kts/ka[hull_line],
na[hull_line]);*/

        /* pitot-static drag */
        Dps=0.715*(0.00205*3.281*3.281)*(ro/2)*
v*v;
        off_Dps=vcg-(.3+.13/2)*mtf;

        // drag on rudder support brackets
        Db=0.6*(0.0012*3.281*3.281)*(ro/2)*v*v;
        off_Db=vcg-0.05*mtf;

        /* Shoenherr friction drag coefficient for
rudder*/
        limit=.0001;
        rer=v*.25*mtf/nu;
        cfr=.003;
        decr=.001;
        f1=log(rer*cfr)/kl10-k9/pow(cf,.5);

        while(pow(f1*f1,.5)>limit||pow(decr*decr,.
5)>limit)
                {
```

```
                f0=f1;
                cfr=cfr-decr;
                f1=log(rer*cfr)/k110-
k9/pow(cfr,.5);
                if(f0==f1)
                        return(1);
                decr=decr*f1/(f0-f1);
                }
        Dr=ro*(.066*3.281*3.281)*cfr*1.08*v*v;
        off_Dr=vcg-(-.1*mtf);
        Da=Dps+Db+Dr;

        /* offset of appendage drag */
        off_fa=(Dps*off_Dps+Db*off_Db+Dr*off_
Dr)/Da;

        /* offset of centre of pressure N */
        cpbh=.75-1/(5.21*cv*cv/lr/lr+2.39);
        off_e=lcg-cpbh*lr*bpx;

        // offset of interaction vector
        //off_i=lcg-l_tc-1;

        /* offset of centre of drag */
        off_ff=vcg-(bpx/4)*tan(ba);

        /* offset of aerodynamic drag force */
        off_fw=(-
0.0208*trim*trim+0.1794*trim+0.4279)*bpx;

        /* net bow down? pitching moment -based
on Savitsky equations */

        f1=
        dispi*(off_e*cos(taui+epsilon)+sin(taui)*of
f_f)

        +(Df+Da)*(off_f+off_e*sin(epsilon))

        +(Da*off_fa+Df*off_ff)*cos(epsilon)

        +Dw*((cos(alpha)*sin(taui+epsilon)

        +cos(taui+epsilon)*sin(alpha))*-off_e
                        -off_fw*cos(epsilon)+
                        off_f*cos(taui+alpha))
                +ivector*(off_i-
off_e)*cos(epsilon);

        if(f1>0)
                tau_max=(taui+2*tau_max)/3;
        else
                tau_min=(taui+2*tau_min)/3;
                decr=pow(pow(old_tau-
taui,2),.5)*57.3;

        limit=50;
        }

/* END OF MAIN BODY */


if (bf[hull_line]=='Y')
{
/* Blount and Fox correction factor relation resulting
from analytical curve fitting of experimental results
(only applies if Froude no.< 3.7 */

if (fv<3.7)
        {
        k=fv-.85;
        m=.98+2*pow(lgbx,1.45)*pow(e,-2*k)-
3*lgbx*pow(e,-3*k);
        }
else
        m=1;
}
else
        m=1;

/* total resistance =Tcos(taui+epsilon) */
rti=cos(taui+epsilon)/cos(epsilon)*((sin(taui)*dispi+D
f)*m
        +Dw*cos(taui+epsilon)+Da);

if (force_u[0]=='K')
        nlbi=.2247;
else
        nlbi=1;

/* estimated horse power */
//ehp=rti_fs*v/550/nlb;
Lki=(lr+tan(ba)/(2*PI*tan(taui)))*bpx;
Re = (v*(Lki-(l_in+l_tc)))/nu;
Rep = pow(Re,0.2);
f1=1;decr=1;limit=.0025;Q=.25*mtf*mtf*mtf;dC=0.7
;
bldelta=dC*0.37*(Lki-(l_in+l_tc))/Rep;
n=log10(Re);
        while(pow(f1*f1,.5)>limit||decr>.001)
        {
        f0=f1;
        Q=Q-decr;
        step=0.001;err =
0.003;QQ=0;hlow=0;hhigh=1;
        An=pow(dj_i,2)*PI/4;

                while(pow(pow(Q-
QQ,2),0.5)/Q>err)
                {
                i=0;
                h =
0;QQ=0;mmoment=0;intakeflux=0;
                hmax = (hlow+hhigh)/2;
/*calc height of st.tube*/
                        while(h < hmax)
/*calc intake flux & Q*/
                        {
                        i++;
                        h = i*step;
                        hb = h/bldelta;
                        if (h < bldelta)
                        vi = pow(hb,(1/n))*v;
/*calc b.l. vel.*/
                        else
                                vi = v;
                        if (h<hmax)
```

```
                                        width =
s_width*pow((1-h*h/hmax/hmax),0.5); /*equ for
elipse*/
                                else
                                        width=0;
                                mm =
ro*pow(vi,2)*width*step;
                                intakeflux += mm;
                                mmoment += mm*h;
                                q = vi*width*step;
                                QQ += q;
                                }
                        if (QQ<Q)

        hlow=(hmax+2*hlow)/3;
                        else

        hhigh=(hmax+2*hhigh)/3;
                        }
        intakeoffset=mmoment/intakeflux;
        nozzleflux=ro*Q*(Q/An)*1.0015;      /*
where 1.002 is a factor based on
                                        nozzle
velocity profile */
        ivr=(Q/Ai)/v;
        TH=nozzleflux*cos(taui+phi-xi)-
intakeflux*cos(taui-xi);
        TV=nozzleflux*sin(taui+phi-xi)-
intakeflux*sin(taui-xi);
        T=pow(pow(TV,2)+pow(TH,2),.5);
        f1=(rti-TH)/rti;
        if (f0==f1)
                return (1);
        decr=decr*f1/(f0-f1);
}
new_epsilon=atan(TV/TH)-taui;

/* offset of T vector from CG */
nbdm=nozzleflux*cos(phi-xi)*(vcg-l_st-lcg*tan(phi-
xi));
ibdm=intakeflux*(intakeoffset+vcg-(l_dk-
lcg)*sin(xi));

new_off_f=(ibdm-nbdm)/T;

//f2=pow(pow((epsilon-
new_epsilon),2),.5)/new_epsilon
//        +pow(pow((off_f-
new_off_f),2),.5)/new_off_f;
epsilon=new_epsilon;off_f=new_off_f;
}

/*need rwave,rapp*/rbh=rbh/nlbi;rti=rti/nlbi;

//Adjusted Values using towing test adjustments

if(fv<2.75)
        corrf_r=(fv4*0.190757-
fv3*1.67079+fv2*5.4486-fv*7.8106+5.1138);
else
corrf_r=1;
rti_fs=rti*corrf_r;

if(fv<2.5)
        corrf_t=(fv3*.29479-
fv2*1.87523+fv*3.98979-1.8932);
else
        corrf_t=0.96;
taui_fs=taui*corrf_t;

corrf_l=(-fv3*0.0145+fv2*0.1026-fv*0.1385+.9511);
Lki=(lr+tan(ba)/(2*PI*tan(taul)))*bpx;
Lki_fs=Lki*corrf_l;

Rerror=(tprop_fs-rti_fs)/tprop_fs*100;
Lerror=(Lkprop_fs-Lki_fs)/Lkprop_fs*100;
terror=(tauprop_fs-taui_fs)/tauprop_fs*100;

ierror=Rerror*Rerror+Lerror*Lerror+terror*terror;

return(0);
}
```

A-7.4 FUEL.C

```
#include <stdio.h>
#include <conio.h>
#include <math.h>
#define PI 3.14159

void main()
{

float   q,dq,c,g,lcfinal,vcfinal,cm,
        vm,
        fuelw,
        h,h1,h2,
        hflag,hmax,hstep,l,length,width,depth,
        xfill,xend,rho,taudeg,tau;

clrscr();
printf("FUEL LOADING");
printf("\n\n\nEnter dipstick level in metres: ");
scanf("%f",&hmax);
printf("\nEnter trim angle in degrees: ");
scanf("%f",&taudeg);
/*set default values*/
depth=.249;
width=.488;
length=2.18;
xfill=1.844;
xend=length-xfill;
hstep=.0005;
tau=taudeg*PI/180;
rho=736;                        /*shell super*/
g=9.81;
/*calc initial fill params. to bottom of dipstick*/
hflag=(xfill*tan(tau)*cos(tau));
for(h=hstep;h<=hflag;h+=hstep)
        {
        l=h/tan(tau)+h*tan(tau);
        c=l/2-h*tan(tau);
        dq=(l*hstep*width);
        q+=dq;
        cm+=c*dq;
        vm+=h*dq;
        }

/*calc h values*/
if(tau<(6.81*PI/180))
        {
        h1=xend*tan(tau);
        h2=depth-(xfill*tan(tau));
        }
else
        {
        h1=depth-(xfill*tan(tau));
        h2=xend*tan(tau);
        }

/*calc rest of tank*/
for(h=hstep;h<h1;h+=hstep)
        {
        if(h>=hmax)
                break;
        l=xfill/cos(tau)+h/sin(tau);
        c=l/2-(xfill*tan(tau)+h)*sin(tau);
        dq=(l*hstep*width);
        q+=dq;
        cm+=c*dq;
        vm+=(hflag+h)*dq;
        }
for(;h<h2;h+=hstep)
        {
        if(h>=hmax)
                break;
        if(tau<(6.81*PI/180))
                {
                l=length/cos(tau);
                c=l/2-(xfill*tan(tau)+h)*sin(tau);
                }
        else
                {
                l=depth/sin(tau);

        c=xfill*cos(tau)+(h/tan(tau))*cos(tau)-l/2;
                }
        dq=(l*hstep*width);
        q+=dq;
        cm+=c*dq;
        vm+=(hflag+h)*dq;
        }
for(;h<=hmax;h+=hstep)
        {
        if(h>=hmax)
                break;
        l=(depth-h)/sin(tau)+xend/cos(tau);
        c=length*cos(tau)-l/2-(h-
xend*tan(tau))*sin(tau);
        dq=(l*hstep*width);
        q+=dq;
        cm+=c*dq;
        vm+=(hflag+h)*dq;
        }


lcfinal=cm/q;
vcfinal=vm/q;
fuelw=q*rho*g;
printf("fuel volume is %5.3f m^3\n",q);
printf("fuel weight is %4.0f N\n",fuelw);
printf("lc of g from lower corner of tank is %5.3g m
\n",lcfinal);
printf("vc of g from lower corner of tank is %5.3g
m",vcfinal);

}
```

A-7.5 INTAKE.C

```
#include <stdio.h>
#include <math.h>
#include <conio.h>

/*Function declarations*/

void get_parms(float *p1, float *p2, float *p3, float
*p4, float *p5,
                float *p6, float *p7, float
*p8,float *p9, float *p10,
                float *p11);
void clrscr();
float get_bldelta(float Vs, float Lk);
void flowrate();
//FILE *fptr, *fopen();

const float G = 9.81E+0F;

float
Vs,dVs,Lk,dLk,Q,QQ,dQ,dC,ddC,Ws,dWs,dn,bldelta,
Re,Rep,intakeoffset,
        intakeflux,hlow,hhigh,n,mmoment,lbratio,r
ho,drho,nu,dnu,
        frho,fnu,fVs,fLk,fQ,fdC,fWs,fdn,z,zpc,IVR,
Ai,
        ifxtotal,ifxave,ifxvar,ifxstdev,
        ifstotal,ifsave,ifsvar,ifsstdev;
float ifs[7000],ifx[7000];
int j1,j2,j3,j4,j5,j6,j7,j8,i;
//char filename[50];
/*Main Function*/

main()
{
frho=1024;
drho=1;
fnu=1.2E-6F;
dnu=63.6E-9F;
Ai = 0.06565;
/*printf("Enter filename...");
gets(filename);*/
        do
        {
        get_parms(&fVs,&dVs,&fLk,&dLk,&fQ,&
dQ,&fdC,&ddC,&fWs,&dWs,&fdn);
//          fptr=fopen(filename,"w");
            ifxtotal=0;ifstotal=0;
            ifxvar=0;ifsvar=0;
            clrscr();
            printf("RESULTS\n\n");
            z=0;
            for(j1=-1;j1<2;j1++)
                {
                Vs=fVs+dVs*j1;
                for(j2=-1;j2<2;j2++)
                    {
                    rho=frho+drho*j2;
                    for(j3=-1;j3<2;j3++)
                        {

        nu=fnu+dnu*j3;
                                        for(j4=-
1;j4<2;j4++)
                                            {

        Lk=fLk+dLk*j4;

        for(j5=-1;j5<2;j5++)

        {

        Q=fQ+dQ*j5;

        for(j6=-1;j6<2;j6++)

                {

                dC=fdC+ddC*j6;

                for(j7=-1;j7<2;j7++)

                        {

                        Ws=fWs+dWs*j7;

                        for(j8=-1;j8<2;j8++)

                                {

                                dn=fdn*j8;


        bldelta=get_bldelta(Vs,Lk);

                                flowrate();


        ifx[z]=intakeflux;


        ifs[z]=intakeoffset;


        //fprintf(fptr,"%6.0f
        %6.3f\n",ifx[z],ifs[z]);

                                z++;

                                }

                        }

                }

        }

        zpc=z/6561*100;

        gotoxy(1,5);

        printf("zpc= %3.0f",zpc);
                                }
                            }
                        }
                }
```

```
                    for(i=0;i<(z-1);i++)
                    ifxtotal+=ifx[i];
                    ifxave=ifxtotal/z;

                    for(i=0;i<(z-1);i++)
                    ifxvar+=(pow((ifx[i]-
ifxave),2)/(z-1));
                    ifxstdev=pow(ifxvar,0.5);

                    for(i=0;i<(z-1);i++)
                    ifstotal+=ifs[i];
                    ifsave=ifstotal/z;

                    for(i=0;i<(z-1);i++)
                    ifsvar+=(pow((ifs[i]-ifsave),2)/(z-
1));
                    ifsstdev=pow(ifsvar,0.5);

                    IVR = (fQ/Ai)/Vs;

                    printf("\nifxave= %5.0f N
ifxstdev= %5.0f N   IVR=
%5.2f",ifxave,ifxstdev,IVR);
                    printf("\nifsave= %5.4f m
ifsstdev= %5.4f m" ,ifsave,ifsstdev);
                    printf("\n\nPress q to quit, any
other key to continue...");
          }
          while (getch() != 'q');
return(0);
}


/*Function defintions*/
void get_parms(float *p1, float *p2, float *p3, float
*p4, float *p5,
                    float *p6, float *p7, float
*p8,float *p9, float *p10,
                    float *p11)
{

                    do {
                    clrscr();
                    printf("\t\tWelcome to Hamish's
Global Flow Program\n\n\n ");
                    printf("\n\nEnter required ship
speed, Vs in m/s ");
                    scanf("%f",p1);
                    printf("Enter delta ship speed in
m/s ");
                    scanf("%f",p2);
                    printf("Enter Lk in m ");
                    scanf("%f",p3);
                    printf("Enter delta Lk in m ");
                    scanf("%f",p4);
                    printf("Enter required flow rate, Q
in m^3/s ");
                    scanf("%f",p5);
                    printf("Enter delta Q in m^3/s ");
                    scanf("%f",p6);
                    printf("Enter B.L. const ");
                    scanf("%f",p7);
                    printf("Enter delta B.L. const ");
                    scanf("%f",p8);
                    printf("Enter ST width Ws in m
");
                    scanf("%f",p9);
                    printf("Enter delta ST width in m
");
                    scanf("%f",p10);
                    printf("Enter dn ");
                    scanf("%f",p11);
                    printf("\n\nVs = %5.2f m/s\ndVs
= %5.2f m/s\nLk = %5.2f m\n"
                    "dLk = %5.3f m\nQ = %5.3f
m^3/s\ndq = %5.3f m^3/s\nB.L. const"
                    " = %4.2f\ndB.L. const =
%4.2f\nWs = %5.3f m\ndWs = %5.3f m\n"
                    "dn = %3.1f"

          ,fVs,dVs,fLk,dLk,fQ,dQ,fdC,ddC,fWs,dWs,
fdn);
                    puts("\n\nIs data correct? (y/n)");
          } while (getch() != 'y');
}
float get_bldelta(float Vs,float Lk)
{
          Re = (Vs*Lk) / nu;
          Rep = pow(Re,0.2);
          return ((dC*0.37*Lk)/Rep);
}
void flowrate()
{
float i;
float Ai,h,hb,hmax,step,j,m,q,QQ,v,x,width,err;
hlow=0; hhigh=0.2; step=0.001; err = 0.005;QQ=0;

while(pow(pow(Q-QQ,2),0.5)/Q>err)
          {
          i=0;
          h = 0;QQ=0;mmoment=0;intakeflux=0;
          hmax = (hlow+hhigh)/2;          /*calc
height of st.tube*/
          while(h < hmax)                 /*calc intake
flux & Q*/
                    {
                    i++;
                    h = i*step;
                    n=log10(Re)+dn;
                    hb = h/bldelta;
                    if (h < bldelta)
                              v = pow(hb,(1/n))*Vs;
/*calc b.l. vel.*/
                    else
                              v = Vs;
                    if (h<hmax)
                              width = Ws*pow((1-
h*h/hmax/hmax),0.5); /*equ for elipse*/
                    else
                              width=0;
                    m = rho*pow(v,2)*width*step;

                    intakeflux += m;
                    mmoment += m*h;

                    q = v*width*step;

                    QQ += q;
```

```
                }

        if (QQ<Q)
                hlow = hmax;
        else
                hhigh = hmax;
        }

        intakeoffset = mmoment / intakeflux;

}
```

Deloitte Touche Tohmatsu

Management Consultants
61 Molesworth Street
Wellington
New Zealand

PO Box 1990
Telephone (4) 472 1677
Facsimile (4) 472 8023
Telex 31015

6 December 1996

Dr A J Bowen
Department of Mechanical Engineering
University of Canterbury
Private Bag 4800
CHRISTCHURCH

Dear Tony

Re: Thesis, Hard Bound

Thanks for the pages and suggested edits. Please find replacement pages enclosed (**81**, 82, 141, **142**). I have included the relevant backing page in each case so that the master is not being downgraded with a further generation of copying.

Also enclosed are seven disks containing file phd.zip which spans all seven disks. The files were compressed using pkzip.

Thanks again Tony,

Kind Regards,

Hamish